THERMAL MODELLING OF LASER HYPERTHERMIA IN THE VICINITY OF A LARGE BLOOD VESSEL

by

William Mark Whelan

A Project

Submitted to the School of Graduate Studies

in Partial Fulfilment of the Requirements

for the Degree

Master of Science

(Health and Radiation Physics)

McMaster University

August 1991

Master of Science (1991) MCMASTER UNIVERSITY

(Health and Radiation Physics) Hamilton, Ontario

TITLE: Thermal Modelling of Laser Hyperthermia in the Vicinity of a Large Blood Vessel

AUTHOR: William Mark Whelan, B.Sc. (U.P.E.I.)

SUPERVISOR: Dr. Douglas Wyman

NUMBER OF PAGES: xv , 167

ABSTRACT

In treating cancer with hyperthermia, an understanding of the heat losses associated with the presence of a large functioning blood vessel in or proximal to a treatment area is needed in order to optimize any protocol.

A three-dimensional computer model based on the Bioheat transfer equation (BHTE) has been developed to account for temperature changes in and around functioning blood vessels during laser-induced hyperthermia. The light source is modelled using an approximation to the transport theory solution for an isotropic point source in an infinite homogeneous tissue medium with anistropic scattering. The derived BHTE's for tissue, vessel and blood are solved for temperature using the implicit finite differences method.

The validity of the model was tested by comparing predicted temperatures to measured temperatures from a series of dynamic phantom studies using two vessel diameters and three flow rates. Large experimental temperature variations were observed and

increased proportionally with increasing thermal gradients. The model consistently over-estimates ($\cong$ 1 - 2°C) absolute temperatures close to the source and under-estimates ($\cong$ 1 - 2°C) them far from the source. This could be due to uncertainties associated with the estimated thermal conductivity and measured optical properties of the tissue material.

Both model and experiments show a small convective heat loss due to the presence of a blood vessel. The model predicts that at high flow rates, temperature reductions of 2°C or greater are limited to distances less than 0.3 cm from the surface of a 0.144 cm (outer diameter) vessel and less than 0.8 cm from the surface of a 0.40 cm vessel. The vessel has a negligible effect on temperatures at distances greater than $\cong$ 1.75 cm.

The predicted temperature change due to blood flow and the measured change agree to within experimental errors. There was better agreement with the larger diameter vessel.

ACKNOWLEDGEMENTS

I would like to thank my supervisor, Dr. Douglas Wyman for his encouragement and guidance during the course of my research. I also appeciate the endless input from the other members of my supervisory committee, Dr. Brian Wilson and Dr. Colin Webber.

I would like to thank my friends and collegues in the Physics Department, machine shop and the electronics lab at the Hamilton Cancer Clinic for their willingness to help me at anytime. I especially appreciate the help from Don MacGregor, Carrie-Lynn Swift and John Blenky.

Most importantly, I owe everything to my wife, Michelle, whose words of support and encouragement enabled me to complete this project — thanks for being there.

TABLE OF CONTENTS

		Page
CHAPTER 1	INTRODUCTION	
	1.1 Hyperthermia.....	1
	1.1.1 General classes.....	1
	1.1.2 Historical perspective.....	1
	1.2 Biological rationale.....	3
	1.2.1 Cellular response to heat....	3
	1.2.2 Proposed cellular targets/ mechanisms.....	7
	1.2.2.1 Plasma membrane.....	7
	1.2.2.2 DNA.....	7
	1.2.2.3 Proteins.....	8
	1.2.2.4 Cellular pH.....	9
	1.3 Clinical perspective.....	9
	1.3.1 Clinical practise.....	9
	1.3.2 Clinical research.....	11
	1.4 Hyperthermia modalities.....	11
	1.4.1 Objectives.....	11
	1.4.2 Microwave and RF systems.....	13
	1.4.3 Ultrasound.....	15
	1.4.4 Heated water.....	16

Table of contents (continued)

	Page
1.4.5 Infrared radiation.....	16
1.5 Hyperthermia modelling.....	18
1.5.1 Principles.....	18
1.5.2 Thermal dosimetry.....	19
1.5.3 Limitations.....	20
1.6 Thermal modelling of large blood vessels.....	21
1.6.1 Literature review.....	21
1.7 Scope of this project.....	22
CHAPTER 2 THEORY OF OPTICAL PROPAGATION, PHOTOTHERMAL INTERACTION AND HEAT TRANSFER IN TISSUE	
2.1 Introduction.....	24
2.2 Optical propagation in tissue.....	24
2.2.1 Optical penetration.....	24
2.2.2 Boltzmann equation.....	27
2.2.3 Diffusion theory.....	29
2.2.4 Transport theory.....	30
2.2.5 Anisotropic scattering.....	32
2.3 Photothermal interactions.....	33
2.4 Heat transfer in tissue.....	34
2.4.1 Thermal properties.....	34

Table of contents (continued)

Page

2.4.2 Derivation of bioheat transfer equation..... 36

2.4.3 Heat removal by a single blood vessel..... 43

2.4.3.1 BHTE at vessel/blood boundary..... 43

2.4.3.2 Heat transfer coefficient..... 44

2.4.3.3 BHTE in blood..... 46

2.5 Mathematical model..... 47

2.5.1 Finite differencing..... 47

2.5.2 Model geometry..... 48

2.5.3 Finite difference expressions for BHTE..... 50

2.5.4 Modelling light source..... 54

2.5.5 Code execution..... 55

CHAPTER 3 MATERIALS AND METHODS

3.1 Apparatus..... 57

3.1.1 Light delivery system..... 57

3.1.2 Tissue phantom..... 61

3.1.3 Temperature feedback system.. 66

3.1.4 Microprocessing system..... 66

3.2 Pump calibration..... 67

Table of contents (continued)

		Page
	3.3 Laser power calibration.....	70
	3.4 Temperature measurements procedure.	74
	3.5 Optical properties of tissue material.....	78
	3.5.1 Apparatus.....	78
	3.5.2 Reflectance and transmittance measurements.....	81
	3.5.3 Total attenuation measurements.....	82
	3.5.4 Monte Carlo calculations of optical properties.....	84
	3.6 Application of mathematical model..	88
	3.6.1 Assumptions.....	88
	3.6.2 Computer code.....	92
	3.6.3 Verification of model.....	92
CHAPTER 4	RESULTS AND DISCUSSION	
	4.1 Optimization and verification of the model.....	94
	4.2 Experimental temperature measurements.....	99
	4.2.1 Temperature variation with distance from source.....	99
	4.4.2 Temperature variation with blood flow.....	104

Table of contents (continued)

		Page
	4.3 Model results.....	110
	4.4 Comparison of model predictions with experimental results.....	121
	4.5 Future research.....	135
CHAPTER 5	SUMMARY	136
APPENDIX A	FINITE DIFFERENCE EXPRESSIONS FOR THE BIOHEAT TRANSFER EQUATIONS	139
APPENDIX B	CONTROL PROGRAM FOR EXPERIMENTAL TEMPERATURE MEASUREMENTS	143
APPENDIX C	COMPUTER CODE FOR DEVELOPED THERMAL MODEL	147
BIBLIOGRAPHY		157

LIST OF TABLES

Page

1.1 Tissue transformations as a function of temperature..... 4

1.2 Effect of local hyperthermia..... 10

2.1 Optical penetration depths in tissues..... 26

3.1 Laser power calibration..... 73

3.2 Monte Carlo values for Σ_a and Σ_s' of tissue material..... 87

4.1 Experimental laser power measurements..... 108

4.2 Input parameters to computer model..... 113

LIST OF FIGURES

Page

1.1 Survival curves for mammalian cells..... 6

1.2 Arrhenius plot for heat inactivation of cells.. 6

2.1 Control surface for BHTE derivation..... 38

2.2 Model geometry..... 49

2.3 Schematic of finite differencing scheme..... 52

2.4 Flow chart of computer code..... 56

3.1 Apparatus for measuring temperatures in a tissue phantom..... 58

3.2 Photographic profiles of cylindrically tipped optical fibers..... 60

3.3 Tissue phantom..... 62

3.4 Peristaltic pump calibration..... 69

3.5 Laser power calibration..... 71

3.6 Microthermocouple calibration..... 75

3.7 Procedure for implanting devices into phantom.. 77

3.8 Optical system used to measure optical properties of tissue material..... 79

3.9 Total attenuation of tissue material..... 85

3.10 Normalized photon flux from source fiber..... 89

4.1 Variation of model solution with temporal increment..... 95

List of figures (continued)

Page

4.2 Variation of model solution with convergence criterion..... 95

4.3 Comparison of analytical solution to finite difference solution..... 98

4.4 Dependence of model solutions on radial and axial increments..... 98

4.5 Configuration of fiber and thermocouple implantations..... 100

4.6 Temperature profiles as a function of distance from source..... 102

4.7 Temperature profiles as a function of blood flow in a 0.40 cm vessel..... 105

4.8 Temperature decrease due to blood flow in a 0.40 cm vessel..... 111

4.9 Temperature decrease due to blood flow in a 0.144 cm vessel..... 111

4.10 Predicted model temperatures as a function of blood flow..... 115

4.11 Temperature change as a function of radial distance from vessel..... 119

4.12 Comparison of model predictions and experimental temperatures for a 0.144 cm vessel..... 122

4.13 Comparison of model predictions and experimental temperatures for a 0.40 cm vessel..... 125

4.14 Model temperatures as a function of the thermal conductivity..... 129

List of figures (continued)

Page

4.15 Model temperatures as a function of the total laser power..... 131

4.16 Comparison between predicted and measured temperature decrease due to blood flow in a 0.144 cm vessel..... 132

4.17 Comparison between predicted and measured temperature decrease due to blood flow in a 0.40 cm vessel..... 133

"Those who cannot be cured by medicine can be cured by surgery. Those who cannot be cured by surgery can be cured by fire [hyperthermia]. Those who cannot be cured by hyperthermia are indeed incurable."

Hippocrates (470 - 377 BC)

CHAPTER 1

INTRODUCTION

1.1 Hyperthermia

1.1.1 General classes

Hyperthermia is the elevation of tissue temperatures above normal body temperature. There are three classes of hyperthermia. These are systemic (whole body), regional and local. Each class is defined by the volume of tissue which is to be heated. In cancer therapy, local hyperthermia is most often used. In this the therapeutic temperature elevation (41-46 $^{\circ}$C) is confined to a localized tumor volume. This project will focus on local hyperthermia.

1.1.2 Historical perspective

As a treatment of disease, hyperthermia has been utilized for thousands of years. In the latter part of the nineteenth century researchers such as Busch (1866)

and Bruns (1887) reported the spontaneous regression of tumors, both primary and metastatic, in patients who had an erysipelas infection, a disease which induces a 40°C fever. This led to the popularity of inducing fevers in patients with cancer. William Coley (1893) reported on a cancer therapy in which strains of Streptococcus Erysipelatosis were injected into patients with advanced cancer. He observed tumour necrosis and in some instances complete tumor regression.

With the discovery of x-rays in 1895 and the advent of radiation therapy thereafter, hyperthermia research began to decline. The modern era of hyperthermia began with the works of Gessler et al (1950), Crile (1961) and Cavaliere et al (1967). Up until the 1960's, hyperthermia was pursued with enthusiasm but with little scientific merit. The literature reflects the lack of knowledge of the mechanisms by which heat kills cells. Primary research was focused on testing this potential modality on tumors of different histological types in numerous locations in the body.

It has only been in the last 20 years that a

better understanding of the behavior of cells at elevated temperatures has evolved. With this increasing data base of in vitro and in vivo studies has come a strong revival of interest in hyperthermia as a cancer treatment modality.

1.2 Biological rationale

1.2.1 Cellular response to heat

The investigation into the cellular, subcellular, and physiological mechanisms by which hyperthermia elicits a biological response is an area of active research and controversy. Researchers agree on one point: heat kills cells. The effects of heating tissue are shown in table 1.1. The tissue temperature achieved determines the type of heat induced transformation. In the hyperthermic temperature range the mechanisms of heat inactivation are not as apparent as with higher temperatures.

Figure 1.1 shows a family of survival curves for Chinese hamster ovaries exposed to temperatures from 41.5°C to 46.5°C. These survival curves show the sensitive temperature dependence of cell necrosis. At

Temperature	Effects on tissue
43 - 45 °C	Retraction Hyperthermia (cell mortality)
50 °C	Reduction of enzyme activity
60 °C	Protein denaturation Coagulation
80 °C	Collagen denaturation Membrane permeabilization
100 °C	Vaporization and ablation

Table 1.1 Tissue transformations as a function of the temperature elevation.

lower temperatures there is a flattening out of the survival curve after an extended exposure to hyperthermia, which suggests the development of resistance to the elevated temperature. This phenomenon, known as thermotolerence, is beyond the scope of this project but is well documented in the literature (Gerner and Schneider 1975, Henle 1980). It appears that different tumors have different levels of thermosensitivity and require different temperatures and incubation times for maximum effect (Cavaliere et al 1983).

Using the data from figure 1.1, 1/Do was plotted against 1/T, where Do is the reciprocal of the final slope of the survival curve and T is the temperature (see figure 1.2). The resulting graph, known as an Arrhenius Plot, yields a slope which represents the inactivation energy of the chemical process(es) involved in cell killing. The sharp change in the slope at 43 °C may reflect different cell kill targets/mechanisms. It is believed that more than one target is involved in the heat inactivation of cells (Hall 1988).

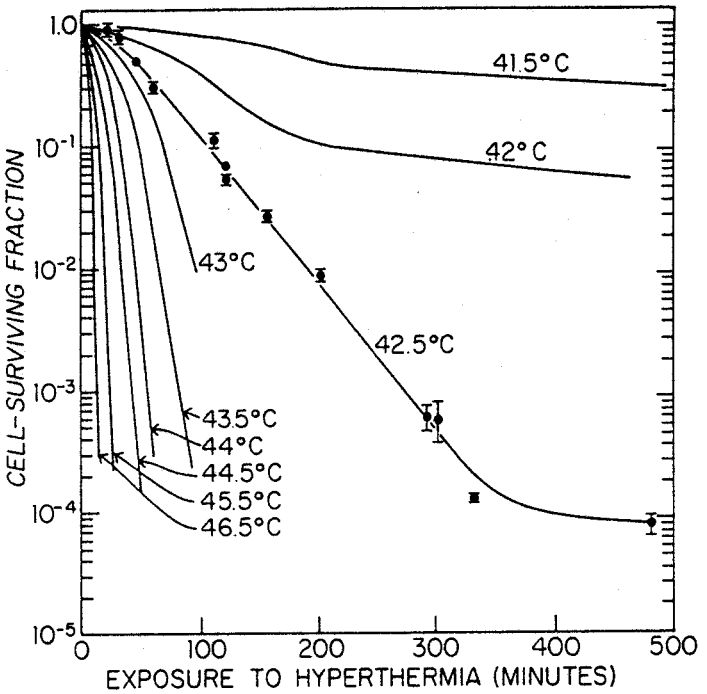

Figure 1.1 Survival curves for mammalian cells (Chinese hamster ovaries) in culture (Reprint from Hall 1988).

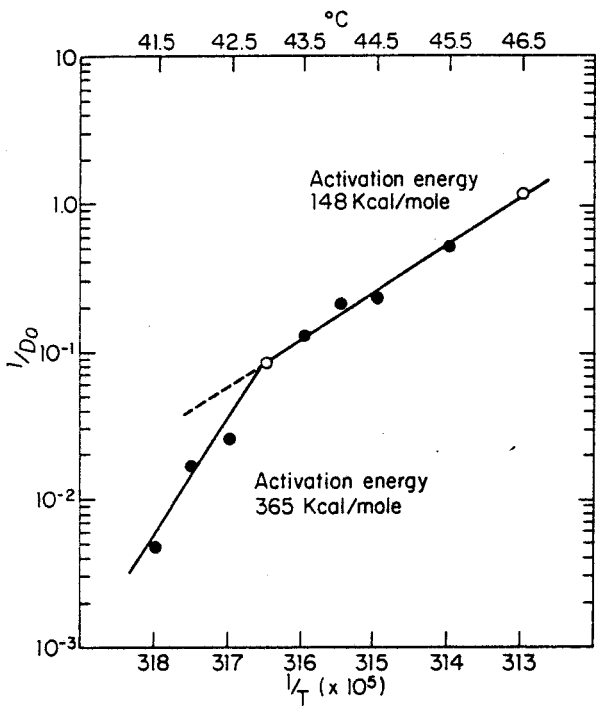

Figure 1.2 An Arrhenius plot for heat inactivation of mammalian cells in culture (Reprint from Hall 1988).

1.2.3 Proposed cellular targets/mechanisms

1.2.3.1 Plasma membrane

Gerner et al (1977) proposed that heating cells increases membrane fluidity and permeability, resulting in a heat sensitive state. Agents which increase membrane fluidity increase the damaged produced by a given dose of heat (Hahn et al 1977, Overgaard 1977).

Borrelli (1986), after heating suspensions of Chinese hamster ovary cells, observed membrane blebbing. The degree of blebbing dictated the ability of the cell to survive.

1.2.3.2 DNA

There have been reports of inhibition of DNA synthesis (McCormick and Penman 1969) and damage to RNA metabolism (Busch and Smetana 1970) in heated cells.

Dewey (1988) observed a correlation between the surviving cell fraction and the frequency of chromosomal aberrations when cells were heated during the S-phase of the cell cycle. In the S-phase, as DNA is being synthesized, cells are most sensitive to heat (Westra and Dewey 1971).

Dewey (1989) observed fewer single or double strand breaks in DNA immediately after heating as compared to the number observed after a dose of radiation yielding the same necrotic endpoint. This suggests the presence of more than one cellular target in heat inactivation.

1.2.3.3 Proteins

Following an exposure to heat, inhibition of protein biosynthesis has been observed (Moricca et al 1977). This inhibition appears to vary with different tumors (Mondovi 1976). It has been suggested that a protein or family of proteins are activated by heat and interfere with DNA synthesis (Wong et al 1989).

The activation energy for cell killing as seen from the Arrhenius plot (figure 1.2) is similar to the inactivation energy for protein denaturation (Johnson et al 1954). Protein denaturation has been observed in cells following an exposure to heat (Brandts et al 1978).

1.2.3.4 Cellular pH

Hyperthermia has been shown to modify intratumor pH in a variety of in vivo systems (Song 1980). It has been proposed that hyperthermia results in a reduction of blood flow which reduces the efficiency of oxygen delivery and metabolite clearance. The reduction in oxygen causes an increase in lactic acid production in the cells. Due to the reduced clearance, the pH is lowered (Hofer and Mivechi 1980). This acidic state at elevated temperatures leads to the increased cytotoxicity.

This theory is supported by reports that cells maintained under acidic conditions exhibit enhanced sensitivity to heat damage (Freeman et al 1977).

1.3 Clinical perspective

1.3.1 Clinical practise

Presently in the clinical environment, hyperthermia is still in its infancy. In the last decade or so there have been several clinical studies which are summarized by Overgaard (1982) in table 1.2. The complete response rate to heat alone is approximately

Study	Number of Tumors	Response		
		Complete	Partial	No
Luk et al	11	1	2	8
U et al	6	0	3	3
Overgaard	13	0	5	8
Fazekas et al	4	1	0	3
Kim et al	19	4	6	9
Perez et al	5	2	0	3
Marmor et al	44	5	14	25
Corry et al	28	5	11	12
Israel et al	36	1	13	22
Marchal et al	12	0	1	11
Abe et al	6	0	1	5
Okada et al	69	15	28	26
Hall et al	35	4	19	12
Hiraoka et al	9	0	2	7
Lele et al	36	6	20	10
Dunlop et al	9	1	2	6
Manning et al	11	2	3	6
Dubois et al	27	1	8	18
All studies	380	48 (13%)	138 (36%)	194 (51%)

Table 1.2 Effect of local hyperthermia alone.

13% and seems to be of short duration. Therefore, the clinical uses of heat alone have been limited to palliative care and for those patients where conventional therapies have failed (Hall 1988, Ferraro et al 1989).

1.3.2 Clinical research

There has been considerable clinical interest in combining heat therapy with radiotherapy or chemotherapy (Overgaard 1982). This is due to the clinical evidence that there is a synergistic effect when radiation and heat or chemotherapy and heat are combined. The combination treatment results exceed the summation of the effect when the two modalities are used individually.

1.4 Hyperthermic modalities

1.4.1 Objectives

There are a number of ideal objectives which are strived for when developing a local hyperthermiasystem. These are:

(i) The therapeutic temperature elevation should be

confined to the treatment volume sparing any surrounding normal tissues.

(ii) The technique should provide for adequate energy penetration in the tissue as well as sufficient power deposition at depth.

(iii) The temperature monitoring system should be reliable and consistent.

(iv) The technique should be easily adapted to physiological changes in the treatment region (i.e. blood vessels, cavities or bone).

(v) The technique should be applicable to both superficial and deep-seated tumors.

With the advances in hyperthermia technology, many of the above objectives can be met. No single technique possesses all these attributes. Hyperthermic systems can be classified as invasive (source implanted in tissue), or non-invasive (source external to the tissue). Non-invasive systems, although desirable, cannot produce the therapeutic temperatures throughout the entire tumor volume while sparing the surrounding normal tissues (Strohbehn et al 1984). It has been reported that invasive systems may be better able to

produce uniform heating patterns within the tumor volume (Strohbehn et al 1984, Dunlop et al 1989). The following is a brief description of the current clinical and experimental hyperthermia systems.

1.4.2 Microwave and radiofrequency systems

The most common hyperthermia systems use electromagnetic radiation in the radio (300 KHz to 300 MHz) and microwave (300 MHz to 300 GHz) frequency ranges.

A major problem with using microwave and RF radiation is the perturbation of the metallic temperature measuring devices such as thermocouples and thermistors. These devices can self heat in the presence of the electromagnetic field reporting inaccurate high temperatures (Christensen 1983).

In general, external microwave systems are limited to the treatment of superficial tumors due to the limited penetration of this frequency of radiation (Paglione 1982). External RF systems with its greater tissue penetration can treat deep-seated tumors but there can also be excessive heating of the subcutaneous

fat (Dunlop et al 1989).

Annular phased array RF systems (Turner 1984, Strohbehn et al 1989) consisting of external applicators aimed at a common focal spot in the center of a deep-seated tumor can provide an enhanced temperature increase proportional to the number of applicators. This can decrease the extent of surface skin heating. There is still difficulty in raising the tumor temperature into the therapeutic range without raising the temperature of normal tissue to dangerous levels (Strohbehn et al 1989).

For heating deep-seated tumors, implantable microwave antennae (Coughlin et al 1983) made of semi-rigid or flexible coaxial transmission lines can be passed through body orifices so as to come in close contact with a tumor or they can be surgically implanted.

Direct tissue heating can be accomplished using implanted metal electrodes which are heated by an external RF generator (Sternhegan et al 1978). The spatial distribution of electrodes is dictated by the size and shape of the tumor as well as its vicinity to

nearby vasculature.

1.4.3 Ultrasound

Ultrasound radiation in the 1-3 MHz frequency range is used to induce hyperthermia (Hynynen and Edwards 1989, Oleson and Samulski 1989). Focused ultrasound systems show great potential for inducing hyperthermia in deep-seated tumors due to the desirable penetration depth in tissue (Hornbeck 1984).

The penetration depth can be increased by decreasing the angle of convergence of the transducer or by reducing the frequency. These adjustments will increase the irradiation area or reduce the energy intensity at the focus, respectively.

Multiple focused ultrasound beams or single focused beams (Lele and Parker 1982) allowed to move three dimensionally provide the means of uniformily heating tumors of different sizes and shapes. These developments remain in the experimental stage.

The disadvantage of ultrasound radiation is its perturbation in the presence of bone and air cavities. Bone/muscle or air/muscle interfaces represent a

mismatch in acoustic impedance which results in a partial or full reflection of the incident wave depending on the degree of mismatch. This phenomenon hinders the penetration depth achievable and the uniformity of temperature elevations.

1.4.4 Heated water

Using heated water is the oldest and simplest way to induce hyperthermia. It is reliable from a thermometry point of view because there is no perturbation of the thermosensors.

In treating superficial tumors, the tumor bearing region is immersed in a temperature controlled waterbath. Uniformity in tumor temperature can only be approximated in thin surface lesions due to the rapid fall off of temperature with distance from the surface of the skin.

1.4.5 Infrared radiation

Using infrared light as the energy source for inducing hyperthermia has been of some interest for the past several years (Svaasand et al 1985, Svaasand 1989,

Dowden et al 1987, Davies et al 1988). Energy can be delivered to any tissue accessible to an optical fiber.

Bown (1983) was the first to use an Nd:YAG laser as the energy source which emits at a near-infrared wavelength of 1064 nm. It has subsequently become the laser of choice in laser-induced hyperthermia research because of the desirable optical penetration of 3-8 mm (Svaasand et al 1985).

The first computer-controlled contact hyperthermia system designed by Daikuzono (1988) uses a single interstitial probe coupled to an Nd:YAG laser operating at a range of powers. The system provides a means of controlling the temperature, via thermocouples, at strategic points within and around the tumor.

Extending Daikuzono's idea to include multiple sources, Wyman et al (1991) at the Hamilton Regional Cancer Center has developed a multi-source, multi-sensor, computer-controlled hyperthermia system. Implanted thermocouples provide temperature feedback which controls the optical power input to the fibers. This provides for a more localized uniform tissue temperature elevation in the target volume.

The advantage of interstitial laser hyperthermia is its potential to confine the therapeutic temperature elevation as defined by the spatial distribution of fibers. The main disadvantage is its invasive nature.

1.5 Hyperthermia modelling

1.5.1 Principles

Thermal modelling of hyperthermia is generally divided into parametric investigations of the potential of hyperthermia (Hayes et al 1985, Eberhart et al 1980, Waterman et al 1989) and comparative investigations of the hyperthermia systems (Engler et al 1989, Stauffer et al 1989).

Present models utilize simplifications of the complex physiological processes governing heat transport in tissue. The mechanisms involved are heat transport by conduction and heat transport by blood flow (convection) in the capillary system (perfusion) and in larger blood vessels.

In modelling hyperthermia, analytical methods have been applied (Bowman 1985, Samulski et al 1989), but numerical methods are better utilized where

irregular boundaries and inhomogeneous tissue properties are found (Strohbehn et al 1984, Lagendijk et al 1984).

One of the major problems in clinical hyperthermia is the determination of the complete temperature field throughout both tumor and normal tissue (Strohbehn et al 1984). In clinical trials temperatures are measured at a few locations in the tissue. Since the temperature in the majority of the tissue is unknown, it is difficult to assess the efficacy of the treatment protocol. It is desirable to be able to predict the thermal field before treatment so that the protocol can be optimized. Computer simulations have been used in an attempt to achieve this goal.

1.5.2 Thermal dosimetry

The computer models can be utilized in four aspects of thermal dosimetry. First, in comparative thermal dosimetry, models are used to investigate the ability of different heating modalities and source configurations to uniformily heat the tumor (Stauffer et al 1989). In prospective thermal dosimetry, patient-specific temperature distributions are

calculated using detailed information on patient anatomy, power deposition patterns and perfusion values. Concurrent thermal dosimetry, involves calculating complete temperature fields during treatment and adjusting power deposition patterns to optimize the treatment (Doss et al 1985). Finally, retrospective thermal dosimetry, is a post-treatment evaluation of the completed therapy by calculating the complete temperature field attained from the measured temperatures (Divrik et al 1984).

1.5.3 Limitations

There are three major problems limiting the progress of computer simulations in hyperthermia. Better methods are needed to predict perfusion values before a treatment. There is a lack of adequate data on the spatial and temporal variation of blood flow in capillaries and larger blood vessels (Jain 1983, Samulski et al 1989). Present numerical algorithms are limited to one and two-dimensional models due to computer limitations. Accurate modelling of many local hyperthermia applications requires three-dimensional

models (Strohbehn et al 1984).

1.6 Thermal modelling of large blood vessels

1.6.1 Literature review

It is generally agreed that blood flow is the main parameter which determines temperature distributions in heated tissue (Lagendijk et al 1984). When modelling hyperthermia, heat transport via convection from capillaries and larger vessels has been evaluated as a single heat loss function (Jain et al 1979, Samulski et al 1989). Chen and Holmes (1980) have reported that vessels with radii larger than precapillary arterioles ($\cong$ 0.001 cm) are "thermally significant" and should be evaluated separately. In the literature, computer modelling of the effect of large blood vessels in or around the treatment field during hyperthermia is limited.

Lagendijk (1982) modelled a block of tissue held at constant temperature traversed by a "thermally significant" blood vessel. He reported inhomogeneities in the temperature distributions caused by the presence of the blood vessel. In 1984, Lagendijk developed a

three-dimensional model, based on explicit finite differencing techniques, which investigated this effect around several blood vessels. He reported good correlation between model and steady-state experimental temperatures (within 0.3 °C when temperatures were in the clinical range).

Glazebrook et al (1985) carried out gel phantom studies using an external RF generator and a lucite transit tube as the vessel. He observed a trough in the temperature profile around the transit tube. His results agree qualitatively with Lagendijk's (1981) theoretical predictions.

1.7 Scope of this project

The scope of this project is to develop a three-dimensional computer model which can predict temperature distributions in and around a "thermally significant" blood vessel during interstitial laser-induced (single fiber) hyperthermia. The validity of the model will be evaluated by comparing model temperatures to experimental temperature measurements obtained from a series of dynamic phantom studies.

This study is one area of a larger research project being conducted at the Hamilton Regional Cancer Centre. The goal of the research is to develop a fully automated multi-fiber system, accessible to surface and deep-seated tumors, which can induce therapeutic temperature elevations localized to the tumor volume. A 20 Watt continuous-wave Nd:YAG laser is the energy source and power deposition is controlled by temperature and/or image feedback. The computer model developed in this project will be used to investigate the changes in thermal profiles due to variations in the source/fiber spacing, estimated blood flow rate, the proximity of a large blood vessel and treatment time.

CHAPTER 2

THEORY OF OPTICAL PROPAGATION, PHOTOTHERMAL INTERACTION AND HEAT TRANSFER IN TISSUE

2.1 Introduction

Laser-induced hyperthermia involves three physical processes: light propagation in tissue, the conversion of light energy into heat and the transport of the heat in the tissue.

2.2 Optical propagation in tissue

2.2.1 Optical penetration

The penetration of light in tissue is determined by two mechanisms: scattering of light and absorption of light. The scattering is determined by the differences in refractive indices between cell components and between cells and the surrounding media. The absorption of light in the visible and near-infrared wavelengths is determined by the presence and abundance of chromophores such as melanin and hemoglobin (Svaasand et al 1985).

From a plane source of light, the fluence rate

eventually decays exponentially with distance. The attenuation coefficient is determined by the scattering and absorption of the incident light. The optical penetration depth, defined as the distance at which the fluence rate is reduced to e^{-1} (0.37) of the initial value, is the reciprocal of the attenuation coefficient. Values of the optical penetration depth at different wavelengths, for various tissues, are found in table 2.1.

Heavily pigmented tissues such as liver or highly scattering tissues such as adult brain will, by definition, have low optical penetration depths. Non-pigmented tissues with low scattering such as neonatal brain will have longer optical penetration depths (Svaasand et al 1985). From table 2.1, one observes that the optical penetration depth increases with increasing wavelength up to 1064 nm. The Nd:YAG laser, emitting at 1064 nm, is currently the laser of choice in hyperthermia applications with an optical penetration depth in the 3-8 mm range (Svaasand et al 1985).

Tissue	Optical penetration depth (mm)		
	488/515 nm	660 nm	1064 nm
Brain (white matter)	0.4-0.6	1.2-1.6	3.2-4.3
Neonatal brain	1.1-1.7	3.7-5.4	7.1-8.8
Brain metastasis	0.6	1.3	2.8
Fair Caucasian skin	0.2	——	1.6

Table 2.1 Optical penetration depths in various human tissues (Svaasand 1989).

2.2.2 The Boltzmann equation

The distribution of light photons emitted from an optical fiber can be described using the linearized Boltzmann Transport Equation. This equation as applied to neutron transport can be derived by balancing the various mechanisms by which neutrons are gained or lost from an arbitrary volume in the system (Duderstadt and Hamilton 1976). The neutron transport equation is given by

$$\frac{\partial n}{\partial t} + v\Omega\cdot\nabla n(r,E,\Omega,t) + v\Sigma t n(r,E,\Omega,t) = \int_{4\pi} d\Omega' \int_{o}^{\infty} dE' \; \Sigma s(E'\rightarrow E,\Omega'\rightarrow\Omega) v n(r,E',\Omega',t) + S(r,E,\Omega,t) \qquad (2.1)$$

The first term on the left hand side of the equation represents the time rate of change of neutrons from an arbitrary volume. The second term represents the net leakage of neutrons into or out from an arbitrary volume. The third term represents the loss of neutrons of the energy of interest, E, travelling in the direction of interest, Ω, due to an absorption interaction or a scattering collision. The first term on the right hand side of the equation represents the number of neutrons of other energies, E', and

directions, Ω', which are scattered into the direction of interest, Ω, with the energy of interest, E. The last term represents the rate of source neutrons that appear travelling in the direction of interest, Ω, with the energy of interest, E.

When applying this equation to the transport of photons a number of simplifications can be made. In photon transport (i) photons can be characterized by a single speed or energy (monoenergetic), (ii) the scattering of light can be considered elastic (no energy loss) and (iii) since we are dealing with continuous-wave laser beams the time variation of n can be eliminated. Therefore equation 2.1 can be written as the one speed transport equation

$$\Omega\cdot\nabla\phi(r,\Omega) + \Sigma_t\phi(r,\Omega) = \int_{4\pi} d\Omega' \; \Sigma_s(r,\Omega'\rightarrow\Omega)\phi(r,\Omega') + S(r,\Omega) \tag{2.2}$$

where $\phi(r,\Omega) = vn(r,\Omega) \equiv$ the number of photons at r moving in the direction of Ω.

In the above description of photon transport $\Sigma_s(r,\Omega'\rightarrow\Omega)$ is the differential scattering cross section, defined as the probability per infinitesimal pathlength that a photon at r moving in the direction Ω' will be

elastically scattered to a new direction Ω. The total scattering coefficient $\Sigma_s(r)$ is obtained by integrating the differential cross section over all final angles

$$\Sigma_s(r) = \int_{4\pi} \Sigma_s(r,\Omega' \rightarrow \Omega) d\Omega \qquad (2.3)$$

The total attenuation of photons in a medium is described by the total attenuation coefficient

$$\Sigma_t(r) = \Sigma_a(r) + \Sigma_s(r) \qquad (2.4)$$

where $\Sigma_a(r)$ is the absorption coefficient defined as the probability per infinitesimal pathlength that a photon at r will be absorbed. Finally, $S(r,\Omega)$ represents the number of source photons at r moving in the direction of interest Ω.

2.2.3 Diffusion theory

Approximate solutions to this transport equation can be obtained for simple geometries using diffusion theory (Duderstadt and Hamilton 1976). Diffusion theory is the simplest approximation to the Boltzmann Equation and is easily applied in three dimensional geometry.

For the case of an isotropic point source in an infinite homogeneous medium, there is no dependence of the photon flux on angle. Therefore, according to

diffusion theory, the photon flux is (Duderstadt and Hamilton 1976),

$$\phi(r) = \frac{Pe^{-r/L}}{4\pi Dr} \qquad (2.5)$$

where P ≡ the source power (W).

$= \phi_o \cdot h\upsilon$

D ≡ the photon diffusion coefficient.

and L ≡ the photon diffusion length.

$= \sqrt{D/\Sigma a}$

Photons coming directly from the source contribute $\frac{e^{-\Sigma t r}}{4\pi r^2}$ to the flux and this in itself is, at small r, greater than the flux given by diffusion theory (Weinberg and Wigner 1958). Therefore, diffusion theory underestimates the flux near r = 0. Since all the photons emitted by the source are absorbed somewhere, the integral $\int \Sigma a \phi \, dr$ over all space must be equal to the total power P. Thus since diffusion theory underestimates $\phi(r)$ near r = 0, it must also overestimate $\phi(r)$ at some r > 0.

2.2.4 Transport theory

Other solutions to the transport equation have been discussed by Weinberg and Wigner (1958), Dowden and

Davies (1988) and Arnfield (1988). Arnfield used an approximation to the rigorous transport theory solution for an isotropic point source with isotropic scattering in an infinite homogeneous medium as given by Weinberg and Wigner (1958)

$$\phi(r) = \frac{P\beta e^{-\varkappa r}}{4\pi D r} + \frac{P e^{-\Sigma' r}}{4\pi r^2} \qquad (2.6)$$

where $P \equiv$ the source power (W).

$= \phi_o \cdot h\upsilon$

$\beta \equiv$ a factor which reduces the diffusion theory value for the flux at large r.

$$= \frac{2\Sigma a}{\Sigma s}\left[\frac{(\Sigma t^2 - \varkappa^2)}{(\varkappa^2 - \Sigma t \Sigma a)}\right] \qquad (2.7)$$

$\varkappa \equiv$ the attenuation coefficient.

$$= \sqrt{3\Sigma t \Sigma a}\ (1 - 2\Sigma a/5\Sigma t) \qquad (2.8)$$

$D \equiv$ the diffusion coefficient.

$$= \Sigma a/\varkappa^2 \qquad (2.9)$$

and $\Sigma' = 5\Sigma t/4 \qquad (2.10)$

The first term in equation 2.6 represents the asymptotic part of the optical distribution far from the source and the second term represents the transient part close to the source.

2.2.5 Anisotropic scattering

In order to account for anisotropic scattering in tissue, the Boltzmann equation must be reduced using an anisotropic phase function in place of isotropic scattering. The result of this lengthy derivation is given by Arnfield (1988). The equation for photon flux is of the same form as equation 2.6. The scattering coefficient is replaced by a reduced scattering coefficient

$$\Sigma_s' = (1-g)\,\Sigma_s \tag{2.11}$$

where g is the mean cosine of the angle of scatter. The parameters therefore become

$$\beta = \frac{2\Sigma_a}{(1-g)\Sigma_s}\left[\frac{(\Sigma_t'^2 - \varkappa^2)}{(\varkappa^2 - \Sigma_t'\Sigma_a)}\right] \tag{2.12}$$

$$\varkappa = \sqrt{3\Sigma_t'\Sigma_a}\,(1 - 2\Sigma_a/5\Sigma_t') \tag{2.13}$$

$$\Sigma' = \frac{5\Sigma_t'}{4} \tag{2.14}$$

where $\Sigma_t' = (1-g)\Sigma_s + \Sigma_a$ (2.15)

Equation 2.6 is a good approximation of photon flux for both small and large r (Weinberg and Wigner 1958); therefore it will be used to determine the optical distributions in this project.

2.3 Mechanisms of laser-tissue interactions

The response of biological tissues to non-ionizing electromagnetic radiation reflect four possible modes of interaction -- electromechanical, photoablative, thermal and photochemical. The type of interaction is dependent on the tissue and laser characteristics for the specific application.

In hyperthermia applications, one is concerned with the conversion of electromagnetic energy into thermal energy. It is a two step process generally given by

$$\text{Absorption} \qquad A + h\upsilon \Rightarrow A^{*} \qquad (2.16)$$

$$\text{De-excitation} \qquad A^{*} + M(E) \Rightarrow A + M'(E + \Delta E) \qquad (2.17)$$

The target molecule A absorbs a photon of energy $h\upsilon$ and is promoted to an excited state. The excited molecule then undergoes inelastic scattering with a nearby molecule M with kinetic energy E. As a result of the collision, molecule M carries away the internal energy released by A^{*}. The kinetic energy of the molecules at $37^{\circ}C$ is $\cong$ 0.027 eV while the energy of a 1064 nm photon is 1.17 eV. The microscopic temperature increase is

proportional to the amount of energy released to M'. These processes are highly efficient in tissue because of the large numbers of accessible vibrational states in biomolecules (10^3 to 10^5) and the high probability of de-excitation due to large collision cross-sections (10^{-18} to 10^{-17} cm^2) (Boulnois 1986).

Effectively, as photons are absorbed by the tissue, the electromagnetic energy is converted into thermal energy creating a number of heat sources. The transfer of the heat from these sources is described next.

2.4 Heat transfer in tissue

2.4.1 Thermal properties

There are three different mechanisms which dictate thermal distributions in tissue: heat transfer via thermal conduction, heat storage and heat transfer through the vascular network (convection).

The first mechanism is described by the coefficient of thermal conductivity k. For most tissues it is described by a single scalar value in the range $3.0 - 5.0 \times 10^{-3}$ W/(cm K) (Svaasand 1989). The thermal

conductivity of water at 37°C is 6.23 X 10^{-3} W/(cm K) (Handbook of Chemistry and Physics 1986). In general, tissues with a high water content such as muscle, kidney, liver and brain, have higher thermal conductivities than those with low water content, such as fat (Bowman et al 1974).

The ability to store heat is described by the specific heat constant c. This quantity is defined as the amount of heat stored per unit temperature increase per unit mass of tissue. The specific heat constant for pure water at 37°C is 4.18 J/g/K (Handbook of Chemistry and Physics 1986) and that for tissue with 70% water content is 3.34 J/g/K (Jacques and Prahl 1987).

A parameter commonly used to describe the thermal response of a material is the thermal diffusivity, X, which is the ratio of the thermal conductivity to the specific heat per unit volume

$$X = \frac{k}{\rho c} \qquad (2.18)$$

where ρ, the tissue density, is typically 1.09 g/cm^3 for tissue with a 70% water content (Jacques and Prahl 1987). The thermal diffusivity for most tissues is approximately 1.2 X 10^{-3} cm^2/s (Welch 1984) and that for

water at 37°C is 1.5 X 10^{-3} cm^2/s (Handbook of Chemistry and Physics 1986)

The thermal diffusivity can be used to determine the thermal diffusion length, L, in tissue

$$L = \sqrt{4Xt} \qquad (2.19)$$

where t is the exposure time. This parameter can be used to approximate the size of the resulting thermal field.

The ability of the tissue to transfer heat via the vascular network is governed by the rate of blood flow, described by an average volumetric perfusion rate in capillary beds and a mean velocity in large blood vessels, and by the heat transfer between the blood and the surrounding tissue. This process will be discussed, in detail, in the next section.

2.4.2 Derivation of bioheat transfer equation

The processes by which tissue accommodates energy inputs in the form of heat are governed by the laws of thermodynamics. The equation describing the individual heat transfer mechanisms in tissue was first derived by Pennes (1948) and is known as the Bioheat Transfer Equation (BHTE). It can be derived by

considering a representative control volume of tissue which is in continuous communication with surrounding tissue through heat transfer and blood flow across the control surface (figure 2.1).

This energy balance equation is expressed as

RATE OF ENERGY STORAGE = RATE OF HEAT TRANSFER BY CONDUCTION + RATE OF HEAT TRANSFER BY BLOOD FLOW

+ RATE OF METABOLIC HEAT GENERATION + RATE OF ENERGY ABSORBED FROM SOURCE (2.20)

The integral expression for these mechanisms is (Bowman 1982)

$$\frac{\partial}{\partial t}\int_V \rho c T \, dV = \int_A k_{ij}\left(\frac{\partial T}{\partial x_j}\right) n_i \, dA +$$

$$+ \int_A c_b T_b f_i n_i \, dA + \int_V Q_M \, dV + \int_V Q_L \, dV \qquad (2.21)$$

where ρ ,c and k_{ij} are the density, specific heat and thermal conductivity of tissue respectively; T is the local tissue temperature; n_i is the normal vector; c_b and T_b are the specific heat and temperature of the blood respectively; f_i is the blood perfusion rate

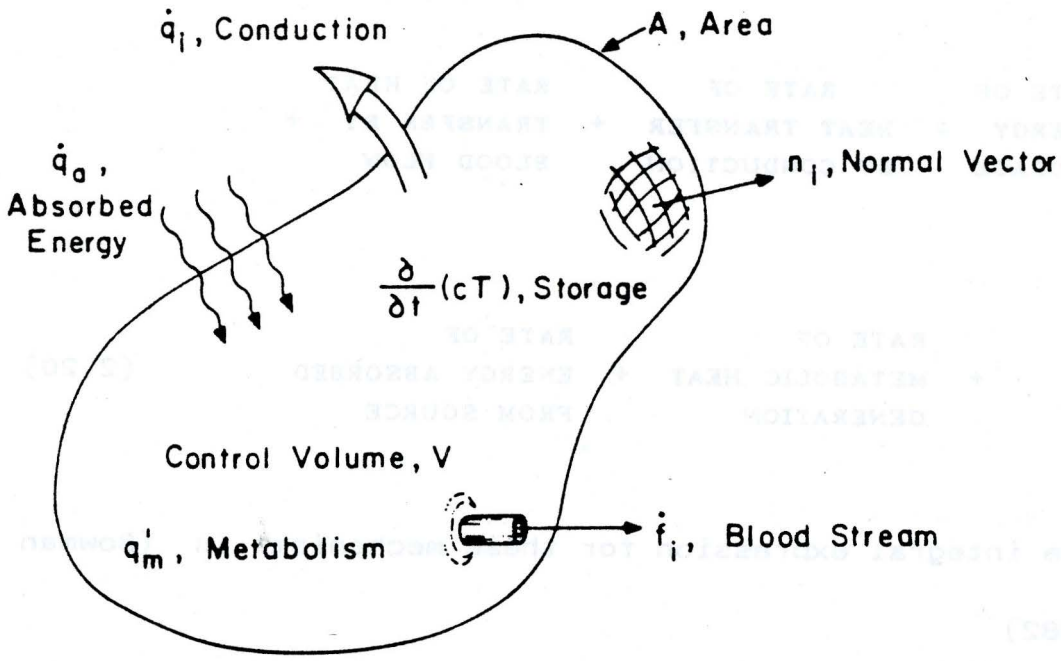

Figure 2.1 Control surface for derivation of BHTE

(Reprint from Bowman 1982).

vector; Q_M is the metabolic heating rate; and Q_L is the energy absorption rate from a power source.

The left side of the equation represents the rate of change of stored thermal energy in the control volume. On the right side of the equation, the first term, the total heat conduction, is arrived at by integrating the conduction heat flux vector $q_i = k_{ij} \frac{\partial T}{\partial x_j}$ over the control surface. The thermal conductivity, k_{ij}, is expressed as a second order tensor which is dependent on position and temperature. The second term represents the net thermal energy transported by the blood vessels across the control surface (convection). The third term represents the total heat generated from metabolic processes in the tissue. The last term represents the total energy absorbed in the control volume from a power source.

It is impossible to model the detailed structure of the microvasculature (i.e. arterioles and capillaries). In tumors the direction and magnitude of blood flow vary with time. This complex problem of solving the convection term in equation 2.21 has thus far proved mathematically intractable (Jain 1983).

Therefore it is assumed that the blood flow within the tissue is nondirectional at the capillary level. The arterial blood arrives at a particular location with a temperature, T_a, equal to the body temperature. It quickly equilibrates with the surrounding temperature, T, as it is slowly transported through the capillary system. Then the thermal energy which has been stored in the blood is carried away as the venous blood leaves the location. This process is described by

$$Q_B = w_b c_b (\gamma - 1)(T - T_a) \qquad (2.22)$$

where Q_B is the rate of heat transfered by capillary blood flow (perfusion), w_b is the average volumetric perfusion rate which is the amount of blood which perfuses through a unit volume of tissue per unit time, c_b is the specific heat of blood, γ is an equilibrium constant that serves as a measure of the effectiveness of the heat transfer between the tissue and the venous blood ($0 < \gamma < 1$); T is the local tissue temperature, and T_a is the arterial blood temperature. It is reasonable to assume that because of slow blood flow in the capillary bed (Guyton 1981), γ will be close to zero and therefore the venous blood is in equilibrium with

tissue (Jain 1982).

Using Gauss' Law and rewriting equation 2.21 in differential form, the BHTE reduces to its general form

$$\rho c \frac{\partial T}{\partial t} = k\nabla^2 T + Q_M + Q_B + Q_L \qquad (2.23)$$

where $Q_B = \omega_b c_b (T_a - T)$ (2.24)

and k_{ij} is replaced by k because the thermal conductivity can be adequately expressed as a scalar (Svaasand 1989). This equation will be used to describe the transfer of heat in tissue.

Equation 2.23 neglects two physical processes: (i) heat conduction within the blood due to the temperature distribution in the blood and (ii) countercurrent heat transfer that occurs between the arterial and venous blood flows which are in close proximity to each other. By this latter process, arterial blood gives up much of its stored energy to the venous blood entering the region rather than to the local environment. Therefore the heat given up to the local region is reduced. The effects of countercurrent heat transfer may be important in the larger vessels (Cravalho 1980, Lagendijk et al 1990).

The limitations of the BHTE have been under

close scrutiny for many years with the major concern being the convection term (equation 2.24). Wulff (1974) criticized the scalar treatment of the convective heat transport by blood. He further argued that the perfusion term, obtained from the global energy balance for the blood in the entire domain, cannot be applied to the local energy balance for an infinitesimal control volume. He therefore introduced a blood velocity vector ub into the BHTE. Any attempt to specify the vector at the microscopic level is marred by the complex nature of the system.

It has been reported that this scalar treatment of the convection term gives a reasonable estimate of the average convective contribution to the heat transfer mechanism through blood perfused tissues (Svaasand 1989).

Due to the lack of detailed knowledge of vascular architecture, as well as the mathematical complexity of describing the vasculature system, the model described by Pennes is most often used in the modelling of hyperthermia treatments (Eberhart et al 1980, Divrik 1984, Waterman et al 1989) and will

therefore be used to describe heat transfer in this project.

2.4.3 Heat removal by a single blood vessel

2.4.3.1 BHTE at vessel blood boundary

The presence of a discrete blood vessel can be described by applying a boundary condition to the BHTE for tissue (equation 2.23) at the surface of the vessel. This boundary condition which describes the heat flux (W/cm^2) through the vessel wall into the blood is given by (Carslaw and Jaegar 1959)

$$k_{bc}\frac{\partial T}{\partial r} = h_s(T_v - T_b) \quad \text{at } r = R_v \qquad (2.25)$$

where k_{bc} is the thermal conductivity of the boundary (vessel wall), h_s is the heat transfer coefficient, R_v is the vessel radius and T_v and T_b are the temperatures of the vessel wall and the blood, respectively. This equation states that the heat flow through the vessel wall is equal to the heat loss to the blood.

The heat flow across the two interfaces, tissue/vessel/blood, can be described by an effective thermal conductivity.

The actual blood vessel is thin-walled with two

boundaries: the tissue/vessel boundary and the blood/vessel boundary. An expression for an effective thermal conductivity at a single vessel boundary defined by r = Rv can be derived (Reece 1986).

At tissue/vessel boundary: $k_{tv} = \frac{(2k_t k_v)}{(k_t + k_v)}$ (2.26)

At blood/vessel boundary: $k_{bv} = \frac{(2k_b k_v)}{(k_b + k_v)}$ (2.27)

At a single vessel boundary:

$$k_{bc} = \frac{(2k_{tv}k_{bv})}{(k_{tv} + k_{bv})} = \frac{(4k_t k_v k_b)}{k_b(k_v + k_t) + k_t(k_b + k_v)} \quad (2.28)$$

where k_t, k_v and k_b are the thermal conductivities of tissue, vessel and blood, respectively.

2.4.3.2 Heat transfer coefficient

The convective heat transfer coefficient, h_s, can be expressed in terms of the thermal conductivity of the fluid k, the diameter of the channel d and a dimensionless parameter Nu (Duderstadt and Hamilton 1976)

$$h_s = \frac{k}{d} Nu \quad (2.29)$$

where Nu, known as the Nusselt number, describes the physical properties of the fluid and the characteristics of its flow.

Assuming that the blood flow is laminar, that

there is no conduction in the direction of flow and that a parabolic velocity profile is established and maintained, the Nusselt number has been shown experimentally to be a series function of the dimensionless "Graetz-group", $\frac{\rho c \langle v \rangle d^2}{kL}$, where L is the length of the channel (Drew et al 1936a,b). Lagendijk (1982) uses this series solution to determine the heat transfer coefficient for laminar flow

$$h_s = \frac{1.08 k_b}{2R_v} \left(\frac{\rho_b c_b \langle v \rangle 4R_v^2}{k_b L_v} \right)^{1/3} \qquad (2.30)$$

where ρ_b, c_b and k_b are the density, specific heat and thermal conductivity of the blood, respectively and L_v is the length of the blood vessel.

Laminar blood flow was assessed using the Reynolds number, a dimensionless quantity which characterizes the fluid flow

$$Re = \frac{\rho \langle v \rangle d}{\mu} \qquad (2.31)$$

where $\langle v \rangle$ is the average fluid velocity and μ is the fluid viscosity. A Reynolds number less than 2100 is characteristic of laminar flow (Duderstadt and Hamilton 1976).

2.4.3.3 BHTE in blood

By considering an elemental length of blood vessel ∂z surrounded by tissue, the heat absorbed in the blood over the length ∂z at a point z is (Lagendijk 1982)

$$q_{abs}(z) = \pi R_v^2 \langle v \rangle c_b \rho_b \{T_b(z+\partial z) - T_b(z)\} \quad (2.32)$$

where R_v is the vessel radius, $\langle v \rangle$ is the average blood velocity, and c_b and ρ_b are the specific heat and density of blood, respectively. This equation is used to describe the heat flow in the vessel due to the mass flow of blood.

An expression for the energy balance in the blood of the vessel can be derived in the same manner as the BHTE for tissue (equation 2.21)

$$\frac{\partial}{\partial t} \int_V \rho c T_b \, dV = \int_A k_{ij} \left(\frac{\partial T_b}{\partial x_j}\right) n_i \, dA + \int_V Q_M \, dV -$$

$$\int_V \frac{\pi R_v^2 \langle v \rangle c_b \rho_b \{T_b(z+\partial z) - T_b(z)\}}{\pi R_v^2 \partial z} \, dV + \int_V Q_L \, dV \quad (2.33)$$

Simplifying this equation yields

$$\rho_b c_b \frac{\partial T_b}{\partial t} = k_b \nabla^2 T_b + Q_M + Q_B + Q_L \quad (2.34)$$

where $Q_B = - \langle v \rangle c_b \rho_b \frac{\partial T_b}{\partial z}$

Given the boundary condition (equation 2.25) at the

vessel wall, it is assumed that the blood is thoroughly mixed to a uniform temperature at each cross-section of vessel. Therefore the calculated blood temperature distribution is averaged at each cross-section.

2.5 Mathematical model

2.5.1 Finite differencing

Finite differencing has been used to model heat transfer in a number of applications (Dowden and Davies 1989, Doss et al 1985, Hayes et al 1985).

Finite differencing is a numerical method in which derivatives at any given point are approximated with finite difference expressions. Therefore the solution of differential equations is reduced to the solution of a set of algebraic equations. Accuracy in such an approximation is controlled by choosing the appropriate interval sizes between grid points.

Error is introduced at each step of calculation due to approximations involved in finite differencing and numerical calculations. There is a cumulative effect of such errors on the final solution. The use of a fine grid, although desirable for better approximation of the

differential equation, increases the cumulative effect of round-off errors and computer time (Gordon 1965).

2.5.2 Model geometry

The model geometry is shown in figure 2.2. A thin walled blood vessel of radius Rv and length Lv traverses the interior of a cylinder of tissue defined by λ and Lv. A line source of light of length L_s is situated at a distance, Dt (cm) from the vessel axis (also the z-axis). The axial position of the line source is given by Z_1 and Z_2.

Three-dimensional cylindrical coordinates are used in the model. Therefore the temperature at each grid point is denoted by

$$T(r,\theta,z,t) = T(i\Delta r, j\Delta\theta, k\Delta z, s\Delta t)$$
$$= T^{s}_{i,j,k} \qquad (2.35)$$

where i,j,k and s are integer values; $\Delta r, \Delta\theta$, and Δz are spatial and angular increments and Δt is a temporal increment.

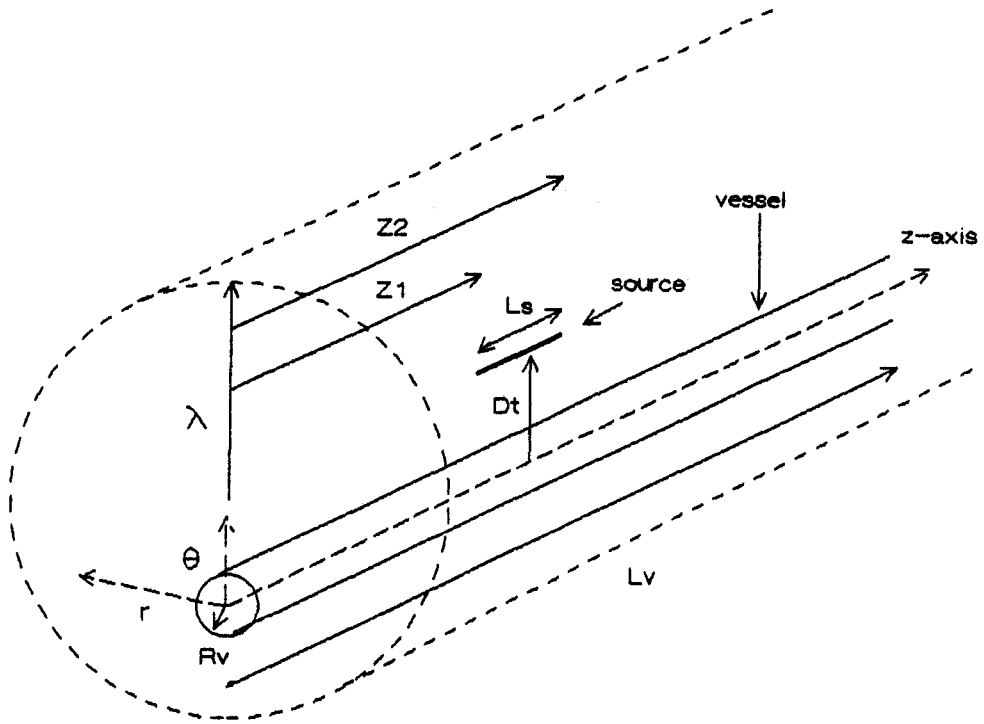

Figure 2.2 Model geometry.

2.5.3 Finite difference equations for BHTE

In cylindrical coordinates, the general form of the BHTE (equation 2.23) becomes

$$\rho c\frac{\partial T}{\partial t} = k\left(\frac{\partial^2 T}{\partial r^2} + \frac{1}{r}\frac{\partial T}{\partial r} + \frac{1}{r^2}\frac{\partial^2 T}{\partial \theta^2} + \frac{\partial^2 T}{\partial z^2}\right) + Q_B + Q_M + Q_L \quad (2.36)$$

where $T = Tt$ and $Q_B = wbcb(Ta - Tt)$ in the tissue;

$T = Tv$, $Q_B = 0$ and $Q_L = 0$ in the vessel; and

$T = Tb$, $Q_B = -\langle v\rangle cb\rho b\frac{\partial Tb}{\partial z}$ in the blood. The heat transfer coefficient assumes no conduction in the direction of blood flow, therefore $kb\frac{\partial^2 Tb}{\partial z^2} = 0$ for flowing blood. The initial and boundary conditions are

$T = 37^{\circ}C$ at $t = 0$

$T = 37^{\circ}C$ at $r = \lambda$, $z = 0$ and $z = Lv$

$kbc\frac{\partial Tv}{\partial r} = hs(Tv - Tb)$ at $r = Rv$

where Tt, Tv and Tb are the tissue, vessel and blood temperatures, respectively.

The differentials in equation 2.36 are written as implicit finite difference expressions. The radial and angular expressions are nonuniformily differenced so that a vessel of any diameter can be modelled and accurate modelling (fine grid) around the light source can be achieved.

$$\frac{\partial T}{\partial t} = \left[\frac{T^{s+1}_{i,j,k} - T^{s}_{i,j,k}}{\Delta t}\right] \tag{2.37}$$

$$\frac{\partial T}{\partial r} = \left[\frac{\Delta r_2^2\, T^{s+1}_{i+1,j,k} - \left(\Delta r_2^2 - \Delta r_1^2\right) T^{s+1}_{i,j,k} - \Delta r_1^2\, T^{s+1}_{i-1,j,k}}{\Delta r_1 \Delta r_2 (\Delta r_1 + \Delta r_2)}\right] \tag{2.38}$$

$$\frac{\partial^2 T}{\partial r^2} = \left[\frac{2\Delta r_2 T^{s+1}_{i+1,j,k} - 2\left(\Delta r_1 + \Delta r_2\right) T^{s+1}_{i,j,k} + 2\Delta r_1 T^{s+1}_{i-1,j,k}}{\Delta r_1 \Delta r_2 (\Delta r_1 + \Delta r_2)}\right] \tag{2.39}$$

$$\frac{\partial^2 T}{\partial \theta^2} = \left[\frac{2\Delta\theta_2 T^{s+1}_{i,j+1,k} - 2\left(\Delta\theta_1 + \Delta\theta_2\right) T^{s+1}_{i,j,k} + 2\Delta\theta_1 T^{s+1}_{i,j-1,k}}{\Delta\theta_1 \Delta\theta_2 (\Delta\theta_1 + \Delta\theta_2)}\right] \tag{2.40}$$

$$\frac{\partial^2 T}{\partial z^2} = \left[\frac{T^{s+1}_{i,j,k+1} - 2T^{s+1}_{i,j,k} + T^{s+1}_{i,j,k-1}}{\Delta z^2}\right] \tag{2.41}$$

The temperature at each grid point is solved for the s+1 time interval from the temperature at the s interval as well as from the six surrounding grid point temperatures at the s+1 interval (see figure 2.3). This requires that all grid points at each time interval be set at the initial temperature. The advantage of implicit differencing over its explicit counterpart (i.e. specifying spatially differentiated temperatures

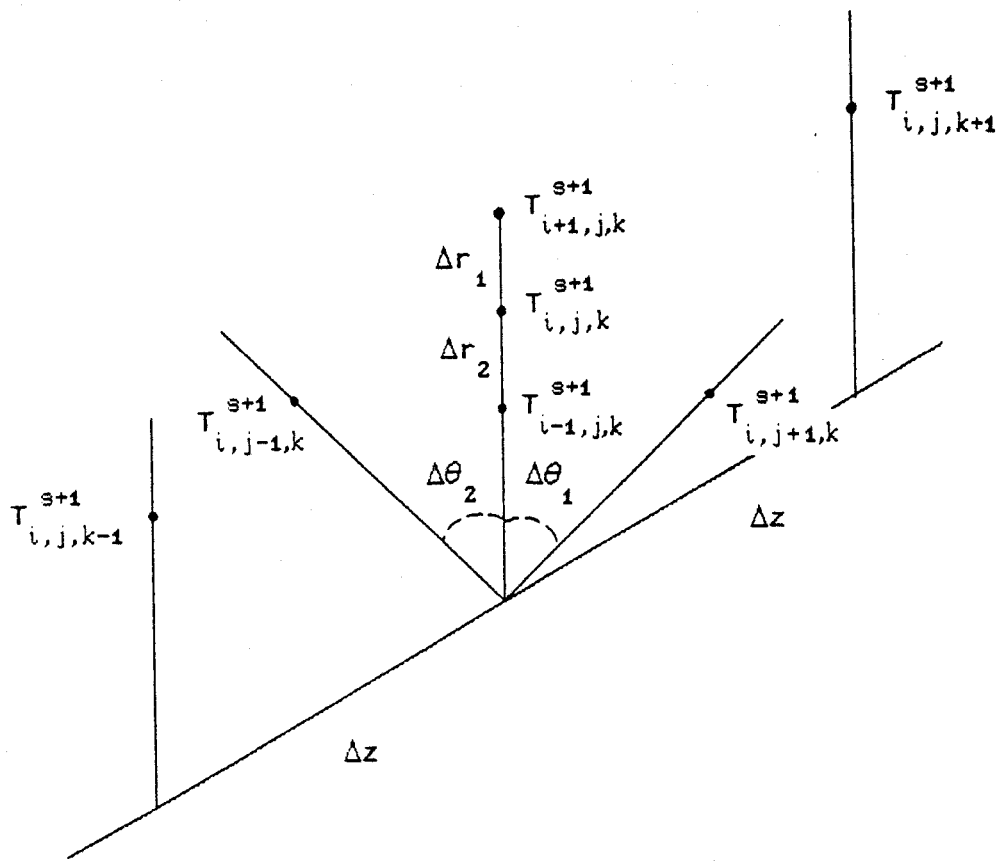

Figure 2.3 Schematic of finite differencing method.

at the s time interval) is that no constraints need to be placed on the values of the radial, angular, axial and temporal increments (Reece 1986). Implicit differencing also eliminates constraints on the range of vessel diameters and flow rates which can be modelled.

The finite difference expressions for the BHTEs for tissue, vessel and blood (flow and no flow) are found in Appendix A. The BHTE's are rearranged and solved for $T_{i,j,k}^{s+1}$

$$T_{i,j,k}^{s+1} =$$

$$\left[\left(B_{i,j}\right) T_{i+1,j,k}^{s+1} + \left(C_{i,j}\right) T_{i-1,j,k}^{s+1} + \left(D_{i,j}\right) T_{i,j+1,k}^{s+1} + \right.$$

$$\left(E_{i,j}\right) T_{i,j-1,k}^{s+1} + \left(F_{i,j}\right) T_{i,j,k+1}^{s+1} + \left(G_{i,j}\right) T_{i,j,k-1}^{s+1} +$$

$$\left(H_{i,j}\right) T_{i,j,k}^{s} + \left(L_{i,j}\right) + \left(M_{i,j}\right) Tb_{k}^{s+1} + \left(QL_{i,j,k} + QM\right) /$$

$$\left. \left(N_{i,j}\right) \right] / \left(A_{i,j}\right) \qquad (2.42)$$

where the model parameters are represented by the coefficients $A_{i,j}$ to $H_{i,j}$, $L_{i,j}$ and $N_{i,j}$. The values of these coefficients depend on the location of the grid point (i.e. blood, vessel or tissue).

2.5.4 Modelling light source

The light source is assumed to have a uniform intensity distribution over its finite length. It is further assumed that the presence of the blood vessel does not perturb the light distribution. These assumptions will be discussed in detail in the next chapter. The light emitted from the source is distributed according to equations 2.6 and 2.11 - 2.15

$$\phi(r) = \frac{P\beta e^{-\varkappa r}}{4\pi D r} + \frac{P e^{-\Sigma' r}}{4\pi r^2} \qquad (2.43)$$

This point source solution is integrated over the line. The integrated form of equation (2.43) becomes

$$\phi(\alpha) = \int_{Z_1}^{Z_2} \left(\frac{S_L \beta e^{-\varkappa \alpha}}{4\pi D \alpha} + \frac{S_L e^{-\Sigma' \alpha}}{4\pi \alpha^2} \right) dz' \qquad (2.44)$$

where Z_1 and Z_2 define the position of the line source along the axial direction, S_L is the source strength (W/cm) and

$$\alpha = \left(r^2 + Dt^2 - 2rDt\cos(\theta) + (z-z')^2 \right)^{1/2} \qquad (2.45)$$

This α substitution facilitates a shift to cylindrical coordinates with the origin on the z-axis. It allows the photon flux $\phi(r,\theta,z)$ to be calculated at defined positions (grid points) in discrete planes along the

z-axis. The absorbed energy at each grid point in a plane is

$$Q_L(r,\theta,z) = \Sigma_a \, \phi(i\Delta r, j\Delta\theta, k\Delta z)$$

$$= Q_{L_{i,j,k}} \qquad (2.46)$$

where Σ_a is the optical absorption coefficient in tissue.

2.5.5 Code execution

Equation (2.42) is solved using an iterative method. During each iteration, temperatures at each grid point are recalculated or "updated". Iterations continue until a point by point convergence criterion is met. The relative change in calculated temperatures between two successive iterations at each grid point is defined as the residual. When the residual is less then or equal to a preset value, the temperature at that grid point is said to have converged. Once all grid point temperatures have converged, the program ends. A simplified flow chart of the computer code is presented in figure 2.4.

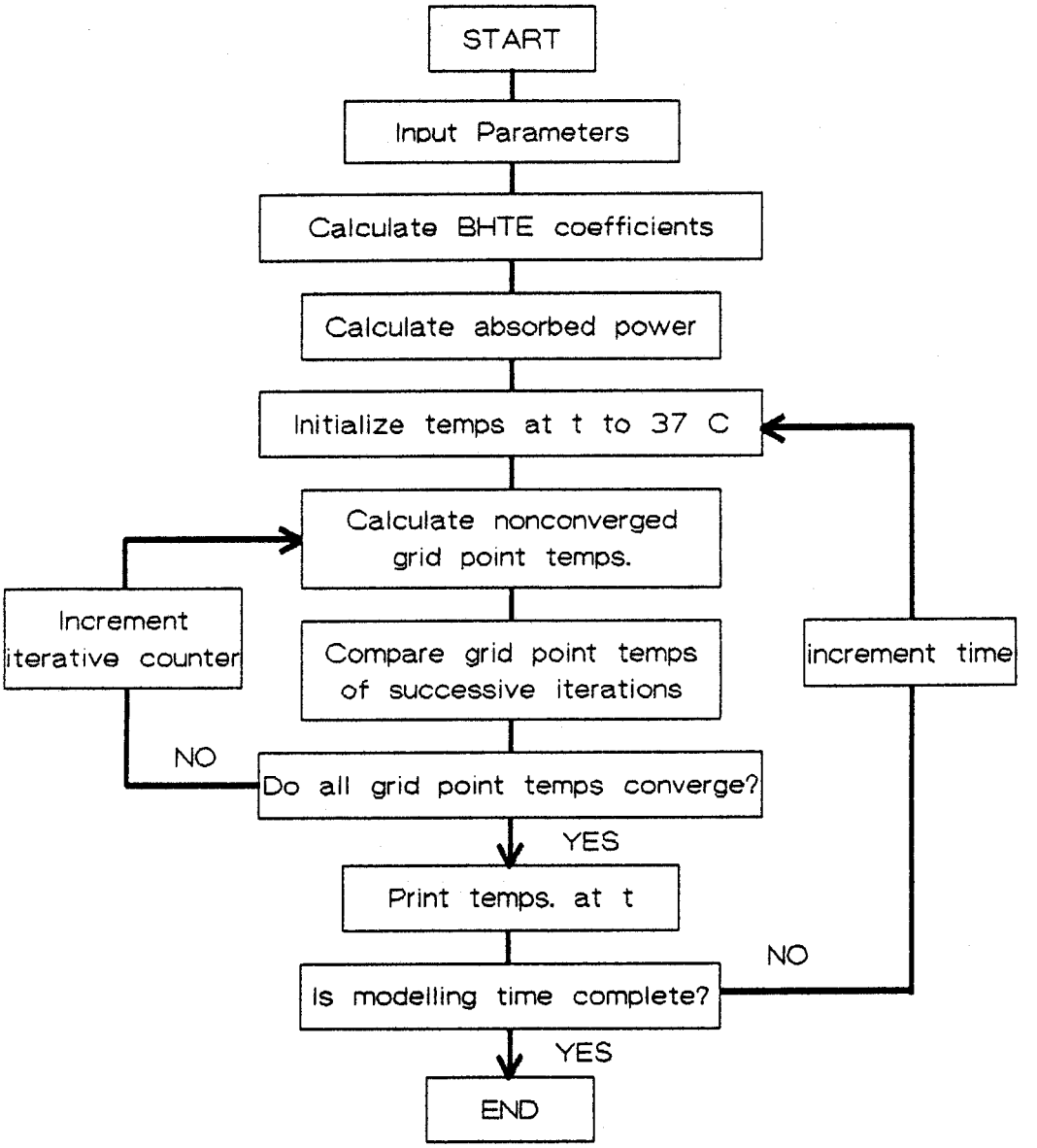

Figure 2.4 Flow chart of computer code.

CHAPTER THREE

MATERIALS AND METHODS

3.1 Apparatus

3.1.1 Light delivery system

The experimental apparatus was set up as in figure 3.1. The energy source was a continuous-wave Nd:YAG laser (Model C95 C.V.I. Laser Corporation, Albuquerque N.M.,U.S.A.) with a maximum power output of 5 W. At the center of this laser system is a 3 mm by 63.5 mm yttrium-aluminum-garnet crystal rod doped with neodymium ions. The crystal sits in a resonator cavity consisting of two mirrors, one highly reflecting and the other partially reflecting. The neodymium ions are excited by absorbing radiation from two 750 W internal tungsten flash lamps in a process known as optical pumping. The excited ions then undergo stimulated emission at three infrared wavelengths, 0.9, 1.06 and 1.35 μm, with 1.06 μm being the most powerful line. Only those ions which emit their energy along the axis of the resonator contribute to the lasing process. The exiting

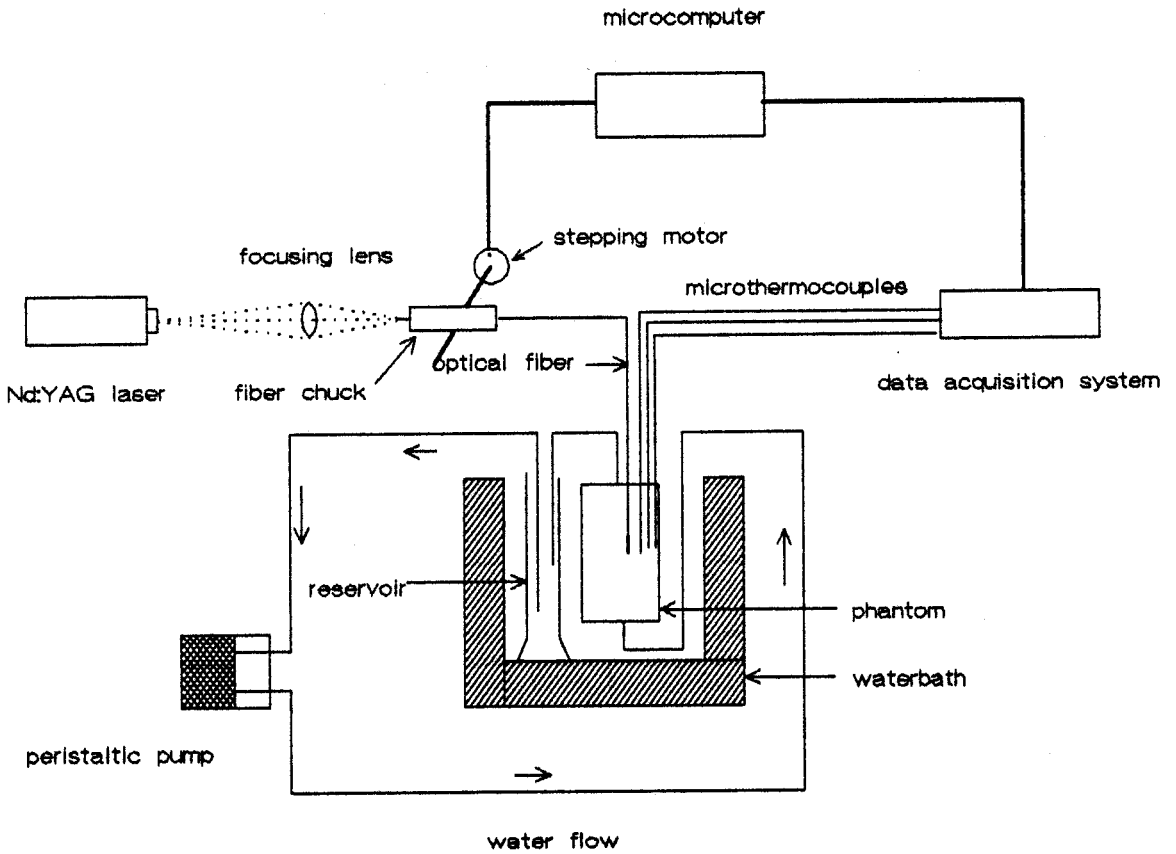

Figure 3.1 Experimental apparatus for measuring temperature elevations in a tissue phantom.

1064 nm multimode laser beam has a diameter of 2.0 mm and a beam divergence of 3.0 mrad.

The beam was directed towards a focusing lens which produced a narrow 200 μm diameter beam at a distance of 19 mm beyond the lens. This beam was coupled to the polished end of a 400 μm core optical fiber (Model 4410 Laser Therapeutics Incorporated, Buellton C.A., U.S.A.) with an internal light transmission of > 85% . The fiber had a 1.5 cm long cylindrical diffusing tip at the output end which provided a finite line source of light.

The fiber was housed in an optical chuck. The chuck was fixed in the center of a lucite block using two tuning screws which were used to manipulate the vertical position of the fiber. The lucite block was fixed to a platform whose horizontal positioning was controlled by a stepping motor (Model M061-FD08, Superior Electric Co., Bristol, CT., U.S.A.) under computer command.

Figure 3.2 shows photographic profiles of the light output from a 2 cm cylindrical tip (Wyman et al 1990). The output is dependent on the angle of incidence

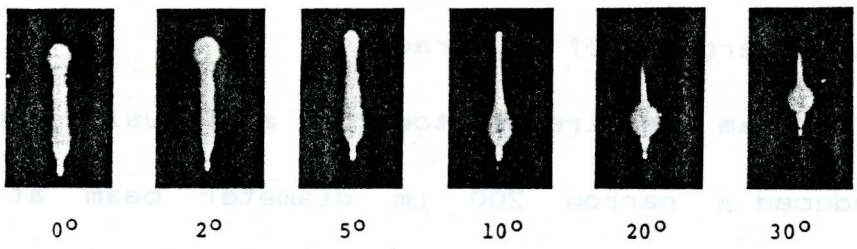

a)

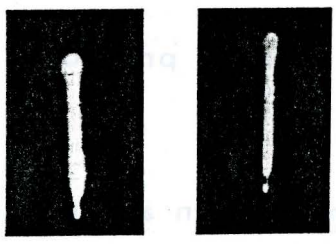

b) c)

Figure 3.2 Photographic profiles of cylindrically tipped optical fibers emitting 632.8 nm supplied by a He-Ne laser. a) well coupled at various angles of incidence, b) normally incident beam well coupled and c) normally incident beam poorly coupled to the fiber.

of the beam onto the fiber and the coupling efficiency. The output was maximized using an angle of incidence equal to zero. This yielded the best approximation of a line source of uniform intensity.

The fiber was implanted into the tissue through a 17 gauge cannula of length 7.5 cm.

3.1.2 Tissue phantom

Tissue phantoms were designed by the author (figure 3.3) and built at the Hamilton Regional Cancer Centre. Two boxes made of 1/4 inch lucite with dimensions 7 by 8 by 11.4 cm were constructed. These dimensions were chosen so as to facilitate simplifications in the mathematical model. It was assumed that due to the rapid decrease of photon flux with radial distance, if the light source could be positioned far from all lucite boundaries then the boundaries would be heated negligibly by the source. Heat transfer across the lucite/water boundary would, therefore, be negligable. The validity of this assumption will be discussed in greater detail in the next chapter.

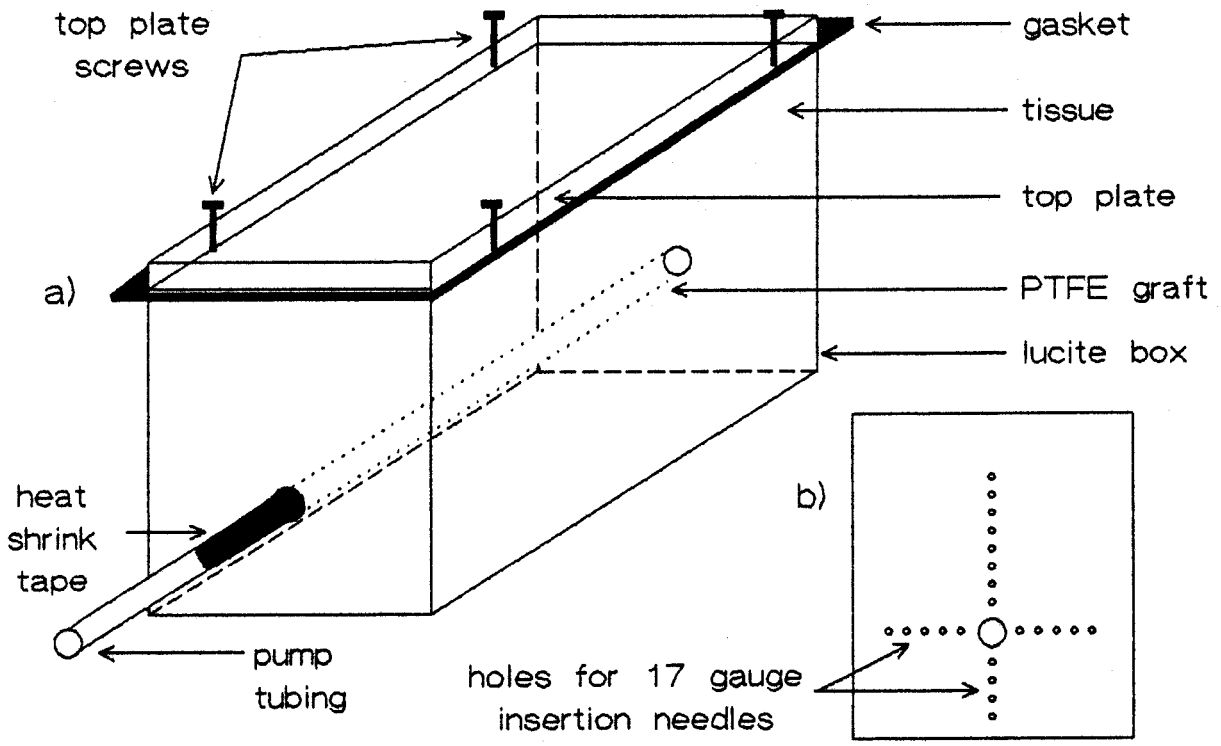

Figure 3.3 Tissue phantom: a) front view and b) back face with machined holes for implanting devices.

The top plate of each phantom was removable to allow packing of the tissue material. This plate was connected to the fixed portion of the box by four screws. A rubber gasket covered with silicone gel formed a waterproof seal between the top plate and the rest of the box. The top plate and one of the side plates were perforated with 1/16 inch diameter holes positioned 0.5 cm apart. These holes provided sites for implanting source fibers and thermocouples. Due to machining constraints, this was the minimum achievable distance between implanted devices.

Traversing the interior of each lucite box was a polytetrafluoroethylene (PTFE) (Impra Incorporated Flagstaff, Arizona, U.S.A.) vascular graft used clinically as a vessel prosthesis. One box housed a 0.40 cm inner diameter (ID) vessel and the other a 0.144 cm ID vessel. The wall thickness of both grafts was measured using a vernier caliper and found to be 0.040 $\pm$ 0.002 cm. The optical transmission of 1064 nm light through this thickness of PTFE is approximately 90% (Handbook of Optics).

A peristaltic pump (Model PJ11T Fred Dungey

Inc., Scarborough Ont.) was used to pump a blood substitute from a reservoir (a 100 ml graduated cylinder) through the vessel and back into the reservoir. The temperature of the blood substitute was kept at 37°C and did not vary more than 0.5°C during any experiment. Water was used as the blood substitute in all experiments for practical reasons.

The tissue material had to satisfy a number of criteria:

(i) It had to be solid so that temperature distortion due to fluid motion would not occur.

(ii) It had to be approximately homogeneous so that the optical properties could be well known.

(iii) It had to allow for tissue collapse around implanted devices so as to minimize the creation of air pockets around these devices.

A ground veal mixture was found to adequately satisfy these criteria. Packaged ground veal was blended with a solution of water, Knox gelatine and formaldehyde. This solution contained 4% (by weight) Knox gelatine and 0.4% (by volume) of a 37% formaldehyde solution. The formaldehyde raised the melting point of

the gelatine from approximately 35°C to at least 60°C (Astrahan 1979).

The veal was homogenized by grinding it in a food blender. This technique provided greater uniformity of the tissue material. The water based solution was then added to the veal in proportions that yielded a 60% veal (by mass) final material. The resulting mixture was poured into the lucite box and allowed to set at room temperature for 24 hours. This time period was required to allow sufficient cross linking of the formaldehyde and collegen molecules (Blechinger et al 1988). During each experiment, the phantom rested on a stand suspending it above the floor of a shaking waterbath (Model 129, Fisher Scientific Co., U.S.A.) set at 37°C, the reference temperature for all experiments. It took approximately 3 hours for the tissue temperature to reach 37.0 ± 0.5 °C, as reported by implanted thermocouples. The temperature of the waterbath was monitored periodically using a Fisher thermometer (range -20 to 110°C) and was found to remain constant to within 0.5°C.

3.1.3 Temperature feedback system

Temperatures were reported at specified sites in the tissue using copper/constantan type T microthermocouples (Model IT-18 Sensortek Inc., Clifton, N.J., U.S.A.) with a time constant of 0.1 seconds. The microthermocouples were covered with a teflon sheath with a wall thickness of 0.64 mm. This protected and increased the rigidity of the wire leads. The thermocouples were implanted into the tissue using 7.5 cm long 17 gauge insertion needles. The thermocouples were fed into a data acquisition and control system (Labmate series 7000, Scientific Instruments Inc., Nepean, Ontario) which housed 16 channels for analog inputs.

3.1.4 Microprocessing system

At the center of the processing system was a 10MHz AST Premium/286 microcomputer. The stepping motor and the Labmate were both interfaced to the computer. The laser pulse and temperature feedback parameters were input into the computer code listed in Appendix B. The laser pulse duration was controlled by the stepping

motor which allowed coupling of the beam to the fiber for a user specified number of temporal increments. The reported temperatures were calculated using the Labmate software (Level1-QB LL version 3.0). This code used least-squares curve fitted polynominals based on the American National Standards Institute tables of thermoelectric voltage as a function of temperature. Using these polynominals, the average error is reported to be 0.012°C over the -30 to 150°C range.

3.2 Calibration of the pump

The output of the peristaltic pump was reported as a percentage speed over a range of 0 to 1000% . The average flow rate through a vessel should vary linearly with the output speed (S) and is given by

$$F = \pi R_v^2 \langle v \rangle \qquad (3.1)$$

where F is the average flow rate, Rv is the vessel radius and <v> is the average output velocity.

The calibration apparatus was set up as in figure 3.1 without the light delivery or temperature feedback systems. The 0.40 cm ID vessel phantom was used. The water bath was set to 37°C so that the

viscosity of the water flowing through the vessel would be consistent with experimental procedures. The flow rate was measured directly by timing the amount of water entering the reservoir. Measurements were taken at 100% increments over the 100% - 700% range. Each measurement was repeated four times. The calibration curve in figure 3.4 represents the mean values of each measurement. The standard deviation for each data point was ± 0.03 ml/min. The data was fit to a straight line by the least-squares method with the equation of the fitted line given by

$$F = 0.2081\ S + 1.0 \quad (ml/min) \qquad (3.2)$$

This equation was used to adjust the variable speed of the pump to the flow rates used during the experiments.

The experiments utilized two flow rates for each phantom. Flow rates in the range of those found in the human body were to be used. Unfortunately, blood flow rates in the body are not well known. For the 0.144 cm vessel phantom, flow rates of 50 and 100 ml/min were used. Flow rates of 100 and 200 ml/min were used for the 0.40 cm vessel phantom. These last flow rates are in the range of in vivo measurements for a brachial artery of

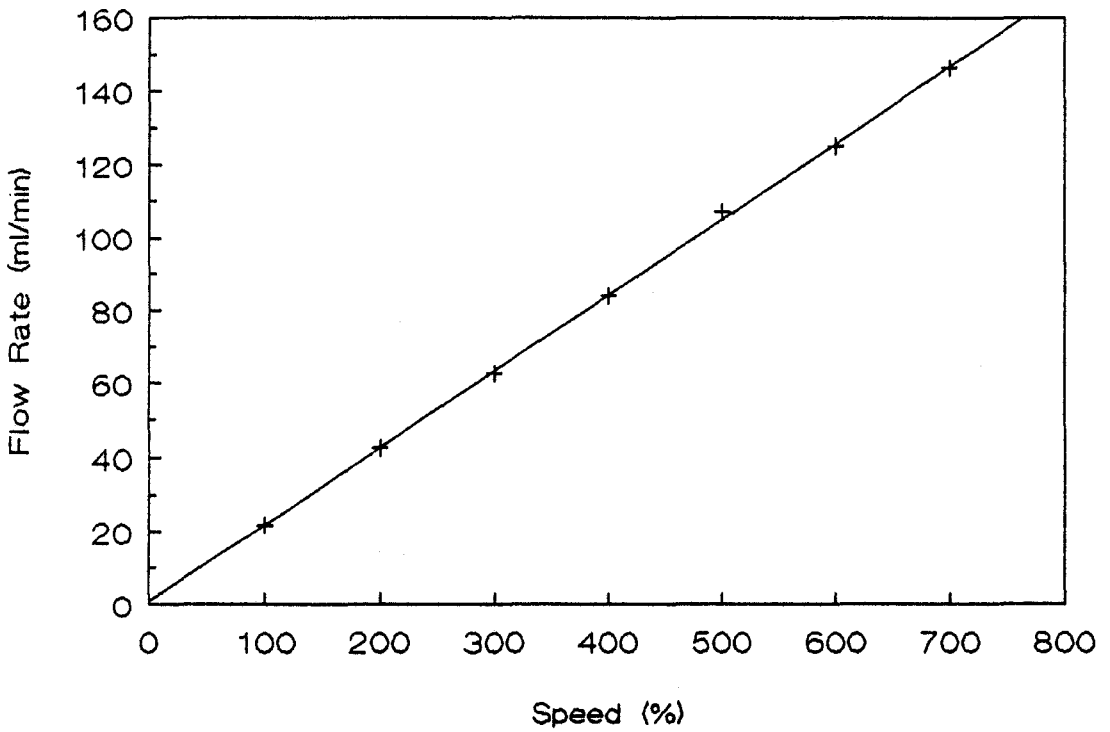

Figure 3.4 Peristaltic pump calibration curve.

diameter 0.474 cm (Anderson 1989).

3.3 Laser power calibration

Optimization of the power emitted from the cylindrical tip was achieved by focusing the laser beam onto the polished fiber end using the stepping motor and the two tuning screws. The power from the laser was then optimized by adjusting the horizontal and vertical positionings of the cavity mirrors until the power reading from the end of the cylindrical tip ($P_{end\ of\ tip,meter}$), as measured by an Ophir laser power meter (Model DG, Optikon, Waterloo, Ontario), peaked to a maximum.

The total power from the entire cylindrical tip could not be measured directly using the available integrating sphere (Labsphere Model 88XL , North Sutton, NH, USA) due to its limited power range. Therefore, a series of four attenuating filters (total optical density at 1064 nm $\cong$ 0.58) were used to attenuate the power into the range of the integrating sphere. The laser power measurement procedure is shown in figure 3.5. The actual total power emitted from the entire

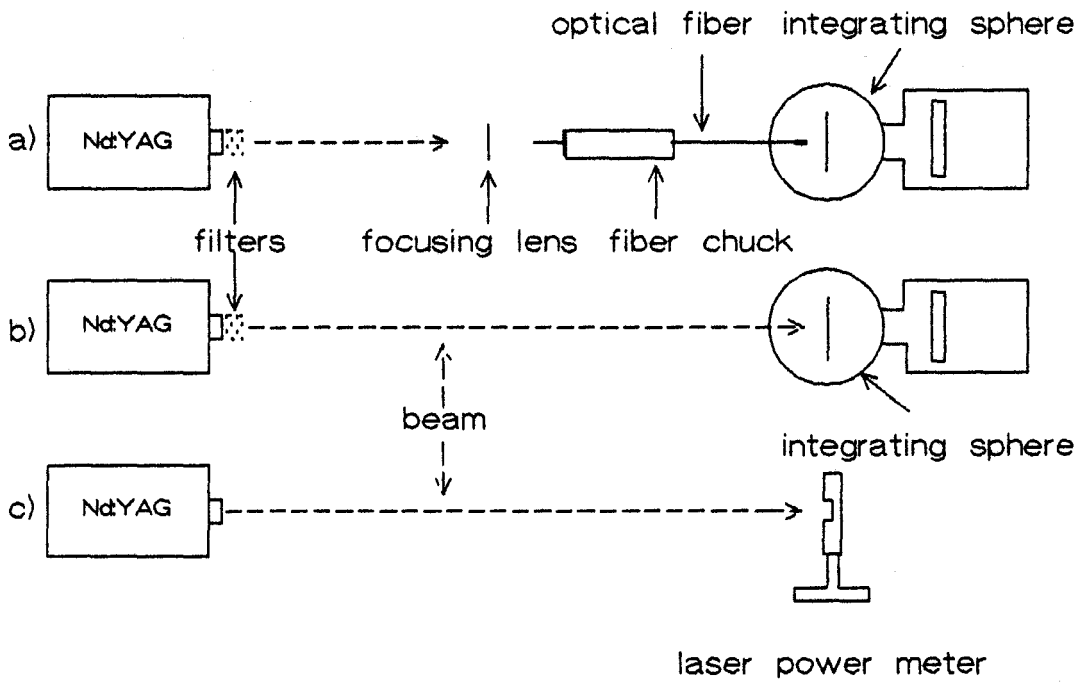

Figure 3.5 Procedure for laser power calibration by measuring a) $P_{lip,sphere} * A$, b) $P_{laser,sphere} * A$ and c) $P_{laser,meter}$.

cylindrical tip was given by

$$P_{actual,tip} = f \, \varepsilon \, P_{laser,meter} \tag{3.3}$$

where $$\varepsilon = \left(\frac{P_{tip,sphere\ A}}{P_{laser,sphere\ A}} \right) \tag{3.4}$$

$\equiv$ the coupling efficiency of the laser beam to the optical fiber.

$P_{actual,tip}$ is the actual integrated power output from the cylindrical tip; $P_{tip,sphere} * A$ is the attenuated power output from the cylindrical tip measured by the integrating sphere (figure 3.5a); $P_{laser,sphere} * A$ is the attenuated power output directly from the laser beam measured by the integrating sphere (figure 3.5b); $P_{laser,meter}$ is the power out of the end of the cylindrical tip measured by the laser meter (figure 3.5c); A is the optical attenuation by the filters; and f is the calibration correction factor for the laser power meter. This correction factor was determined to be 1.00 ± 0.01 over the range of experimental power measurements.

The results of the laser power calibration are found in table 3.1. From these results, one can determine a calibration factor, τ, which will relate the power emitted from the entire cylindrical tip to the

	POWER	
	TRIAL 1	TRIAL 2
Pend of tip,meter	0.75 ± 0.01 W	0.75 ± 0.01 W
Ptip,sphere * A	1080 ± 30 μW	1080 ± 30 μW
Plaser,sphere * A	1700 ± 20 μW	1660 ± 20 μW
Plaser,meter	3.0 ± 0.1 W	2.94 ± 0.05 W

Table 3.1 Laser power calibration.

power measured from the end of the cylindrical tip in the Ophir power meter

$$\tau = \left(\frac{P_{actual,tip}}{P_{end\ of\ tip,meter}\ f} \right) \qquad (3.5)$$

The calibration factor was found to be 2.55 ± 0.10 and was used to determine the total power emitted from the entire cylindrical tip before each experiment.

3.4 Temperature measurements procedure

Seven thermocouples were calibrated over the 31 - 56 °C temperature range in the shaking waterbath. The temperature reported by a thermocouple was compared to that of a Fisher thermometer (range -20 to 110 °C) with a reported tolerance of 1 °C. The results are presented in figure 3.6. The slope of the calibration curve is 1.00 ± 0.01, therefore no correction factors were required.

The laser power out the end of the cylindrical tip was measured before each experiment. The actual total power from the entire cylindrical tip was given by

$$P = P_{end\ of\ tip,meter}\ f\ \tau \qquad (3.6)$$

where $P_{end\ of\ tip,meter}$ was the power from the end of the cylindrical tip measured by the meter before each experiment and f and τ are defined as above.

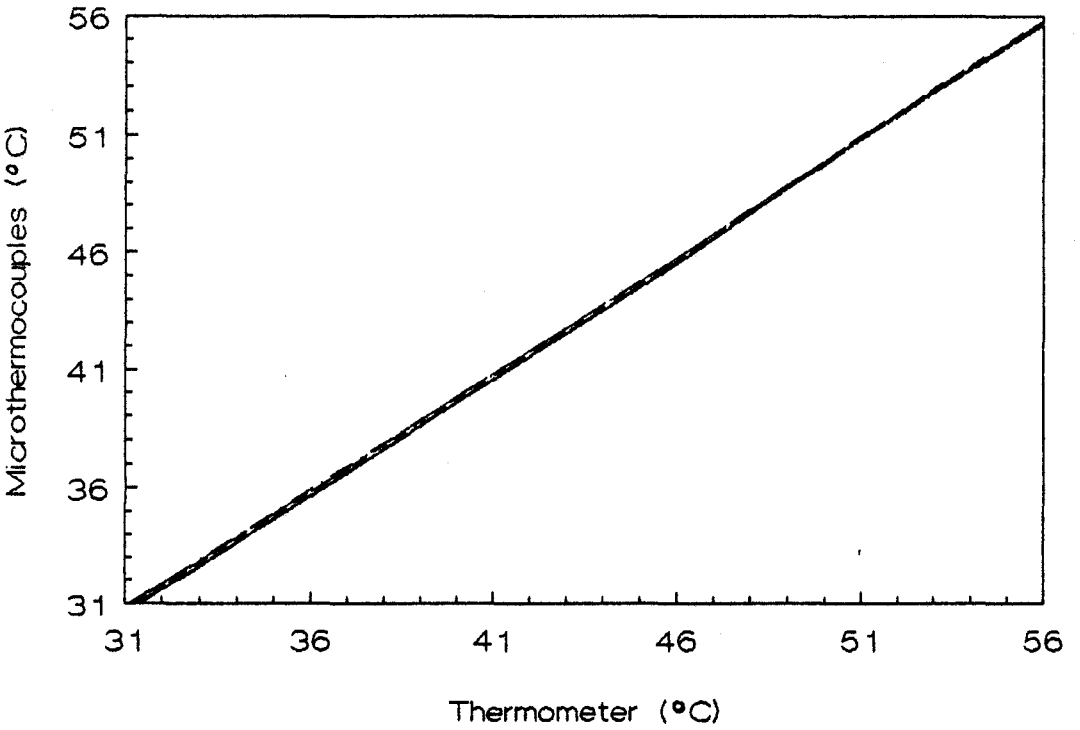

Figure 3.6 Microthermocouple calibration.

The optical fiber and the microthermocouples were implanted into the tissue using the method shown in figure 3.7. Each device was fed into a cannula until it could be viewed at the bevelled end (figure 3.7a). The needle was pushed through a hole on the end plate and into the tissue until less than a centimeter of the needle was visible (figure 3.7b). The needle was withdrawn until a point marked 0.5 cm from the tip of the needle was visible, the device lead held steady. The device lead was then withdrawn until a mark on that lead was flush with the top of the needle (figure 3.7c). This mark was made at 13 and 14 cm from the tip of the thermocouple and optical fiber, respectively. This resulted in the thermocouples being positioned 6 cm from the end plate and the end of the cylindrical tip 7 cm from the end plate.

The 0.5 cm tip of the needle which rested in the end plate provided stability and aided in the reproducability of the fiber/thermocouple positioning. It was estimated that the position of the devices could be reproduced to within 1 mm.

After reviewing the results of preliminary

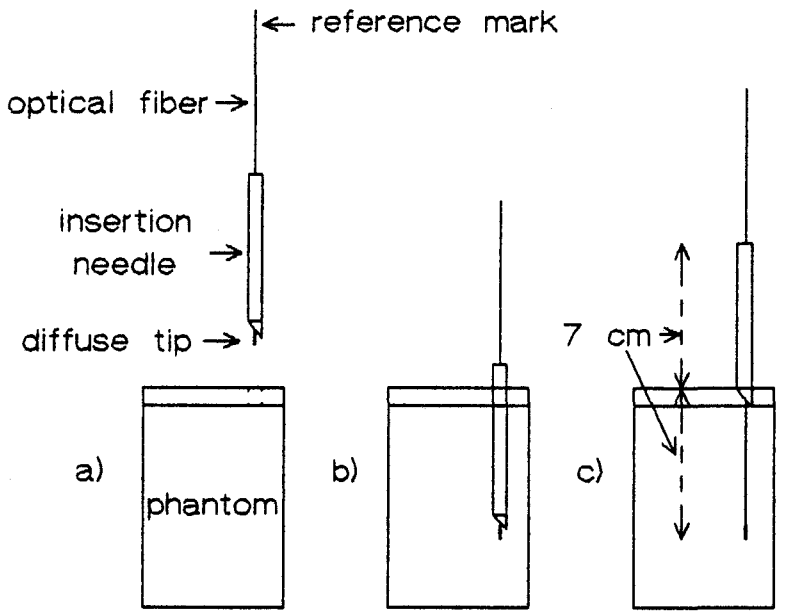

Figure 3.7 Procedure for implanting devices into phantom (optical fiber shown here).

experiments, an exposure of 10 minutes was decided upon. Given this exposure, the maximum temperature attained was approximately 60°C. At temperatures greater than 60°C, the tissue material could melt resulting in temperature perturbations due to fluid motion.

The variable speed on the peristaltic pump was dialed to the desired flow rate. Three background temperature measurements, at 60 second intervals, were taken to ensure that all thermocouples reported 37.0 ± 0.5°C. The laser was allowed to warm up for two minutes with the beam directed towards a beam-stop. The fiber was illuminated for 10 minutes. Temperature measurements were taken every 60 seconds during and after the illumination for a total of 30 minutes.

3.5 Optical properties of tissue material

3.5.1 Apparatus

The optical properties of the tissue material were determined using a procedure as described by Peters et al (1990) (see figure 3.8a). Briefly, light from a high pressure Xenon arc lamp was focused onto the entrance slit of a monochromator. The monochromator was

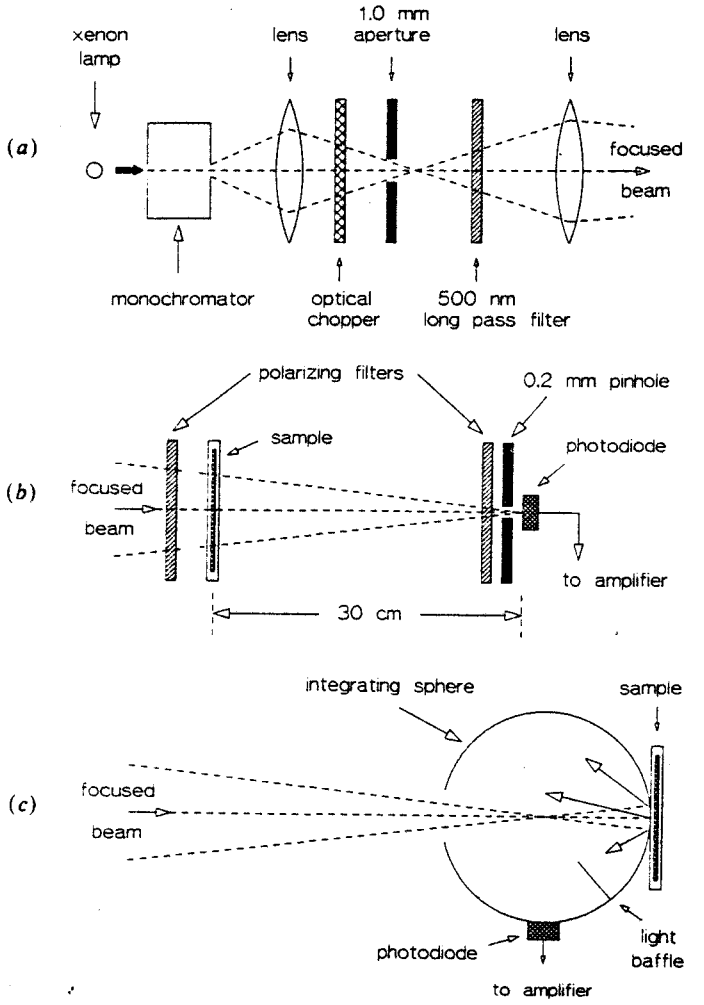

Figure 3.8 a) Optical system used to produce a collimated monochromatic light beam, b) apparatus used to measure the total attenuation coefficient, c) the integrating sphere used to measure reflectance. For measuring transmittance, the sphere was rotated 180° on the vertical axis and a barium sulfate plate was used to cover the open port (Reprint from Peters et al 1990).

selected to emit near infrared light of 1064 nanometers. The light exiting the monochromater passed through an optical system which produced a well collimated 3 mm diameter light beam.

For transmittance and reflectance measurements, the beam was incident upon the entrance port of an integrating sphere which housed a silicon photodiode used to measure the light signal (figure 3.8c). This signal was modulated by an optical chopper in the path of the original beam. A lock-in amplifier filtered the signal and amplified only those components which were modulated at the frequency of the optical chopper. This increased the signal-to-noise ratio.

In measuring reflectance, the sample was placed at the exit port of the integrating sphere; in measuring transmittance the sample was placed at the entrance port of the integrating sphere and a barium sulfate lined plate covered the exit port.

For measuring total attenuation, the beam was collimated by placing an aperture made in black tape over lens #2 (figure 3.8a). This produced a circular 3 mm diameter beam which was incident upon the sample

located 5 cm away from this lens. The light passing through the sample struck a silicon photodiode located approximately 30 cm away (figure 3.8b). The photodiode was coupled to a preamplifier and the signal was again amplified by a lock-in amplifier. Scatter was rejected in these measurements by maximizing the distance between the sample and the detector, and by using a 0.2 mm aperture over the photodiode.

3.5.2 Measuring reflectance and transmittance

Three samples were prepared for the transmittance and reflectance measurements by placing a section of the tissue material between two 1 mm thick glass slides. A sample thickness of 1 mm was achieved by fixing glass slide fragments in between and at the ends of the two intact slides using epoxy. Measurements were taken at four different approximately homogeneous locations on each sample. After each measurement, the monochromator was dialed to 650 nm (red light) in order to locate the next site.

The measured sample reflectance R_M is given by

$$R_M = R_c \, (I_R \, / \, I_{ref}) \qquad (3.7)$$

where Rc is the reflectivity of the barium sulfate coating lining the inside of the integrating sphere which was taken to be 0.965 for all calculations (Peters et al 1990), I_R is the measured reflectance signal and I_{ref} is the reflectance measurement with the barium sulfate reflective plate at the exit port.

The measured sample transmittance is given by

$$T_M = R_c \, (I_T / I_{ref}) \qquad (3.8)$$

where Rc and I_{ref} are the same as above and I_T is the measured transmittance signal.

The sample reflectance and transmittance were calculated using the 12 measured signal values and found to be $R_M = 0.129 \pm 0.013$ and $T_M = 0.434 \pm 0.020$. The errors represent one standard deviation from the mean signal values.

3.5.3 Total attenuation measurments

Thin samples were required for total attenuation measurements due to the high probability that multiply scattered photons in the beam exiting a thick sample could be forward directed and be detected by the photodiode (Peters et al 1990). The samples were

prepared using a block of tissue which had been refrigerated at -70°C for three hours. From this block, thin samples were cut using a Cryostat microtome. The sample thickness ranged from 10 μm to 22 μm at 4 μm increments. Each slice was mounted on a glass slide. A drop of water was placed on each slice to improve the glass-tissue coupling and a glass coverslip was attached to the glass slide using epoxy. This was to prevent dehydration of the sample. Three slides of each thickness were prepared. A water sample, which was used to account for specular reflective losses by the glassware, was also prepared in the same way.

Total attenuation measurements at 1064 nm were taken at four different sites on each sample. The monochromator was dialed to 650 nm after each measurement to enable accurate sample positioning. The attenuation coefficient of the tissue sample is given by

$$\Sigma t = -(1 / t)\ln (I / Io) \qquad (3.9)$$

where I is the detector reading with the sample, Io is the reference reading with the water sample and t is the thickness of the tissue sample.

The mean ln (I / Io) value and associated standard deviation for each sample thickness were plotted against thickness (see figure 3.9). The points were fitted to a straight line by the least squares method. From equation 3.9, the slope of this fitted line yielded a total attenuation coefficient of Σt = 35.1 ± 12.6 mm^{-1}. The error associated with the slope was determined by the least squares method. The large variance of I could be due to air pockets and fat inhomogeneities in the tissue material.

3.5.4 Monte Carlo calculations of optical properties

A Monte Carlo generated data program (Peters et al 1990) was used to derive the optical interaction coefficients from measured reflectance, transmittance and total attenuation values. This data program contained calculated reflectance and transmittance values plotted against the total attenuation coefficients for ranges of g (mean cosine of the scatter angle) and albedo.

For any given sample, the measured reflectance

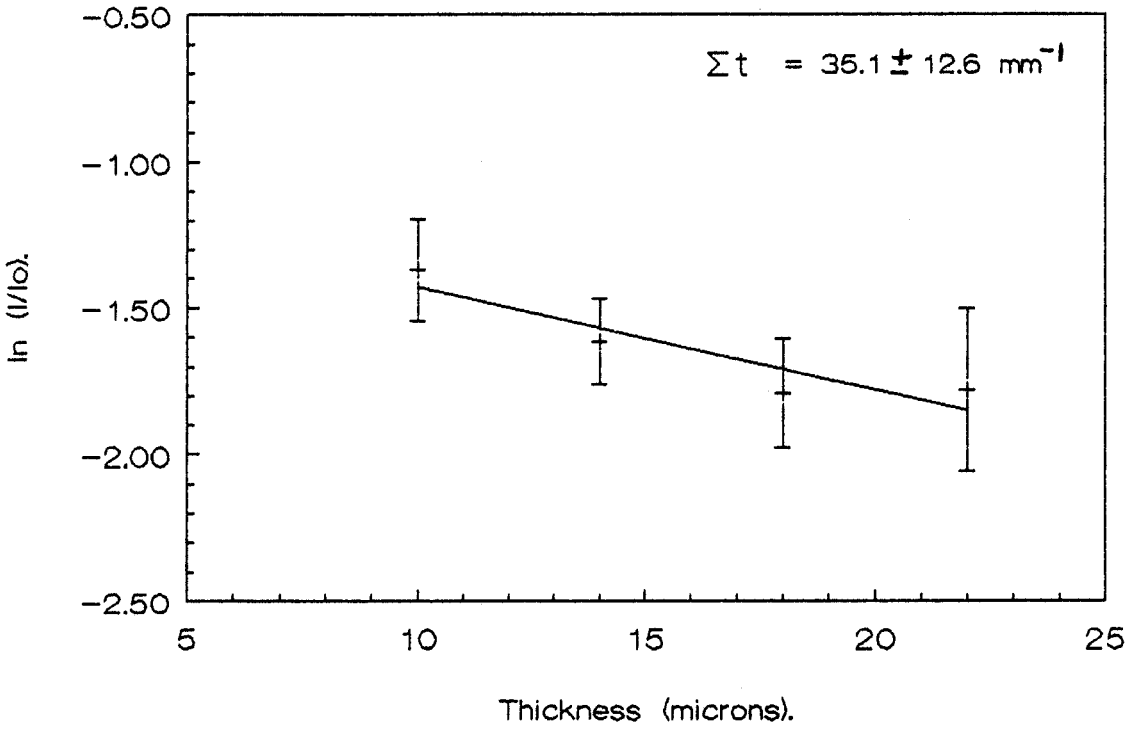

Figure 3.9 Total attenuation coefficient of tissue material.

combined with the measured total attenuation can be used to obtain pairs of compatible values of albedo and g from these plots. Similarly, the measured transmittance combined with the measured total attenuation can be used to obtain a second set of acceptable pairs. The correct values of albedo and g which are the only mutually acceptable values interpolated from the paired data sets determine the optical interaction coefficients (Peters et al 1990).

The absorption and reduced scattering coefficients for the tissue material were obtained by inputting the range of reflectance, transmittance and total attenuation measurements into the Monte Carlo data program (see table 3.2). The final absorption and reduced scattering coefficients represent the mean value and one standard deviation from the mean. These final values were $\Sigma_a = 0.181 \pm 0.026$ mm^{-1} and $\Sigma_s' = 0.806 \pm 0.080$ mm^{-1}. The absorption coefficient for water (blood substitute) at 1064 nm is approximately 0.02 mm^{-1} (Boulnois 1986). These were the values used in the computer model.

Ranges of Σt, R_M and T_M	Σa (mm^{-1})	$\Sigma s'$ (mm^{-1})
Σt_{min}, R_{Mmin} T_{Mmin}	0.225	0.739
Σt_{min}, R_{Mmax} T_{Mmin}	0.186	0.876
Σt_{min}, R_{Mmin} T_{Mmax}	0.192	0.691
Σt_{min}, R_{Mmax} T_{Mmax}	0.158	0.780
Σt_{max}, R_{Mmin} T_{Mmin}	0.203	0.834
Σt_{max}, R_{Mmin} T_{Mmin}	0.175	0.936
Σt_{max}, R_{Mmin} T_{Mmin}	0.169	0.756
Σt_{max}, R_{Mmin} T_{Mmin}	0.142	0.835

Table 3.2 A range of Monte Carlo data for the optical properties of the tissue material.

3.6 Application of the mathematical model

3.6.1 Assumptions

The thermal conductivity, specific heat and density of the phantom material were approximated using published values for tissue and water (found in section 2.4.1) weighted according to the volume of tissue and water used in the final material. The phantom material was 58% veal and 42% water by volume. Therefore the weighted values were determined according to

$$A = 0.58\ At + 0.42\ Av \qquad (3.10)$$

where A, At and Av represent the parameter values of the phantom material, tissue and water, respectively. The values obtained were k = 4.35 - 5.51 X 10^{-3} W/cm/K c = 3.69 J/g/K and ρ = 1.05 g/cm^3. An average thermal conductivity of k = 4.93 X 10^{-3} W/cm/K was used in the mathematical model.

Using the optical properties of the phantom material, a graph of calculated photon flux (equation 2.6), normalized at 0.1 cm, with radial distance from the source was plotted (figure 3.10). This shows that, at 0.7 cm, the flux falls to less than 1% of its value at 0.1 cm. Given that the surface of the PTFE graft is

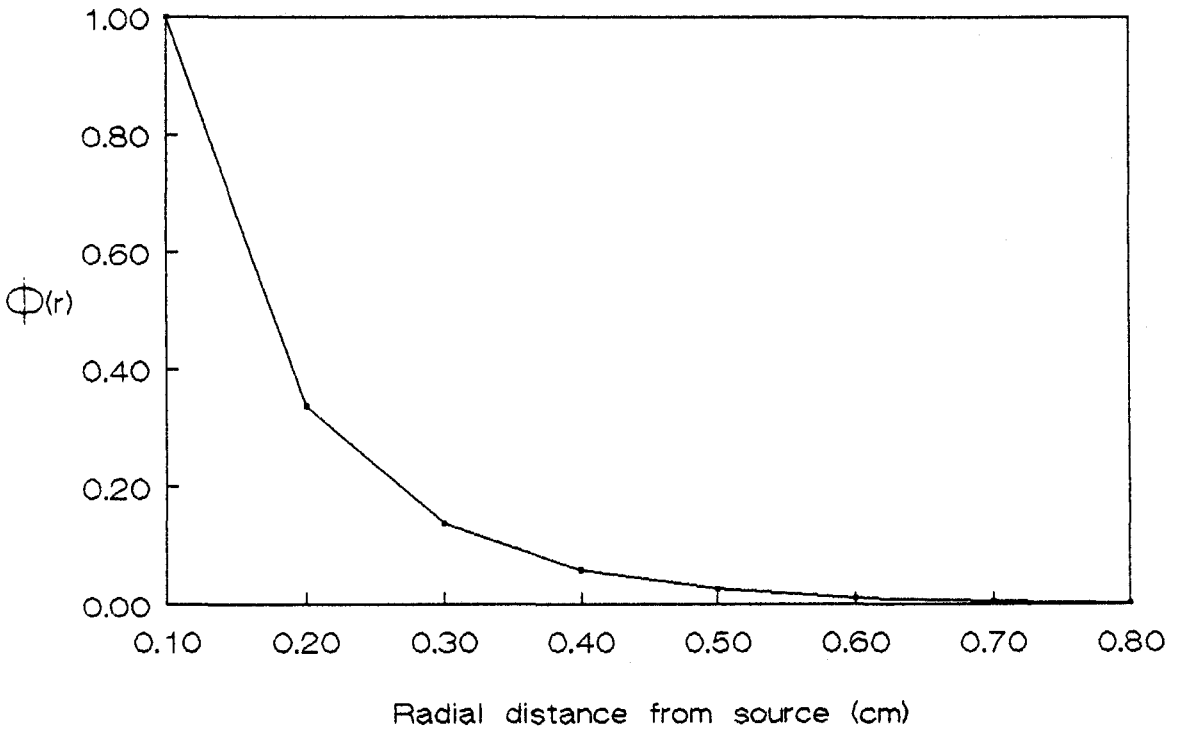

Figure 3.10 Normalized photon flux (calculated) vs. radial distance from a 1.5 cm line source.

always at least 0.8 cm away from the source and the optical transmission of 1064 nm light through 0.04 cm of PTFE is 90% , it is assumed that the graft doesn't perturb the photon flux distribution. The absorption coefficient at the graft is set to zero.

In order to limit the size of the model geometry and hence save computer time, the maximum thermal field extending radially from the light source can be approximated by adding the thermal diffusion length (equation 2.19) to 0.7 cm, the distance at which the photon flux is less than 1% of its value at 0.1 cm

$$\lambda = 0.7 + (4Xt)^{1/2} = 0.7 + \left(\frac{4kt}{\rho c}\right)^{1/2} \qquad (3.11)$$

where X is the thermal diffusivity and t is the total modelling time. Given the approximated physical and thermal properties of the tissue material and a modelling time of 20 minutes (10 minutes with laser on and 10 minutes relaxation), the maximum thermal field was found to be 3.17 cm. This was verified by a computer simulation with a λ value of 5 cm. Therefore, at the boundary defined by λ = 3.2 cm, the temperature was set at a constant 37°C for all numerical calculations.

At the flow rates being investigated convection

dominates radial conduction within flowing blood. This can be seen by solving the coefficients in the BHTE for flowing blood found in Appendix A. For the 0.144 cm vessel with a flow rate of 50 ml/min, radial conduction contributes less than 1% to the blood temperature. For the 0.40 cm vessel this contribution is also less than 1 % . Therefore the conduction term in the BHTE for flowing blood can be neglected at high flow rates. The finite difference expression for the BHTE in flowing blood for high flow rates is

$$Tb_k^{s+1} = \left(QL_{i,j,k} + QM + \left(\frac{\langle v \rangle cb\rho b}{\Delta z} \right) Tb_{k-1}^{s+1} + \left(\frac{\rho bcb}{\Delta t} \right) Tb_k^{s} \right) \Bigg/ \left(\frac{\langle v \rangle cb\rho b}{\Delta z} + \frac{\rho bcb}{\Delta t} \right) \qquad (3.12)$$

Given that the photon flux is negligible at the surface of the blood vessel (source to vessel surface distance is always at least 0.8 cm) and since it was assumed that the blood is thoroughly mixed to a uniform temperature at each cross-section of vessel, $QL_{i,j,k}$ can be replaced by QL_k, the absorbed light along the axis of the vessel.

3.6.2 Computer code

The finite difference approximations of the BHTE were solved using the computer code listed in Appendix C. The code was executed using a MicroVax II (Digital Equipment Corporation) computer which housed the IMSL Math library. A routine, DQDAGS, from this library was used to numerically integrate equation 2.44. A description of the model parameters is found in Appendix C. Round-off errors were minimized by declaring all parameters in the code to be double precision (16 decimal places).

3.6.3 Verification of model

The sizes of the spatial differencing parameters were decided upon by comparing the results of a slightly modified computer model to those of an analytical solution.

The analytical solution is for an infinite continuous line source (i.e. hot wire) in an infinite homogeneous medium given by (Carslaw and Jaegar 1986)

$$\Delta T = \frac{SL}{4\pi k} Ei\left(\frac{-r^2}{4Xt}\right) \qquad (3.13)$$

where ΔT is the increase in temperature and Ei is the

exponential integral. If $\frac{r^2}{4Xt} << 1$ then the integral can be expanded to

$$\Delta T = \frac{SL}{4\pi k}\left[- \ln(x) - \gamma + \frac{x^2}{4} + O(x^3)\right] \qquad (3.14)$$

where $x = \frac{r^2}{4Xt}$ and $\gamma = 0.5772$ (Euler's constant).

The blood vessel was removed from the mathematical model and a 6 cm line source was found to adequately approximate an infinite line source. Temperatures increases were reported radially outwards from the center of the line source.

CHAPTER FOUR

RESULTS AND DISCUSSION

4.1 Optimization and verification of the model

The optimization process began by choosing values for the temporal increment and the convergence criterion. The values of the spatial differencing parameters were initially set to the smallest achievable given the computer memory available

$$\Delta r = 0.1 \text{ cm}, \quad \Delta\theta = 10^{\circ}, \quad \Delta z = 0.1 \text{ cm}$$

The dependence of the model solutions on the temporal increment and the convergence criterion are displayed in figures 4.1 and 4.2, respectively. All temperatures reported in this chapter reflect a change in temperature, ΔT, from an initial temperature of $37^{\circ}C$. Figure 4.1 shows temperatures at 0.1 cm from the source following a 120 s pulse. The final temperatures decrease linearly as the temporal increment is increased from 20

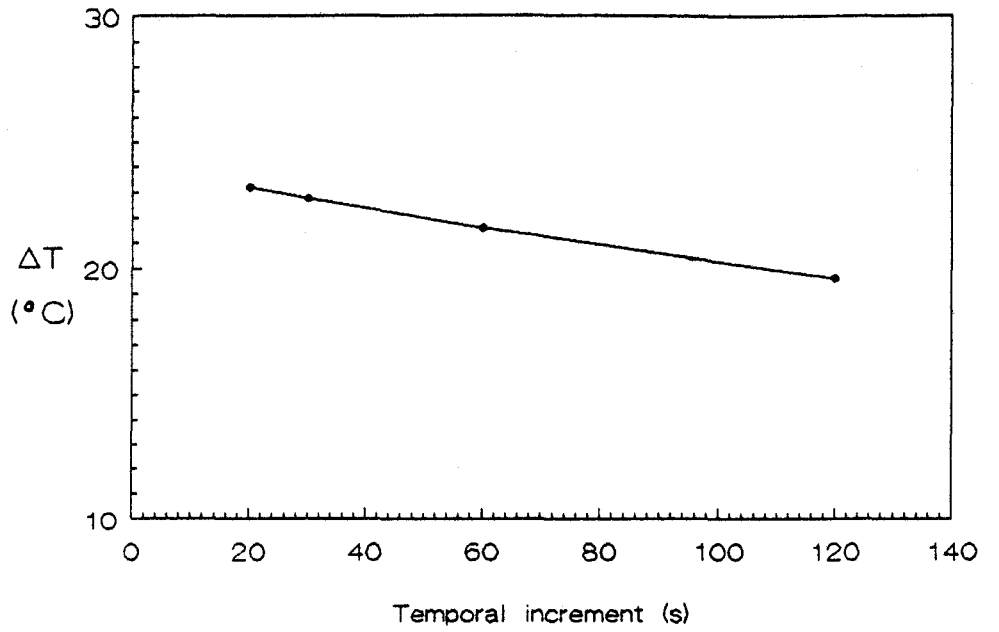

Figure 4.1 Variation of model solutions with the temporal increment.

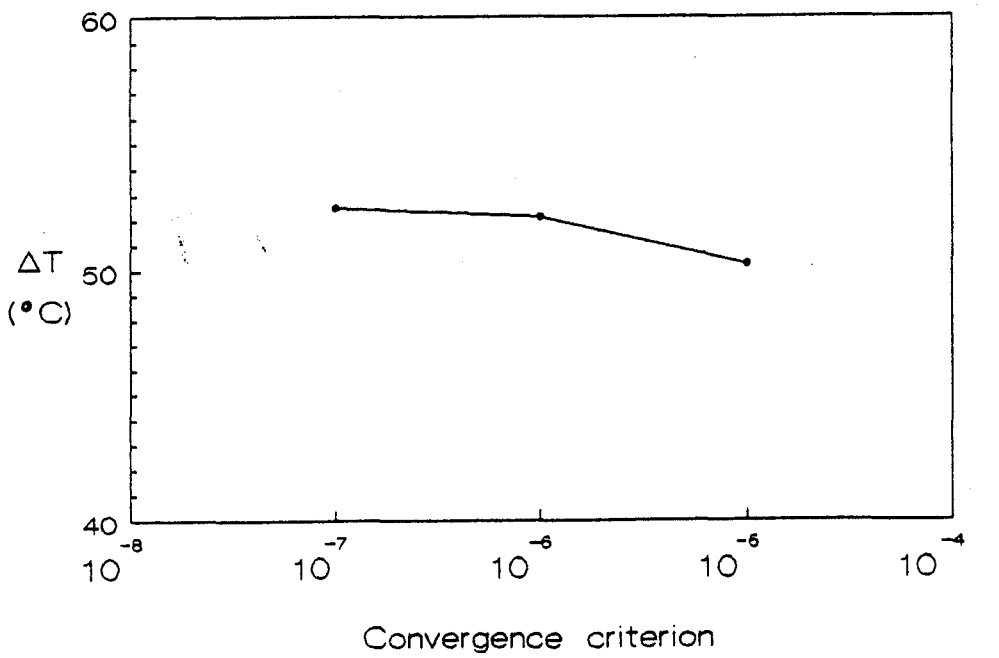

Figure 4.2 Variation of model solutions with the convergence criteria.

to 120 s. There is a 7% decrease in temperature over the 20 to 60 s range. This temperature increase is at a maximum during the first 120 to 180 s of energy deposition as the temperatures are highly transient. A temporal increment of 60 s was chosen in order to minimize the computer time required.

Figure 4.2 shows temperatures at 0.1 cm from the source following a 10 minute pulse. The temperature increase is less than 1% when the criterion is decreased from 10^{-6} to 10^{-7}. Each order of magnitude decrease in the convergence criterion doubles the computer time required. A convergence criterion of 10^{-6} was chosen.

The spatial differencing parameters where chosen by comparing model solutions with forced high optical attenuation to the analytical solution of an infinite continuous line source of heat (i.e. hot wire) in an infinite homogeneous medium as given by equation 3.12. The spatial differencing parameters were set to their initial values and the model was executed using a source strength of 0.5 W/cm and an absorption coefficient of $0.181\ mm^{-1}$.

The absorption coefficient was continuously

doubled until the model was in agreement with the theory (i.e. best approximation to a hot wire). As the absorption coefficient was increased, the radial increments surrounding the source had to be decreased in order for the model to pick up the distributed light. An absorption coefficient of 0.72 mm^{-1} with a radial increment of 0.02 cm surrounding the source yielded the best correlation (see figure 4.3). The analytical solution yields higher temperatures very close to the source (ideal hot wire) and the model solutions are slightly higher as one moves further away from the source, due to the spatial distribution of absorbed light. The area under these two curves as the radial distance approaches infinity should be and are, approximately, equal.

Improvement in the correlation at distances less than 0.1 cm could be made possible by imposing smaller incremental increses in the absorption coefficient and further decreasing the radial increments. As these increments are made smaller, however, round-off errors can be introduced.

The effect of doubling the radial and axial

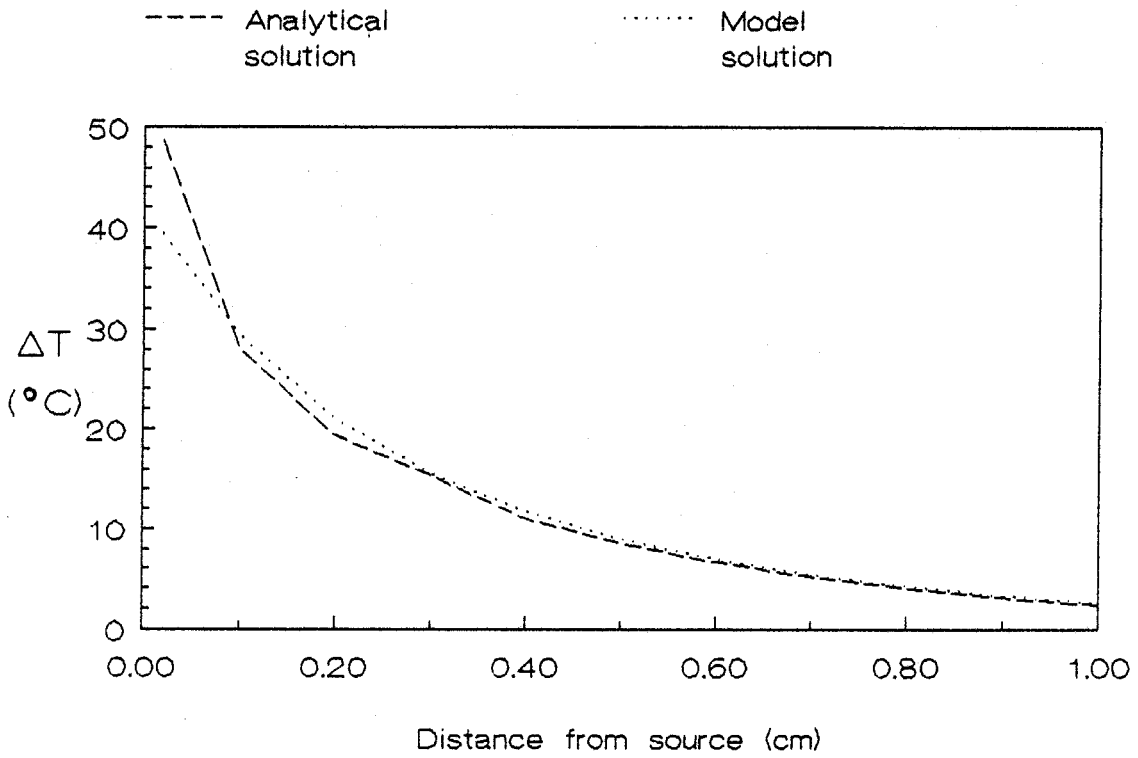

Figure 4.3 A comparison of the analytical hot wire solution to the modified finite difference model.

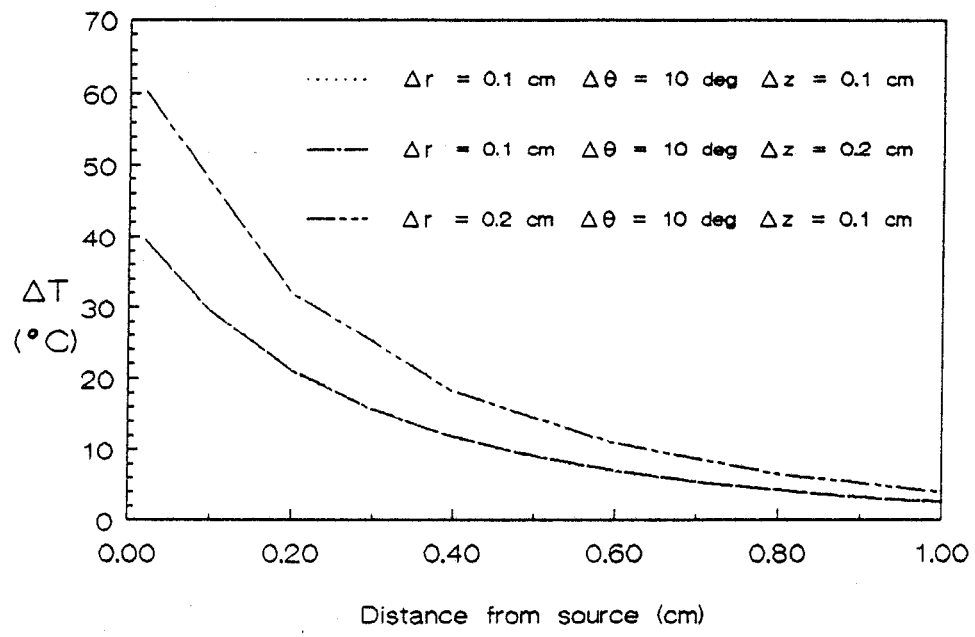

Figure 4.4 Dependence of model solutions on the radial and axial increments.

increments is shown in figure 4.4. When the axial increment was increased to 0.2 cm, there was no change in the calculated temperature profile. Doubling the radial increment yielded higher temperatures. Therefore, the model was considered verified using differencing parameters of

Δr = 0.1 cm, $\Delta\theta$ = 10°, Δz = 0.2 cm and Δt = 60 s

These parameters were used in all computer simulations.

4.2 Experimental temperature measurements

4.2.1 Temperature variation with distance from source

The temperature profiles obtained using the 0.40 cm vessel, a source to vessel distance of 1.0 cm and no flow will be used to illustrate the methods of data analysis. The variability of the temperature profiles was investigated by repeating each experiment three times at a particular flow rate. The temperatures at five thermocouple locations were measured. These locations are described in figure 4.5 and will be referred to by position number throughout this chapter. The temperature profiles at four of these positions are

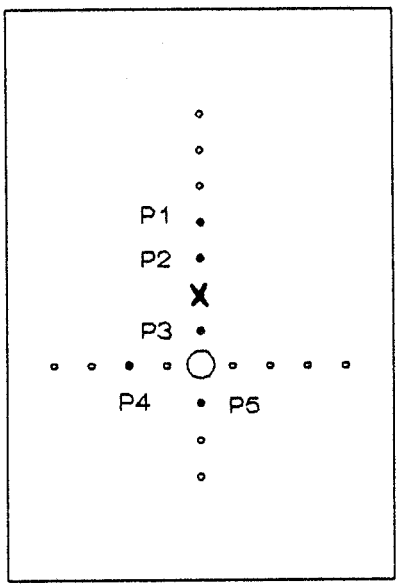

• thermocouple

x optical fiber

Figure 4.5 A diagram of the end plate of the phantom with the radial and angular positions of the implanted thermocouples. Axially, each thermocouple sits in a plane 6 cm from the end plate.

shown in figure 4.6. The average laser power is determined from equation 3.6

$$P_{av} = P_{end\ of\ tip,meter_{av}} \cdot \tau \qquad (4.1)$$

where τ is the laser power calibration factor and $P_{end\ of\ tip,meter_{av}}$ is the average of the power measurements out the end of the cylindrical tip before each experiment. The uncertainty in any one power measurement was 0.01 W.

The curve represents the mean values of temperature increase with time and the error bars represent one standard deviation from the mean. All graphs show that the experimental errors increase with increasing temperature during the 10 minute laser pulse; and they decrease rapidly during the thermal relaxation period. This trend of systematic errors was consistent throughout the entire series of experiments.

Figure 4.6b is a temperature profile obtained from a thermocouple located 0.5 cm from the light source. The model predicts that at that position the temperature gradient could be as large as 5 $^{\circ}$C per mm. From all graphs, it appears that the errors are largest in positions with high thermal gradients. Since it was

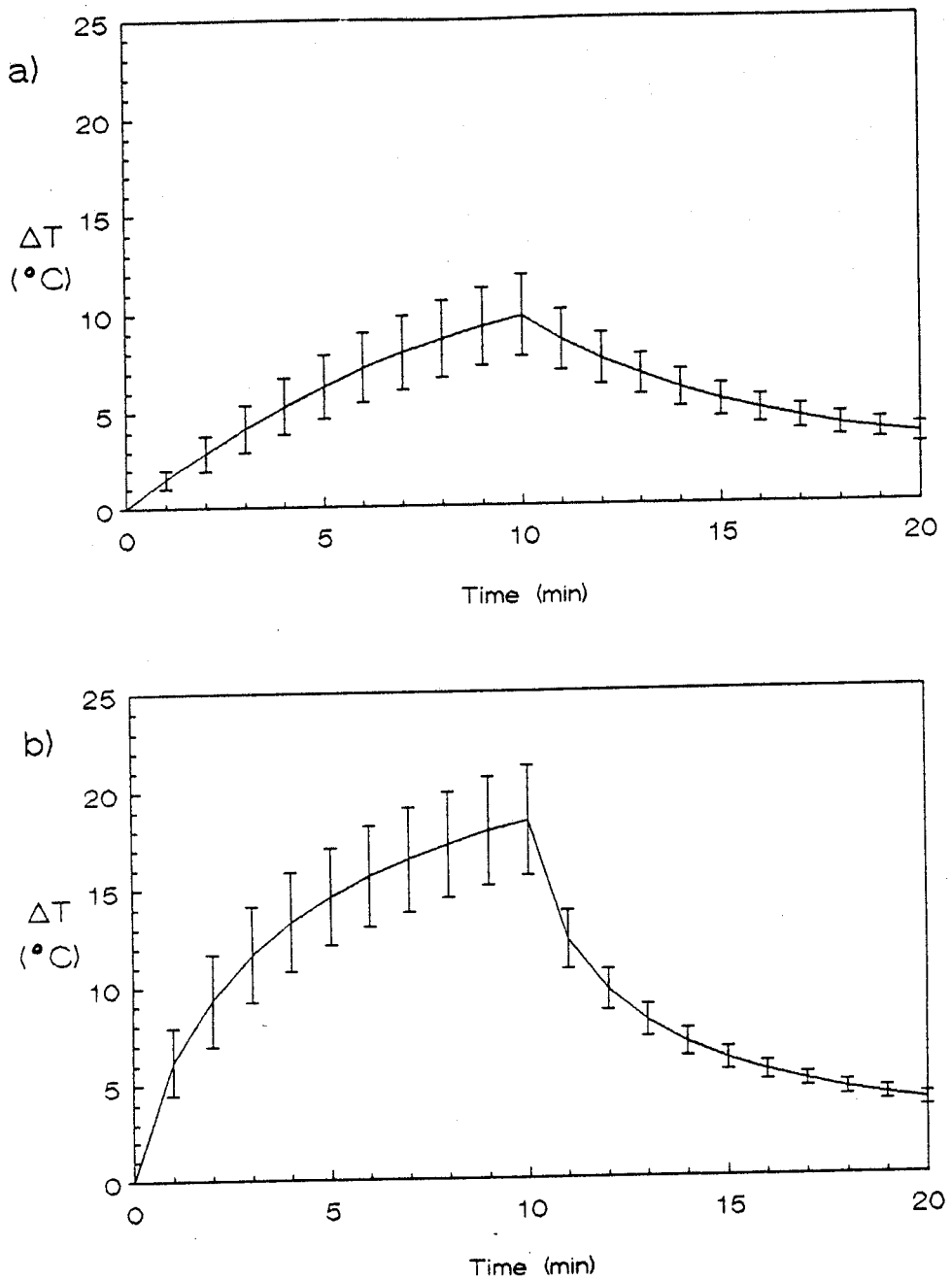

Figure 4.6 Temperature profiles at four thermocouple locations in the absence of blood flow.

a) P1 (1.0 cm from source).

b) P3 (0.5 cm from source).

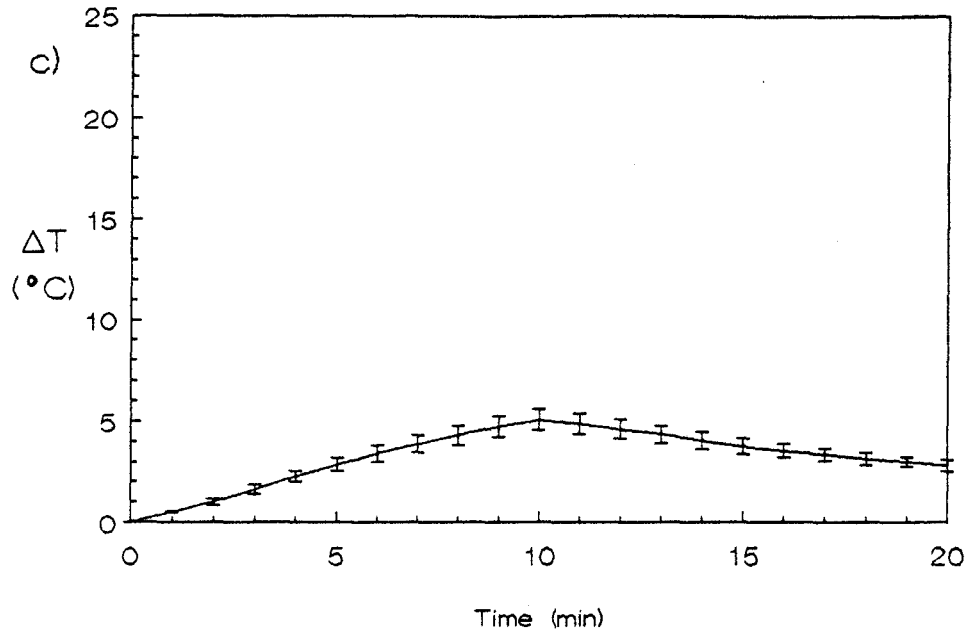

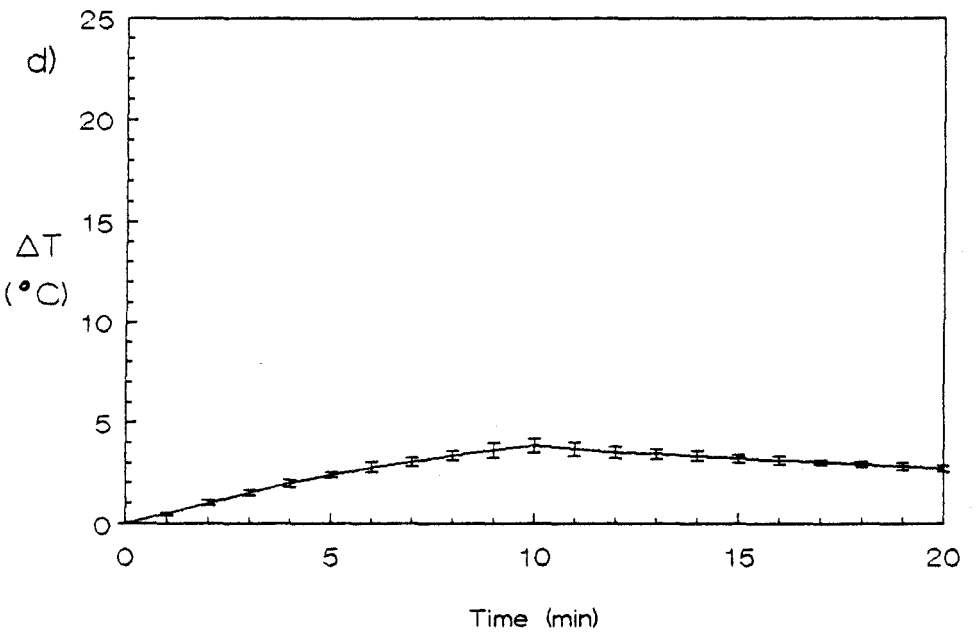

Figure 4.6 (continued)

c) P4 ($\sqrt{2}$ cm from source).

d) P5 (1.5 cm from source).

estimated that thermocouple repositioning could be achieved to within an accuracy of ± 1 mm, the experimental errors are most likely due to the lack of consistent thermocouple repositioning.

The fat content of the veal could change from week to week introducing variability in the thermal properties of the tissue material. It is unlikely that this could produce errors of the magnitude observed.

4.2.2 Temperature variation with blood flow

The mean temperature profiles as a function of flow rate, at the five thermocouple positions, for the 0.40 cm diameter vessel are shown in figure 4.7. The laser power measurements for all experiments are listed in table 4.1. The $P_{end\ of\ tip,meter}$ values were not constant for all flow rates. The increase in the average laser power during the experiment conducted at the highest flow rate is only 3% . At time 10 min, all experimental values are shown. As mentioned in section 4.2.1, there were large temperature variations in regions of high thermal gradients.

During the laser power deposition, there appears

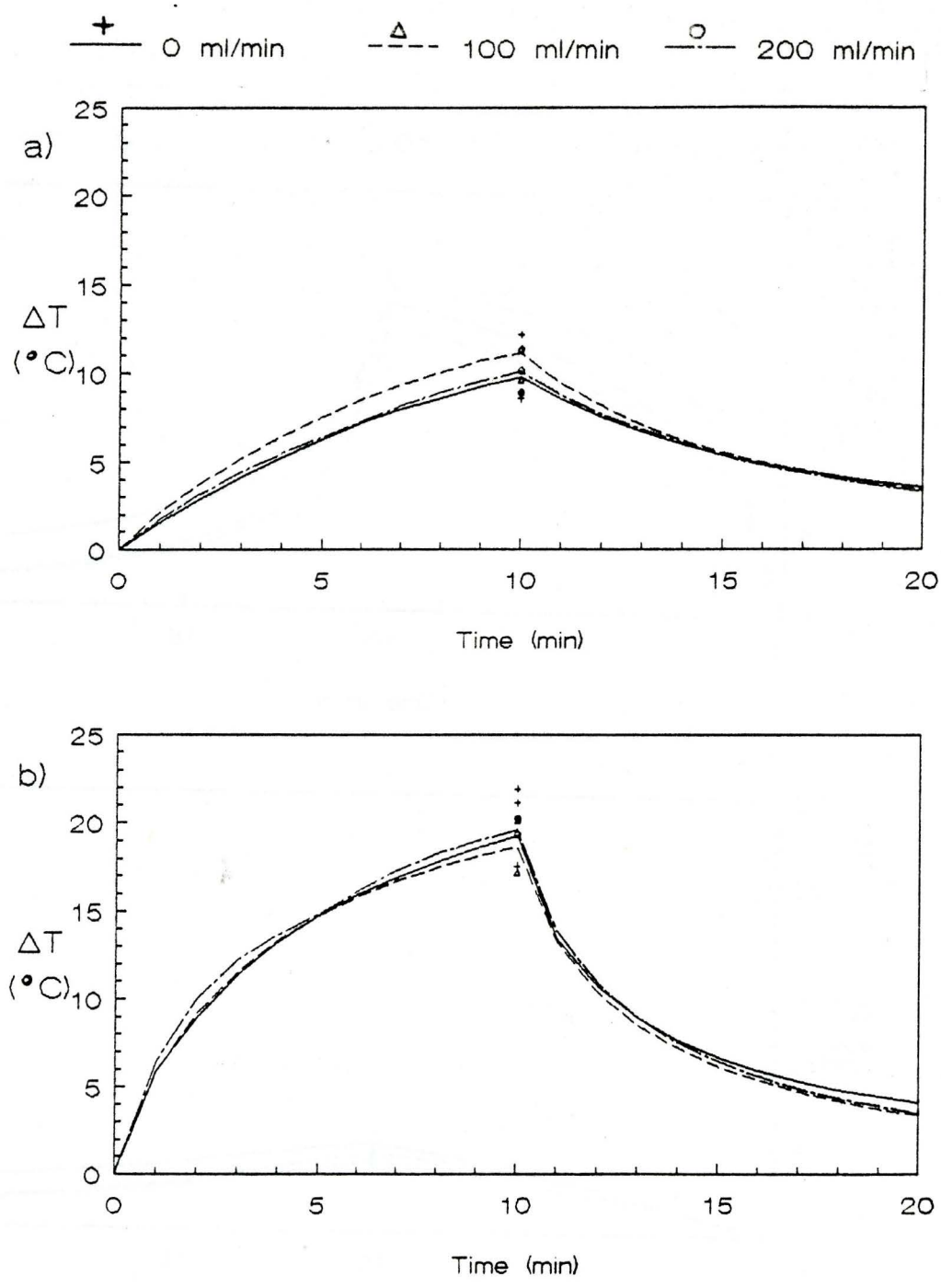

Figure 4.7 Temperature profiles for the 0.40 cm vessel at blood flow rates of 0, 100 and 200 ml/min.

a) P1 (1.8 cm from vessel surface).

b) P2 (1.3 cm from vessel surface).

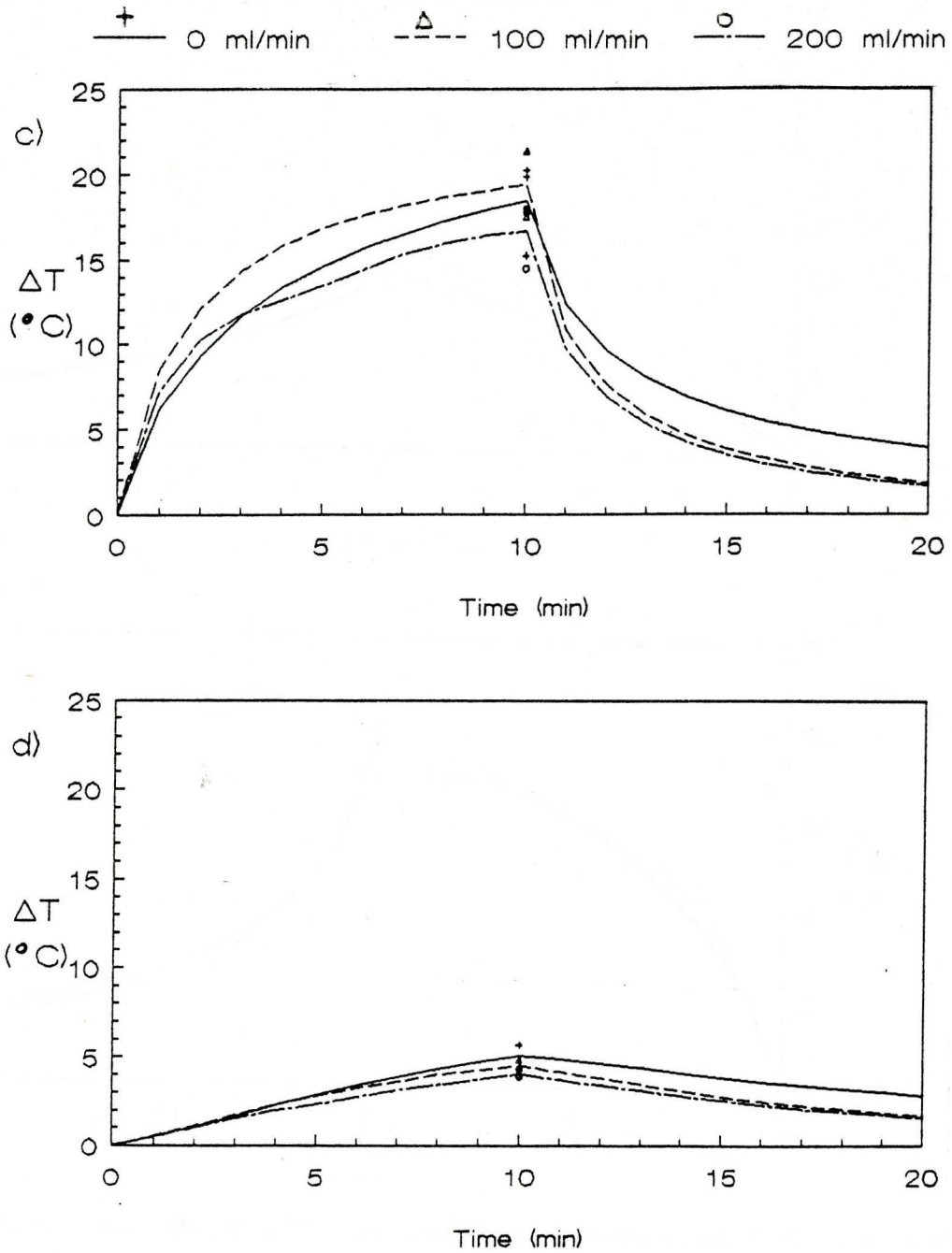

Figure 4.7 (continued)

c) P3 (0.3 cm from vessel surface).

d) P4 (0.8 cm from vessel surface).

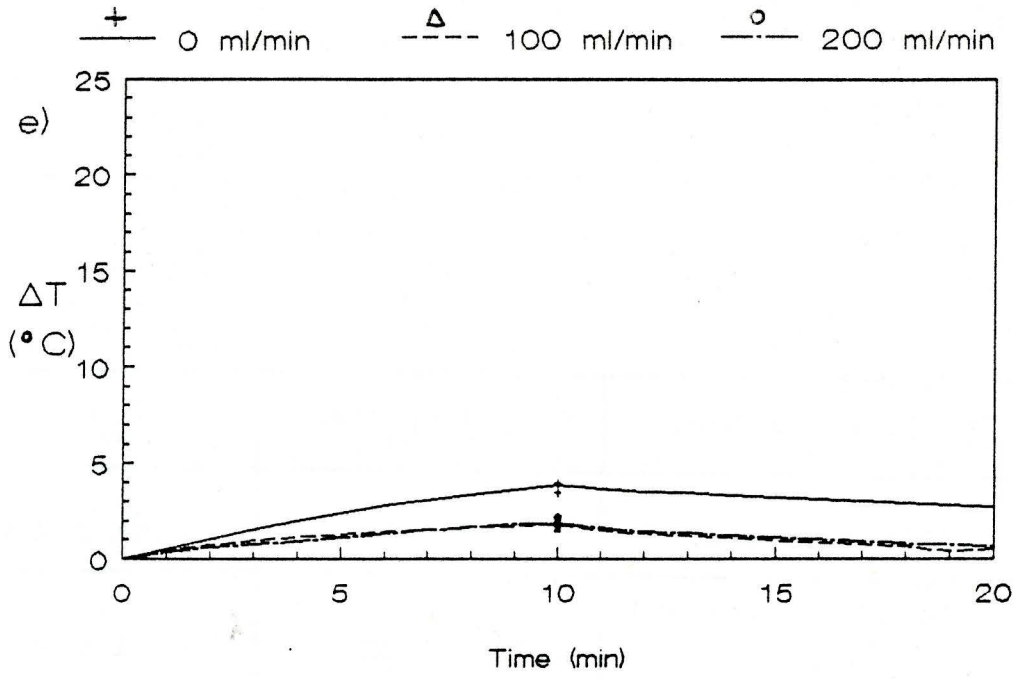

Figure 4.7 (continued)

e) P5 (0.3 cm from vessel surface).

Flow Rate (ml/min)	Pend of tip $_{av}$ (W)	P_{av} (W)
0 (both vessels)	0.79 ± 0.01	2.01 ± 0.08
50 (0.144 cm vessel) 100 (0.40 cm vessel)	0.79 ± 0.02	2.01 ± 0.09
100 (0.144 cm vessel) 200 (0.40 cm vessel)	0.81 ± 0.01	2.07 ± 0.09

Table 4.1 Experimental laser power measurements.

to be no significant decrease in temperature due to the presence of the blood vessel in positions P1 - P4, however, the mean temperatures do show a convective effect. The increasing temperatures for 100 ml/min in positions P1 and P3 probably reflect inconsistent repositioning of the thermocouples. During the 10 minute relaxation period following the laser pulse, there is a significant temperature decrease due to blood flow in positions P3 - P5. Doubling the blood flow rate does not appear to increase this convective heat loss. This suggests that, for both vessels, flow at the initial rate removes most of the removable heat.

At position P2, 0.5 cm from the source, the mean temperature during the laser pulse is slightly higher at 200 ml/min than with no flow. This could reflect the 3% difference in P_{av} at these flow rates. The effects of this difference on the temperature profiles will decrease with increasing distance from the source.

At positions P1 - P4, due to the large experimental temperature variations, the influence of the blood vessel on the temperature distributions during the laser power deposition is unclear. At the end of the

thermal relaxation period, 20 min, the experimental errors are appreciable smaller. Therefore, at time 20 min an investigation into the temperature change due to blood flow can be made.

Using the 0 and 200 ml/min data from figure 4.7, graphs of the mean temperature decrease at 20 min due to convection as a function of distance from the surface of the vessel were plotted (see figure 4.8). The temperature decrease due to convection is inversely proportional to the distance from the surface of the vessel. At distances beyond approximately 2 cm the presence of the functioning blood vessel does not perturb the temperature distributions. A similar plot for the 0.144 cm vessel at 0 and 100 ml/min is shown in figure 4.9. The convective heat loss is smaller with the 0.144 cm vessel. Due to the smaller convective heat loss, the effect of the differences in P_{av} on the temperature distributions becomes more pronounced. This could explain the slight negative values at P1 and P2.

4.3 Model results

The values of the input parameters to the

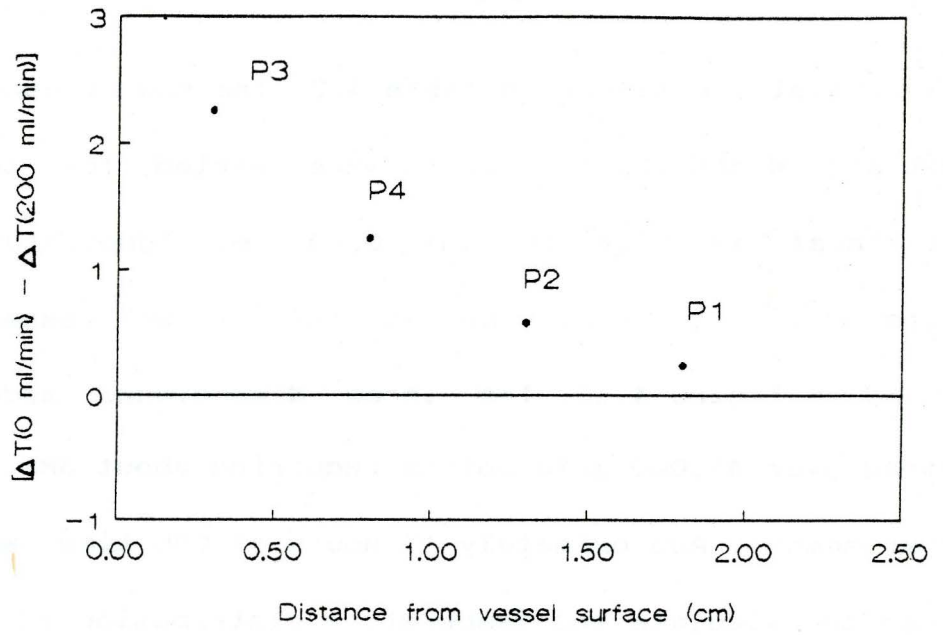

Figure 4.8 Plot of [ΔT(0 ml/min) - ΔT(200 ml/min)] against the radial distance from the surface of the 0.40 cm blood vessel.

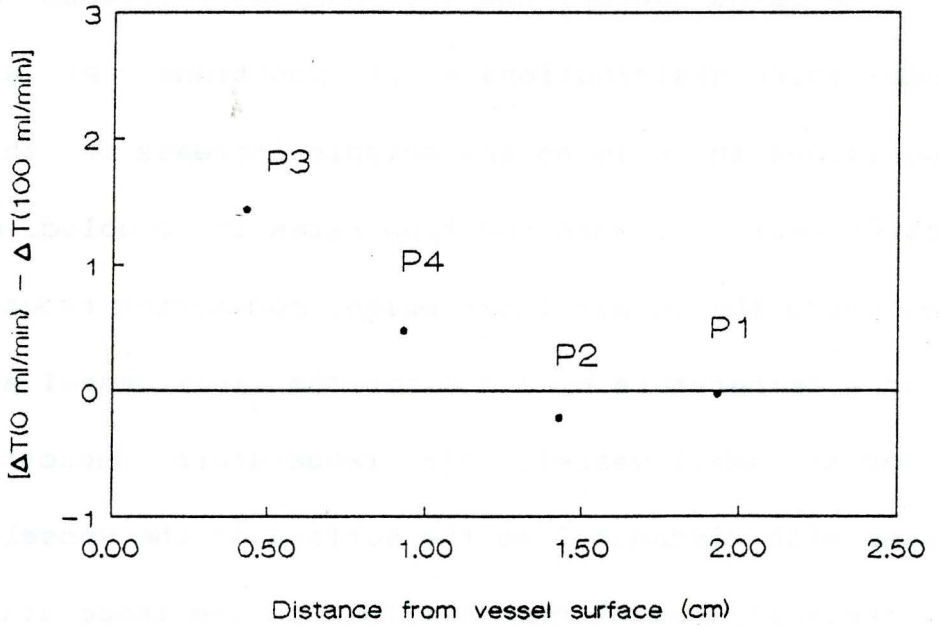

Figure 4.9 Plot of [ΔT(0 ml/min) - ΔT(100 ml/min)] against the radial distance from the surface of the 0.144 cm blood vessel.

computer model are listed in table 4.2. The source power was set at 2 W and the flow rates were varied for two vessel diameters, 0.144 cm and 0.40 cm. Temperature profiles as a function of flow rate for the two vessels are found in figure 4.10. The three dimensional model contained over 45,000 grid points requiring about 3MB of computer memory. Approximately 17 hours of CPU time was required to calculate the temperature distribution at 1 min intervals for a 10 min laser pulse followed by 10 min of thermal relaxation.

The larger vessel has the greatest influence on the temperature distributions at all positions. At all four positions there is no appreciable increase in this convective heat loss when the flow rates are doubled. At P3, following the 10 min laser pulse, convection reduces the tissue temperature by 3.8 $^{\circ}$C for the large vessel and 1.3 $^{\circ}$C for the small vessel. This temperature reduction decreases with distance from the surface of the vessels. At P2, the small vessel has no effect on the temperature as where the larger vessel is still effecting a small temperature change.

Figure 4.11 is a plot of temperature versus

DELTAR	0.1 cm	DIFFT	0.00127 cm^2/sec
DTHETAD	10°	KTISS	0.00493 W/cm/K
DELTAZ	0.2 cm	DIFFB	0.0015 cm^2/sec
ZLENGTH	8.0 cm	KB	0.00623 W/cm/K
DELTAT	60 sec	CB	4.1783 J/g K
TOTALT	1200 sec	DENB	0.99336 g/cm^3
DIV	10	KV	0.0025 W/cm/K
Z1	3.3 cm	CV	1.046 J/g K
Z2	4.8 cm	DENV	3.414g/cm^3
DT	1.0 cm	QM	0 W/cm^3
MUAt	1.81 cm^{-1}	Ta	310 K
MUAb	0.2 cm^{-1}	Wb	0 $g/sec/cm^3$
MUSPt	8.06 cm^{-1}	CRITER	$1\epsilon^{-6}$
LAMBDA	3.2 cm		

Table 4.2 Values of the input parameters to the computer model. a) constant parameters.

	Vessel	
	0.144 cm	0.40 cm vessel
R1	Rv (with flow)	Rv (with flow)
	Rv (without flow)	0.1 cm (without flow)
EVENR	0.128 cm	0.1 cm
VEL	0 cm/sec	0 cm/sec
	51 cm/sec	13.26 cm/sec
	102 cm/sec	26.52 cm/sec
IFLAG	10 (with flow)	9 (with flow)
	10 (without flow)	10 (without flow)
JFLAG	1	1

Table 4.2 (continued)

b) parameters which vary with vessel diameter.

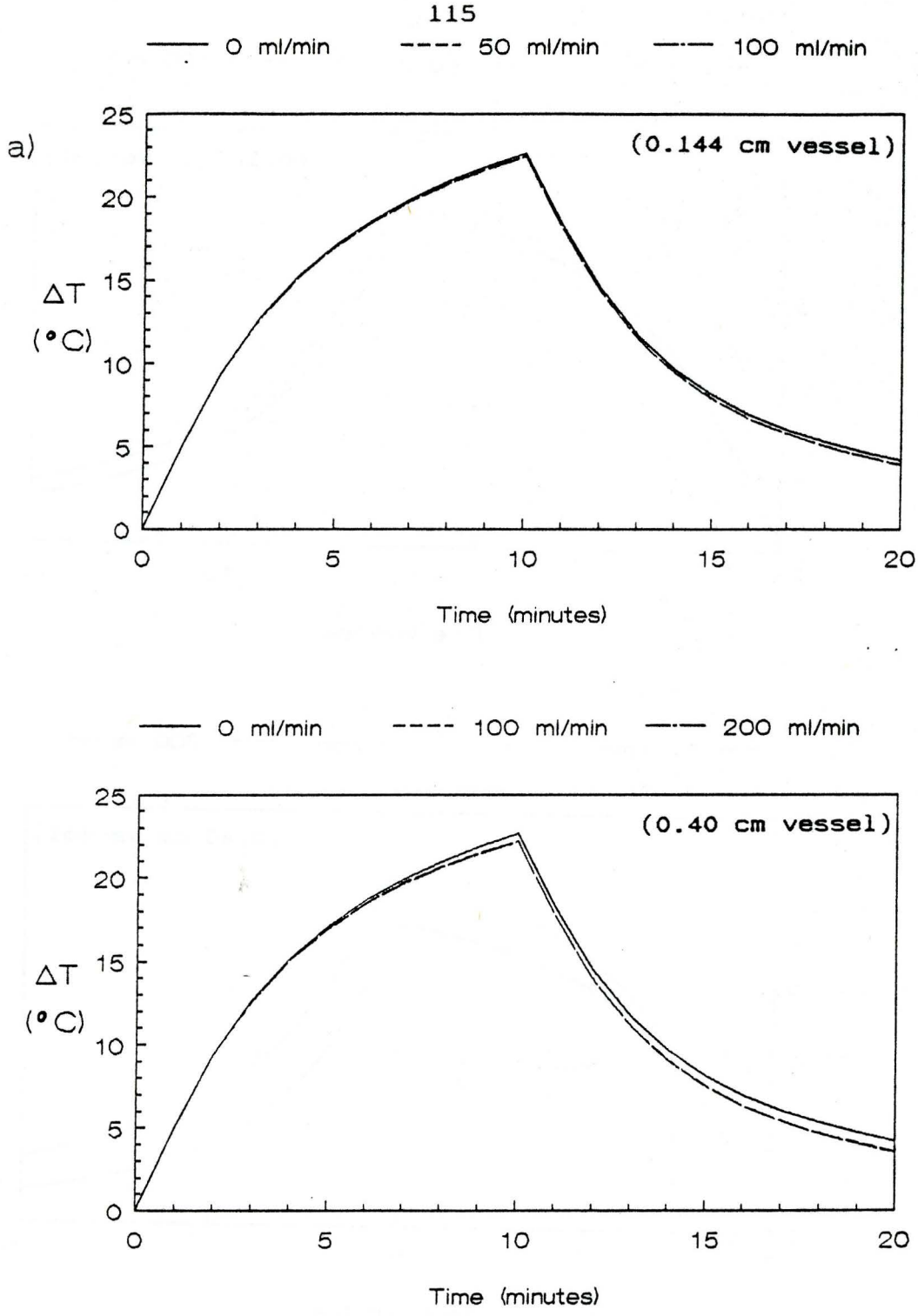

Figure 4.10 Predicted model temperatures for the 0.144 cm and 0.40 cm vessels at positions P2, P3 - P5.

a) P2

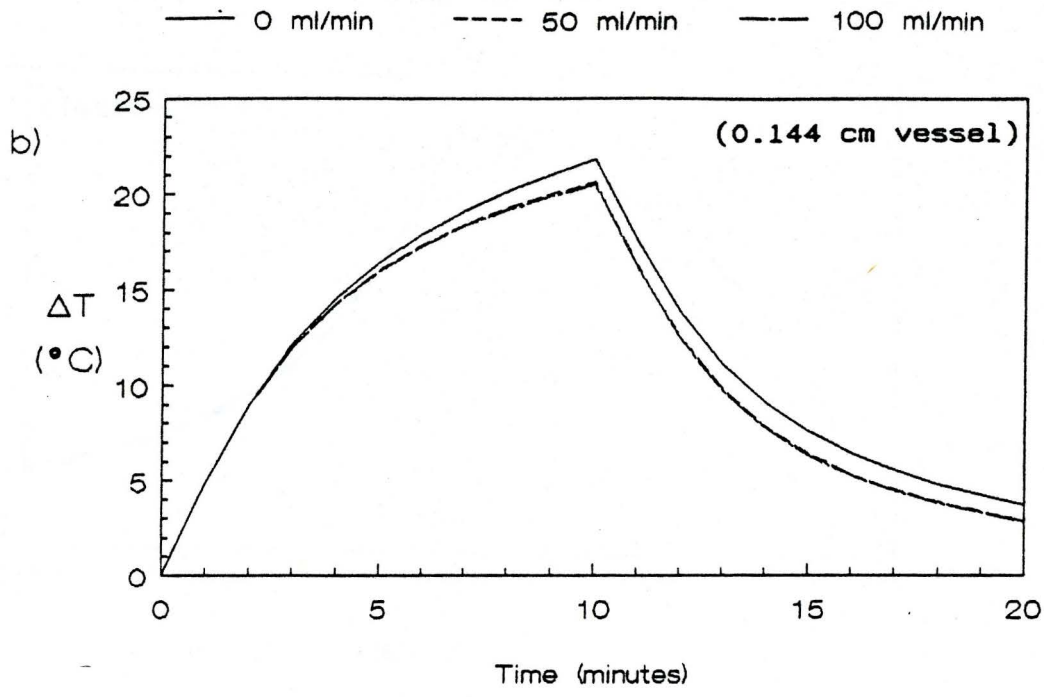

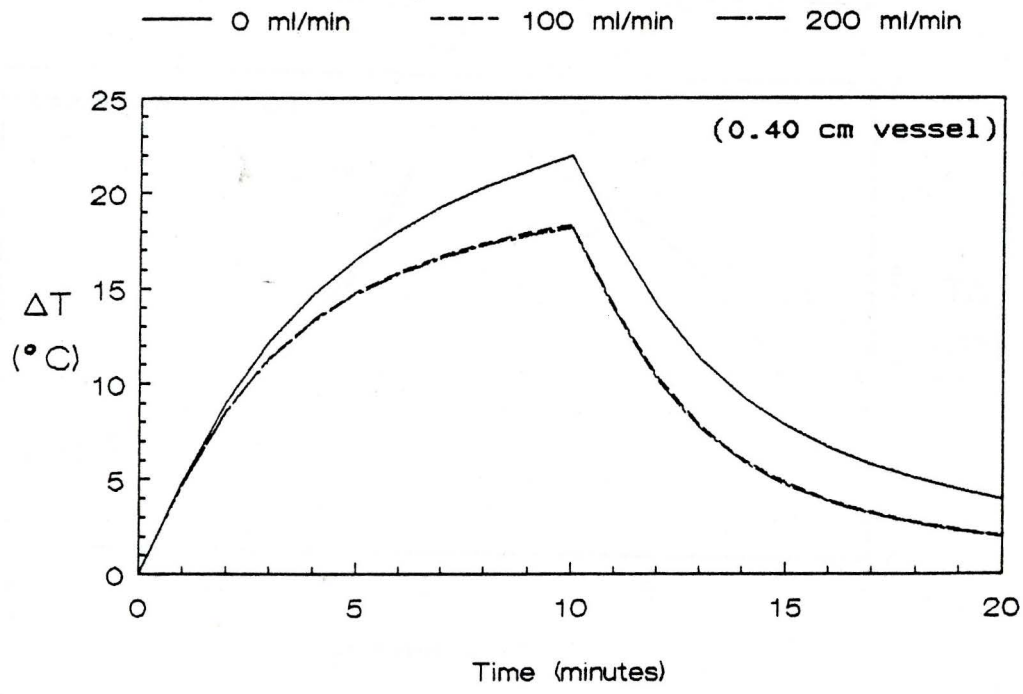

Figure 4.10 (continued)

b) P3

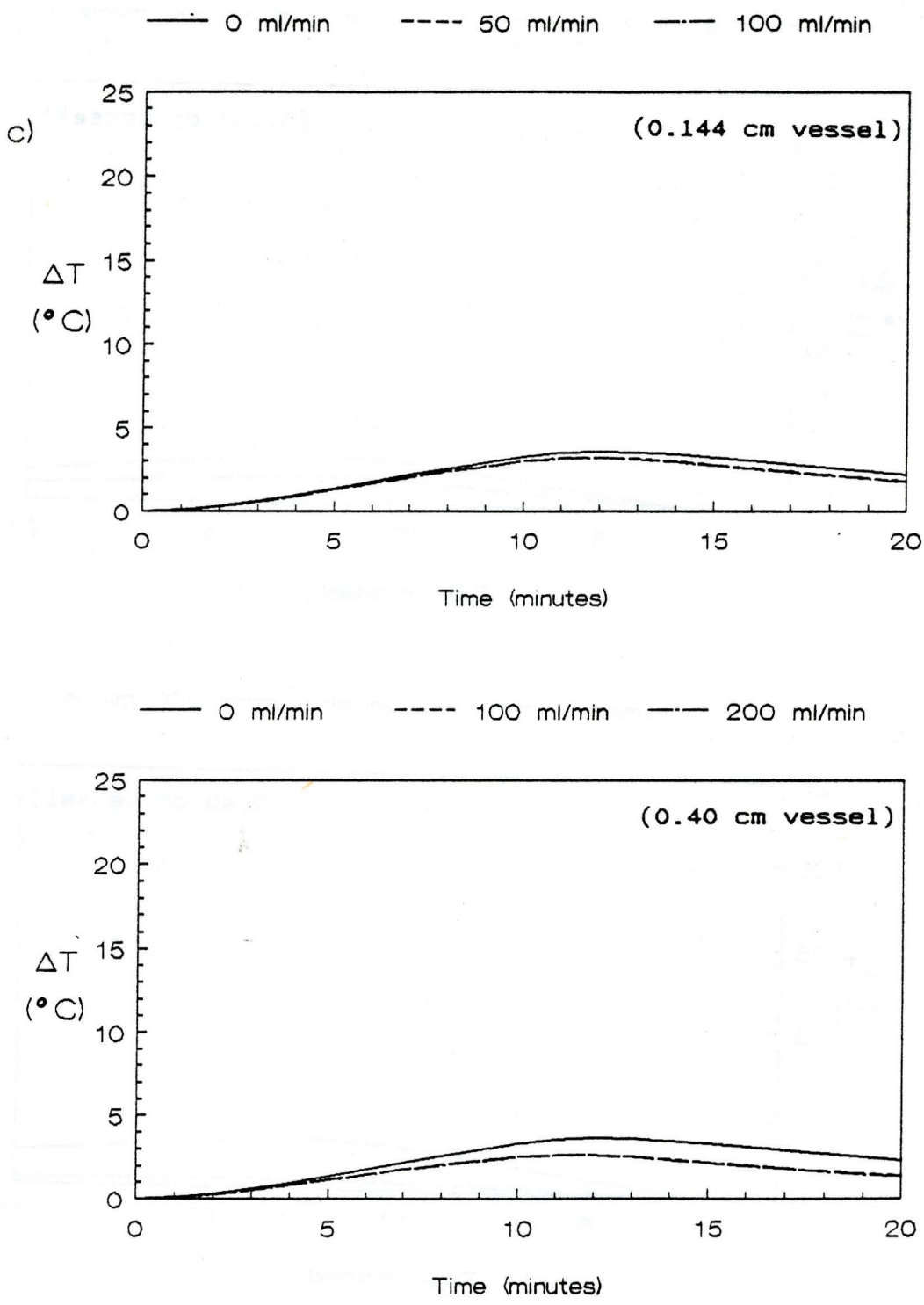

Figure 4.10 (continued)

c) P4

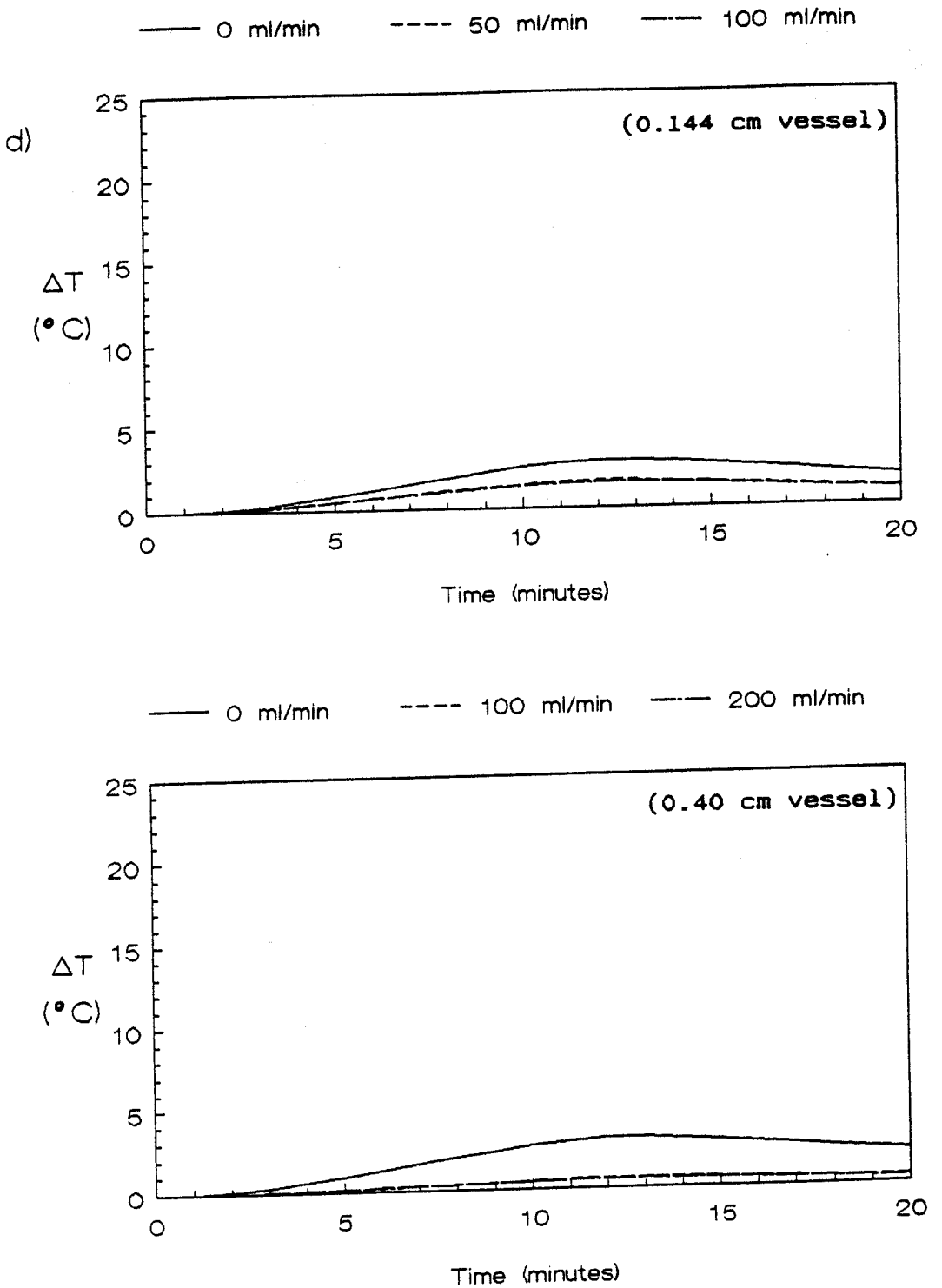

Figure 4.10 (continued)

d) P5

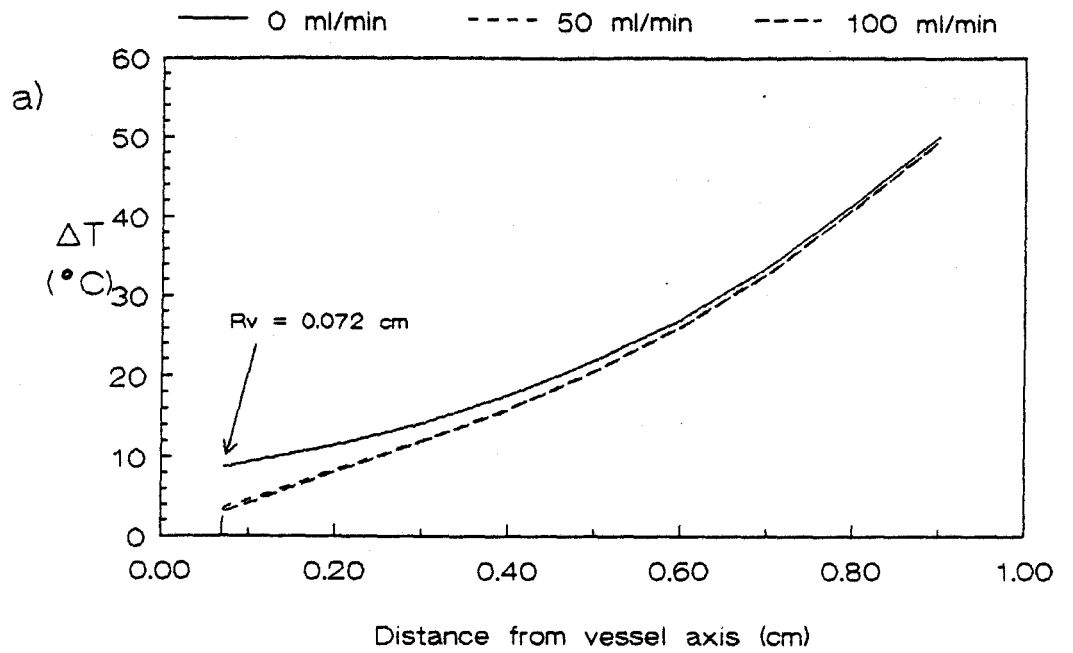

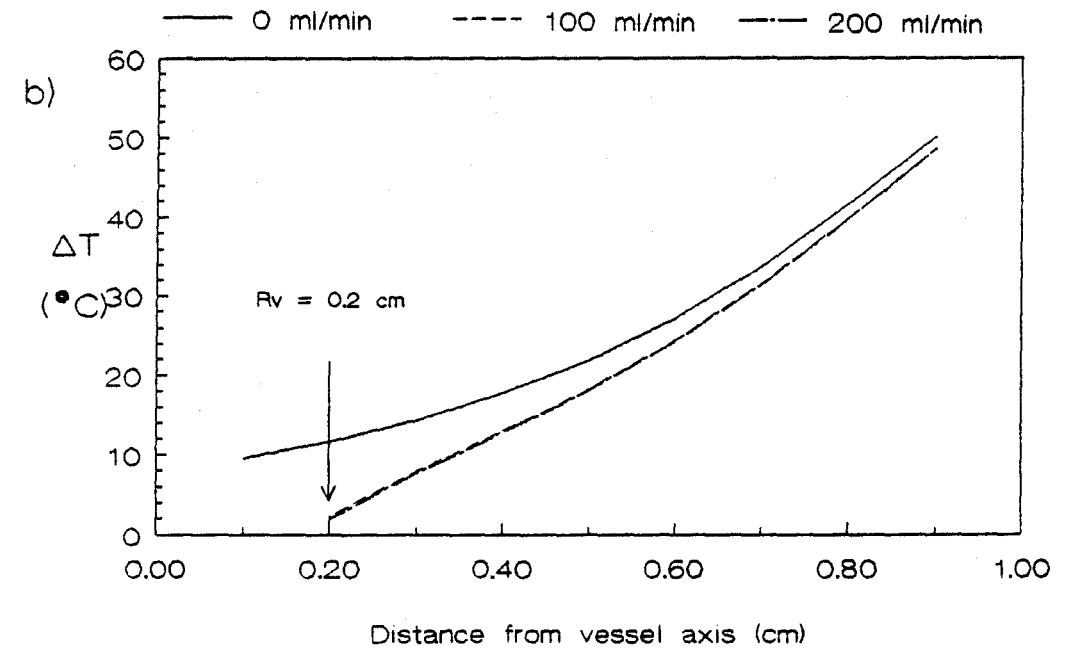

Figure 4.11 Temperature change as a function of radial distance from a functioning blood vessel immediately after a 10 min laser pulse.

a) 0.144 cm vessel.

b) 0.40 cm vessel.

radial distance from the axes of the vessels immediately after the 10 min laser pulse. The temperatures at the surfaces of both vessels for a flow rate of 100 ml/min are appoximately the same.

Given that the surface of the 0.40 cm vessel is closer to the light source, the temperature of the surface in the absence of flow will be greater than the corresponding temperature for the 0.144 cm vessel. Therefore, the temperature decrease at the surface of the 0.40 cm vessel due to a flow rate of 100 ml/min will be greater than that for the 0.144 cm vessel at the same flow rate. This is shown in figure 4.11.

Both vessels show no appreciable increase in convection when the flow rates are doubled. The model predicts that any significant temperature changes due to the presence of a functioning blood vessel are limited to a small region surrounding the vessel. If one considers temperature reductions of 2 $^{\circ}$C and greater to be significant, this would correspond to a distance up to 0.3 cm from the surface of the 0.144 cm vessel and 0.8 cm for the 0.40 cm vessel.

4.4 Comparison of model predictions with experimental results

The proper average power values (P_{av}) for each flow rate for the two vessels were used to generate a new set of model results which could be compared to the experimental findings. A direct comparison between the model and the experiments for the two vessels at three thermocouple positions, P2, P3 and P5, is shown in figures 4.12 and 4.13.

Figures 4.12 and 4.13 show that the model overestimates temperatures near the source and underestimates temperatures far from the source at all flow rates. At P2, the model temperatures are approximately 1 - 2°C above the range of experimental measurements. At P5, the model temperatures are approximately 1 - 2°C below the range of experimental measurements.

The model results are strongly dependent on the thermal conductivity of the material and the total laser power. The temperature difference could be due to errors in these values. The thermal properties were

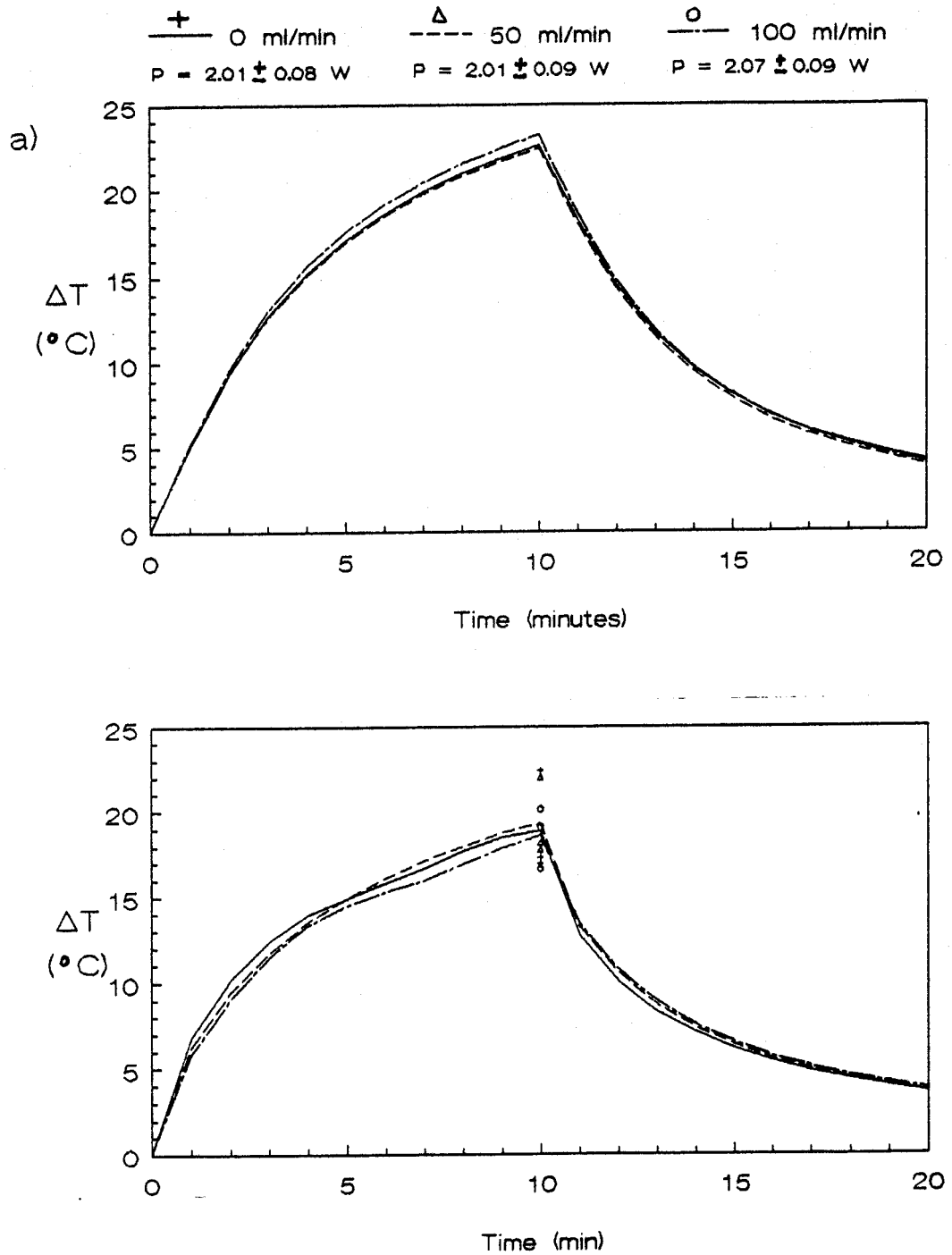

Figure 4.12 Comparison of model predictions (top graph) and experimental temperatures (bottom graph) for the 0.144 cm vessel.

a)at P2

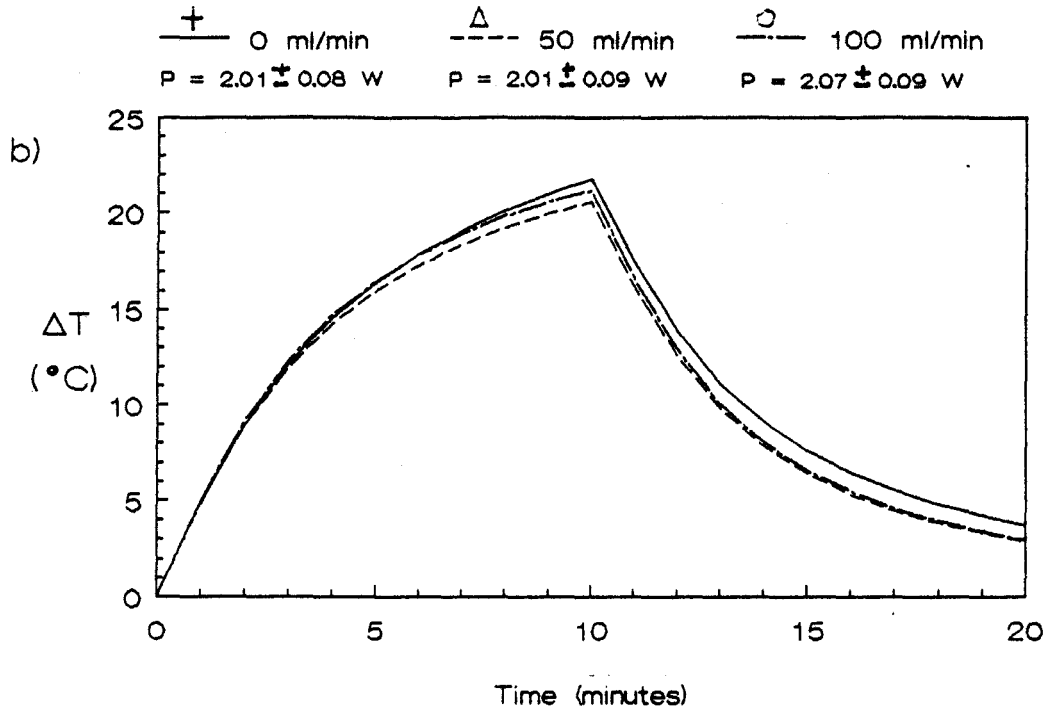

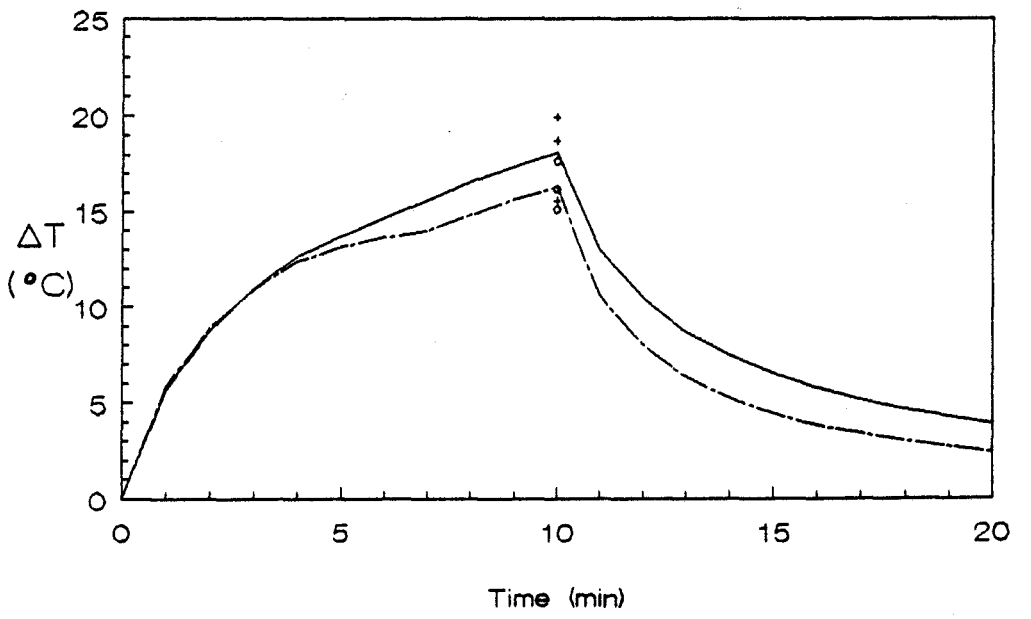

Figure 4.12 (continued)

b)at P3

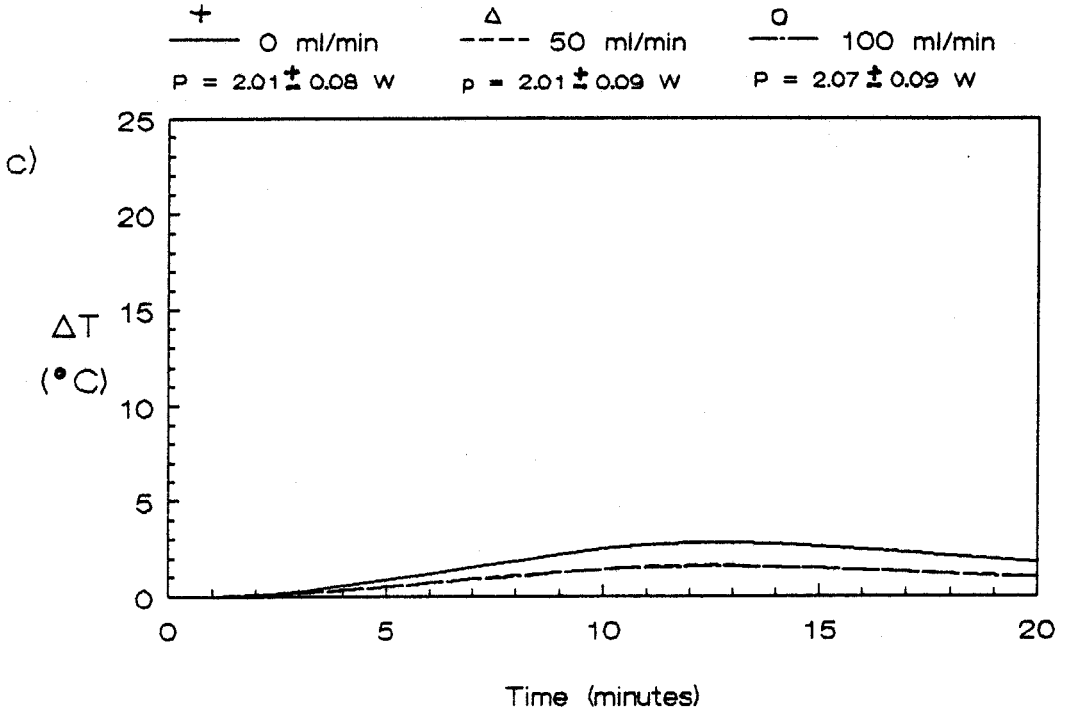

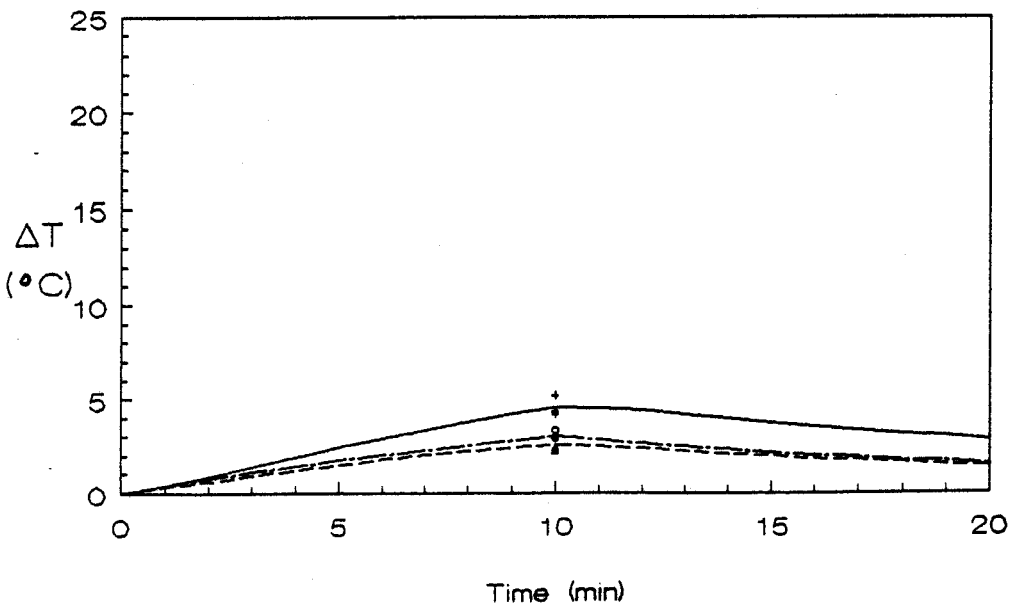

Figure 4.12 (continued)

c)at P5

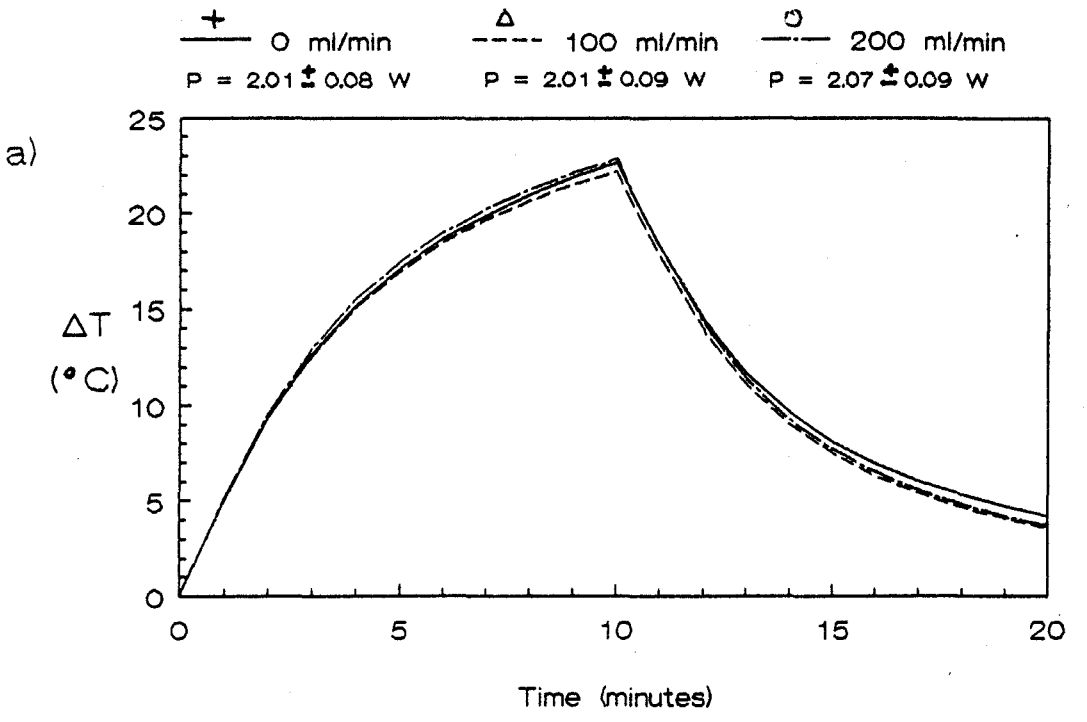

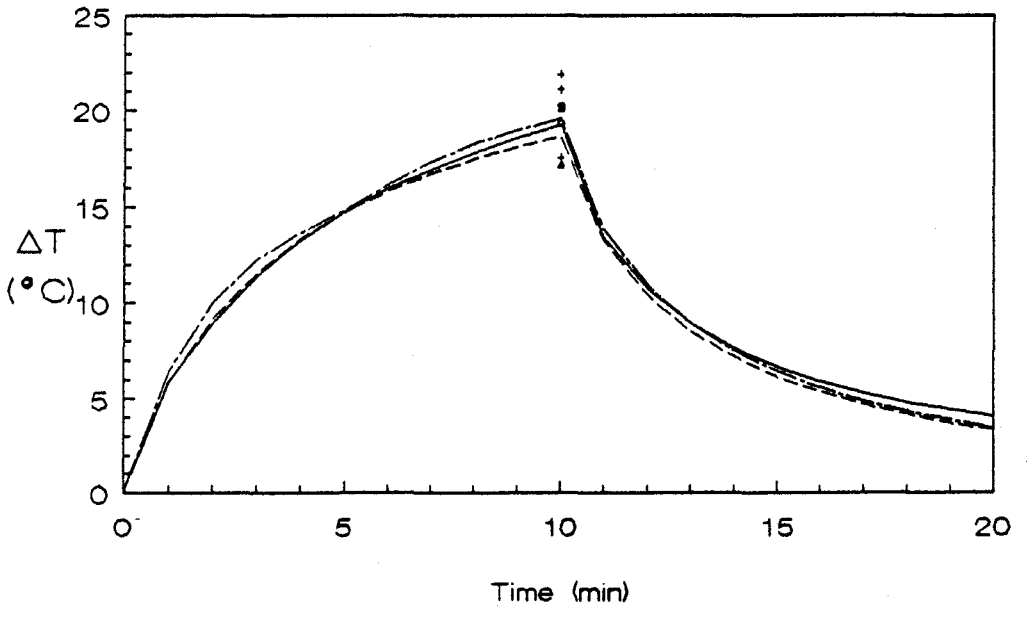

Figure 4.13 Comparison of model predictions (top graph) and experimental temperatures (bottom graph) for the 0.40 cm vessel.

a)at P2

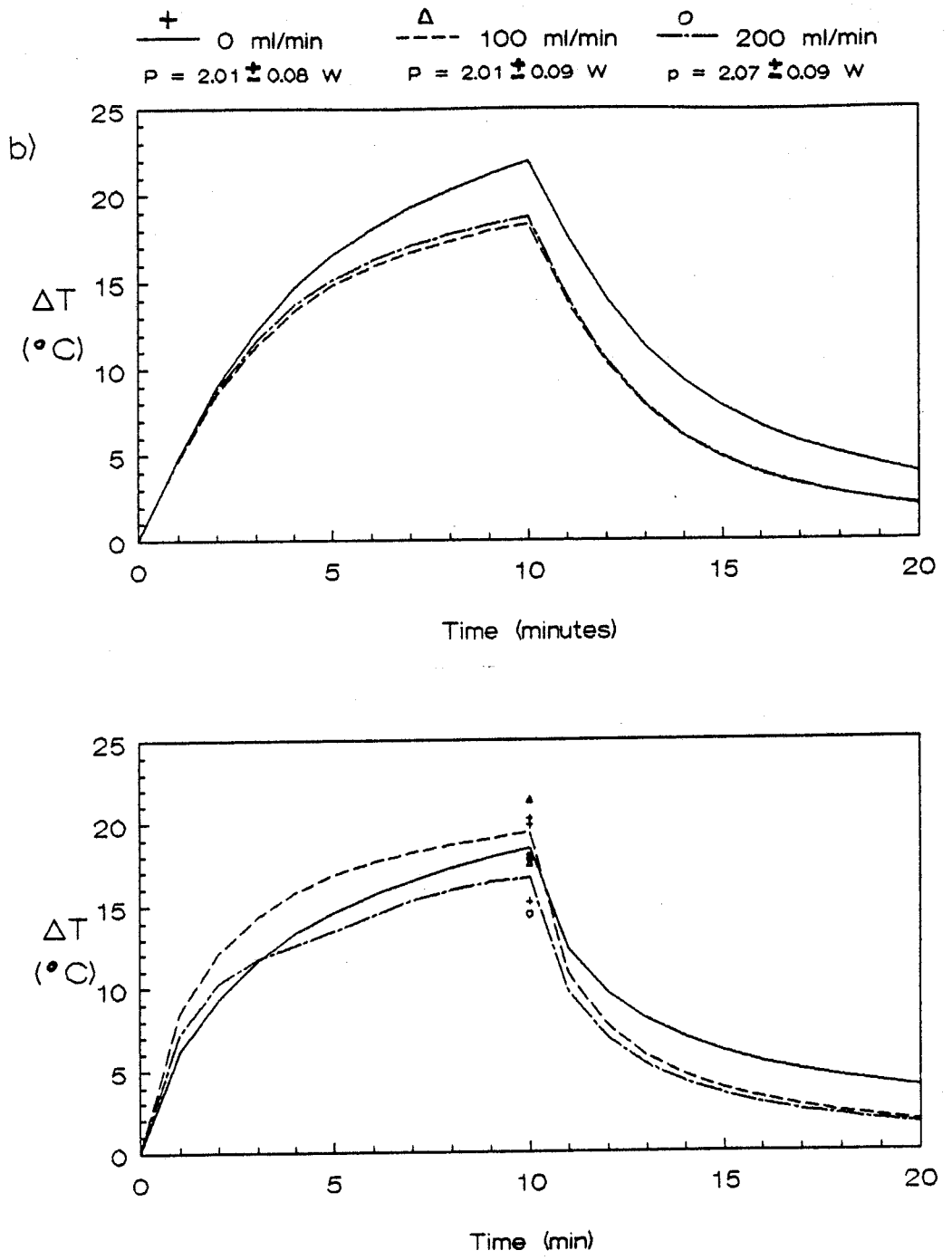

Figure 4.13 (continued)

b)at P3

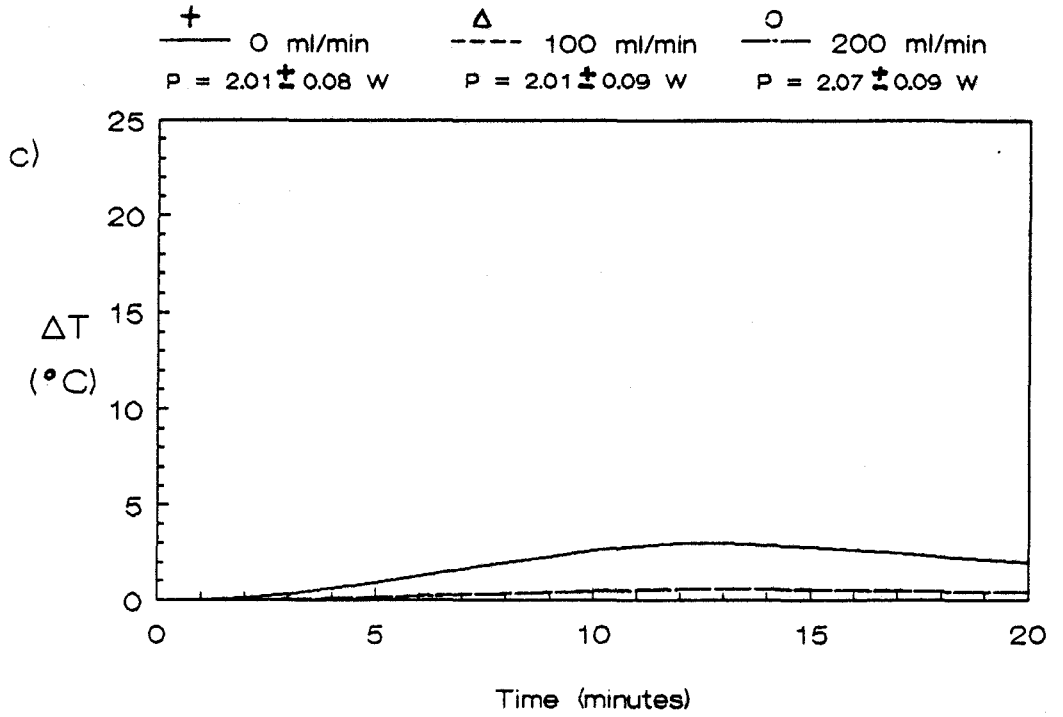

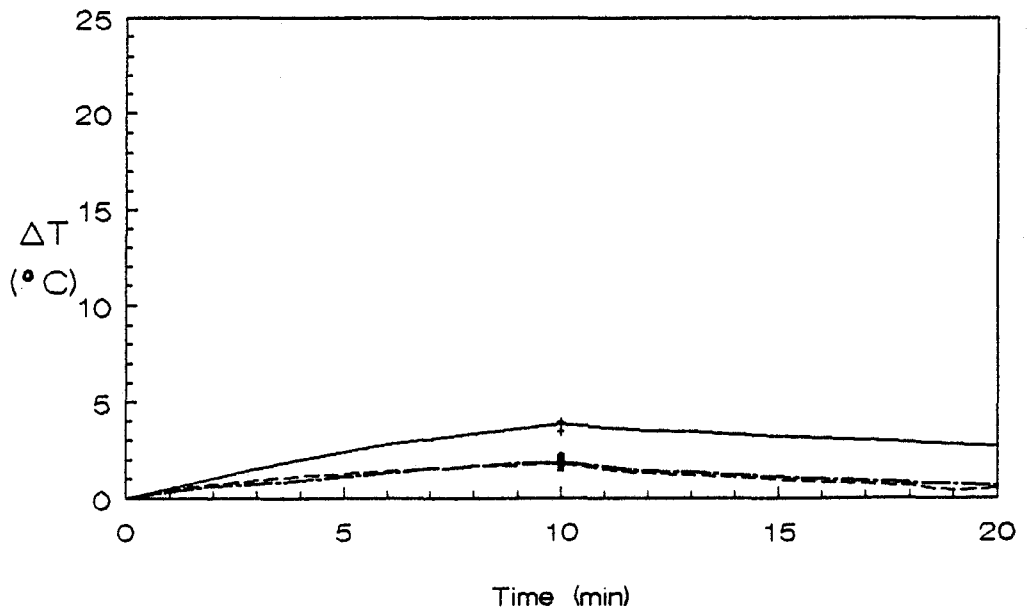

Figure 4.13 (continued)

c)at P5

approximated from published values. The laser power calibration factor had an inherent uncertainty associated with it.

In order to possibly improve the correlation between absolute temperatures, temperature profiles as a function of the thermal conductivity and total laser power were generated. Figure 4.14 shows the results of increasing the thermal conductivity from the average value of 4.93×10^{-3} W/cm K to its determined upper limit of 5.51×10^{-3} W/cm K. At 0.5 cm from the source, P3, there is a consistent decrease in temperature. At 1.5 cm from the source, P5, there is a small increase in temperature. This temperature shift is in a direction that would improve the correlation between absolute model and experimental temperatures. This increase in thermal conductivity brings the model temperatures into the range of experimental values at P2 and P3 for both vessels.

Figure 4.15 shows the dependence of the model temperatures with the total power following the laser pulse at distances radially outward from the source. Total laser power values of 2.0 W, 1.9 W (-5%) and 1.8 W

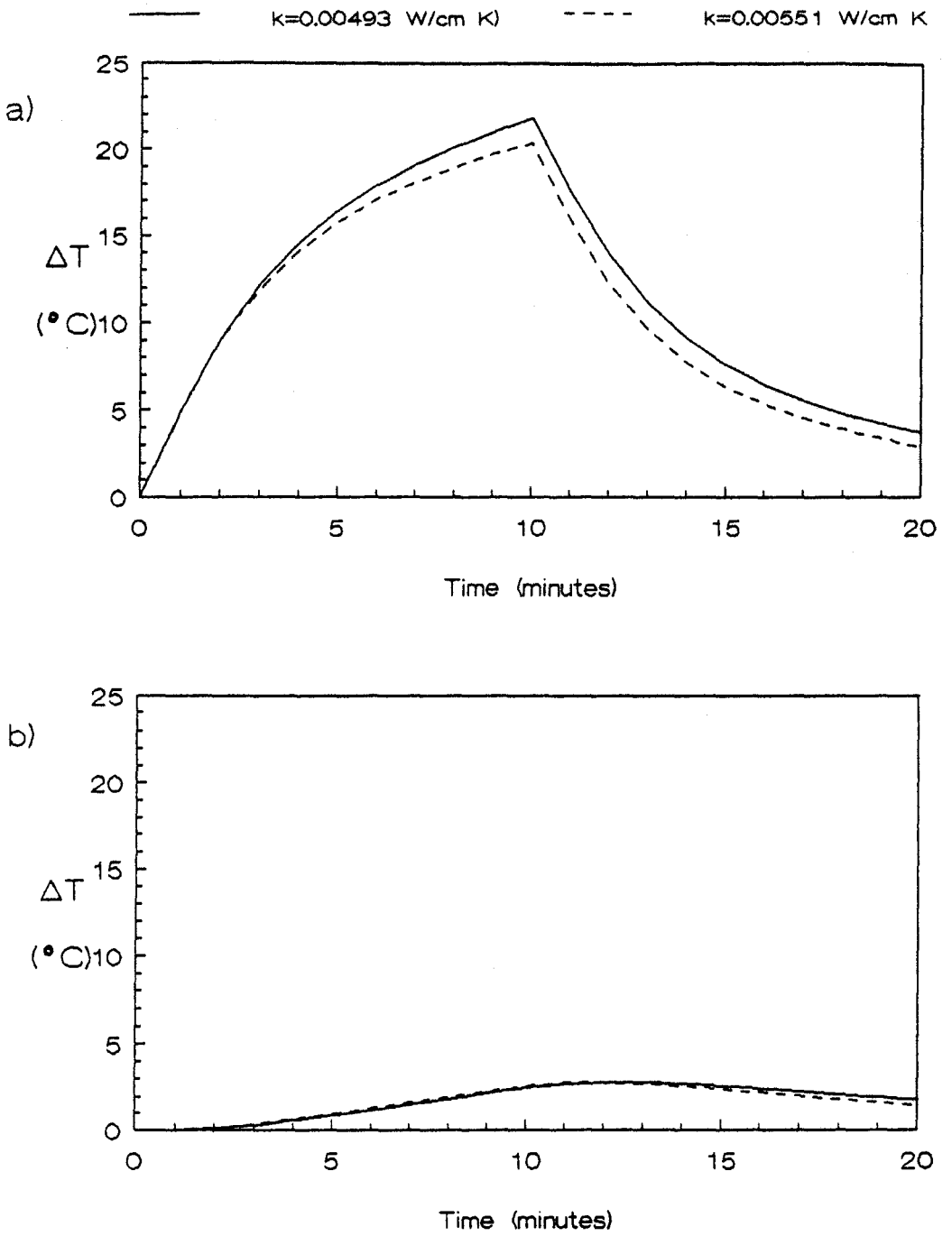

Figure 4.14 Model temperatures as a function of the thermal conductivity.

a)at P3

b)at P5

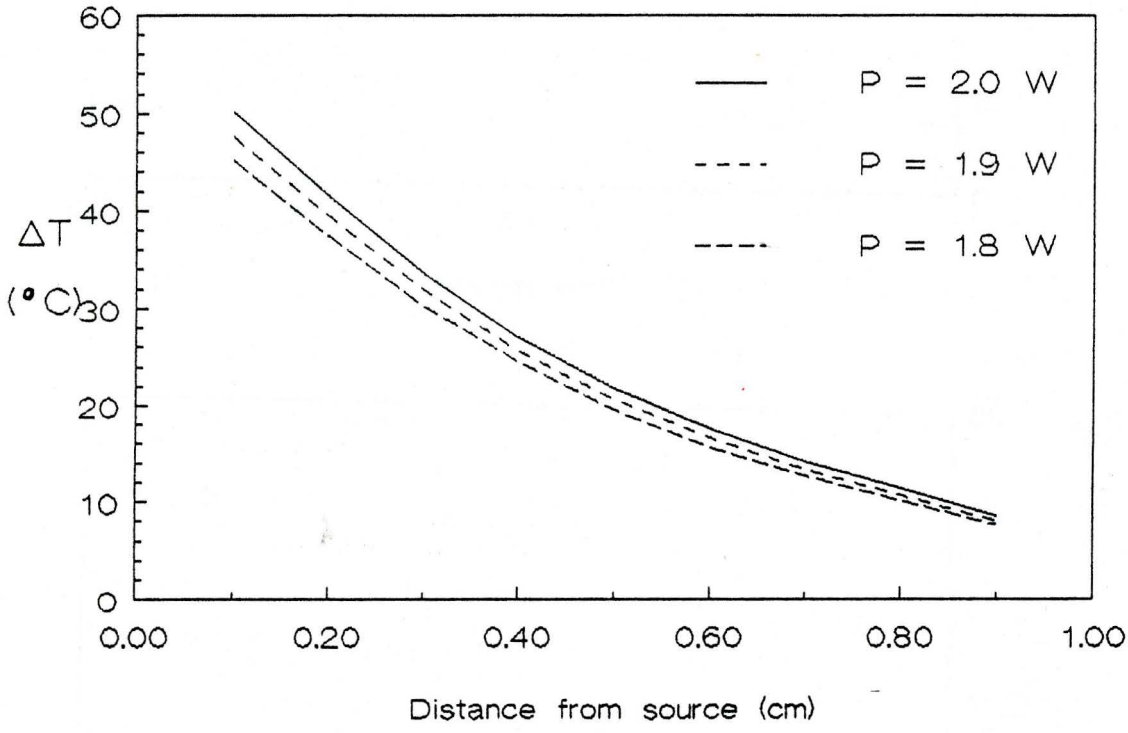

Figure 4.15 Model temperatures at radial distances from the source as a function of the total laser power.

(-10%) were used. The resulting temperatures appear to decrease linearly as power is decreased. At P3, a 10% power decrease corresponds to a 2°C temperature decrease. At P5, there is only a 0.3°C decrease. Using the 0.144 cm vessel with no flow as an example, the total laser power is 2.01 ± 0.08 W.

Assuming the linearity of figure 4.15, the lower range of the total laser power would yield a temperature decrease of 1°C at P3 and 0.2°C at P5. This would improve the correlation between the absolute model and experimental temperatures at points close to the source.

A comparison between the measured and model-predicted convective heat loss due to blood flow is shown in figures 4.16 and 4.17. As mentioned in section 4.2.1, the magnitude of the experimental errors during the laser pulse make such a comparison difficult in that time interval. In figures 4.16 and 4.17 the convective heat loss is shown at 5 and 10 minutes after the laser is turned off.

The errors bars represent one standard deviation from the mean temperatures. At positions greater than approximately 0.3 cm from the surface of these vessels,

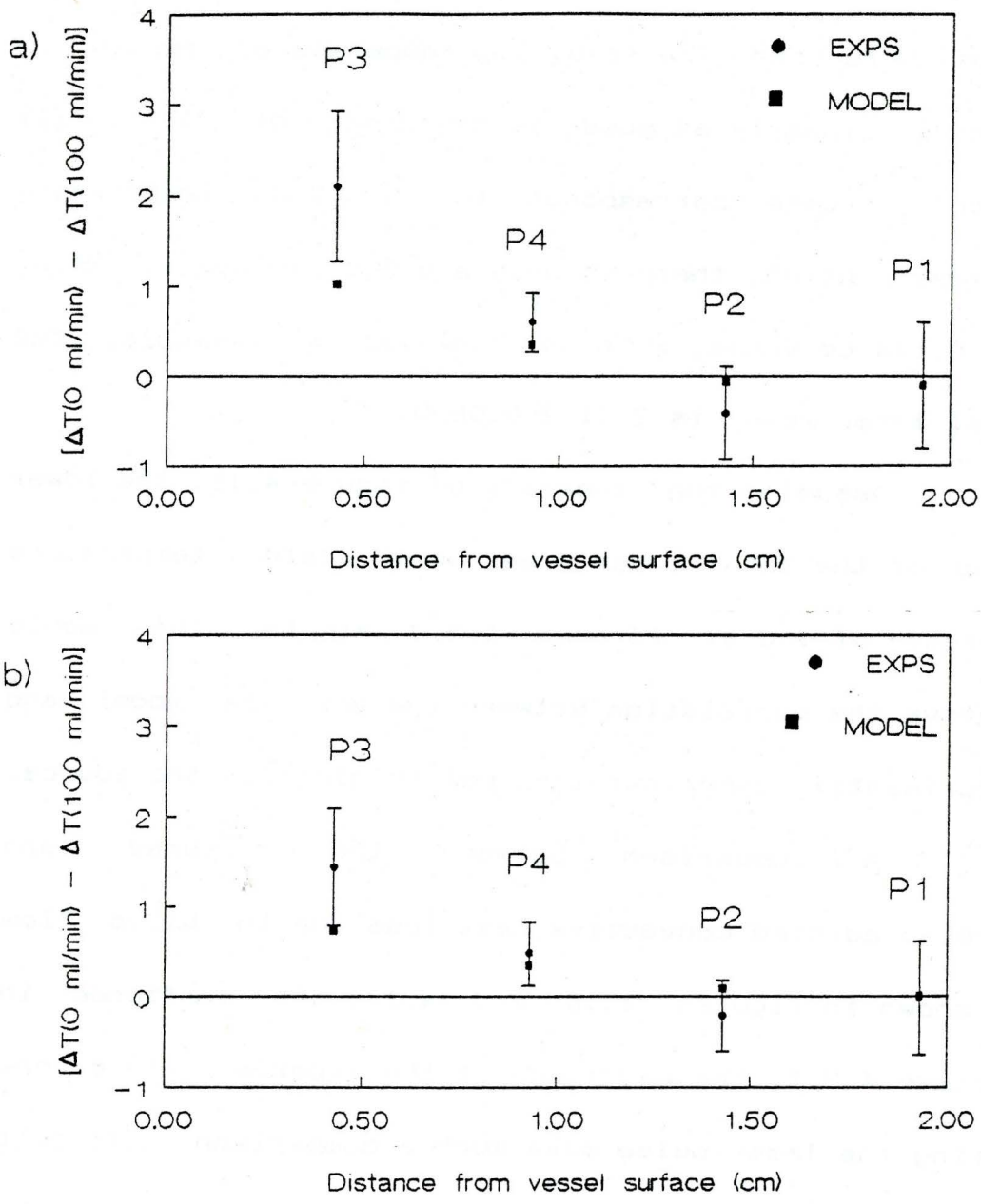

Figure 4.16 Correlation between the predicted and measured temperature decrease due to blood flowing in a 0.144 cm vessel at a rate of 100 ml/min.

a) at 5 minutes following laser pulse.

b) at 10 minutes following laser pulse.

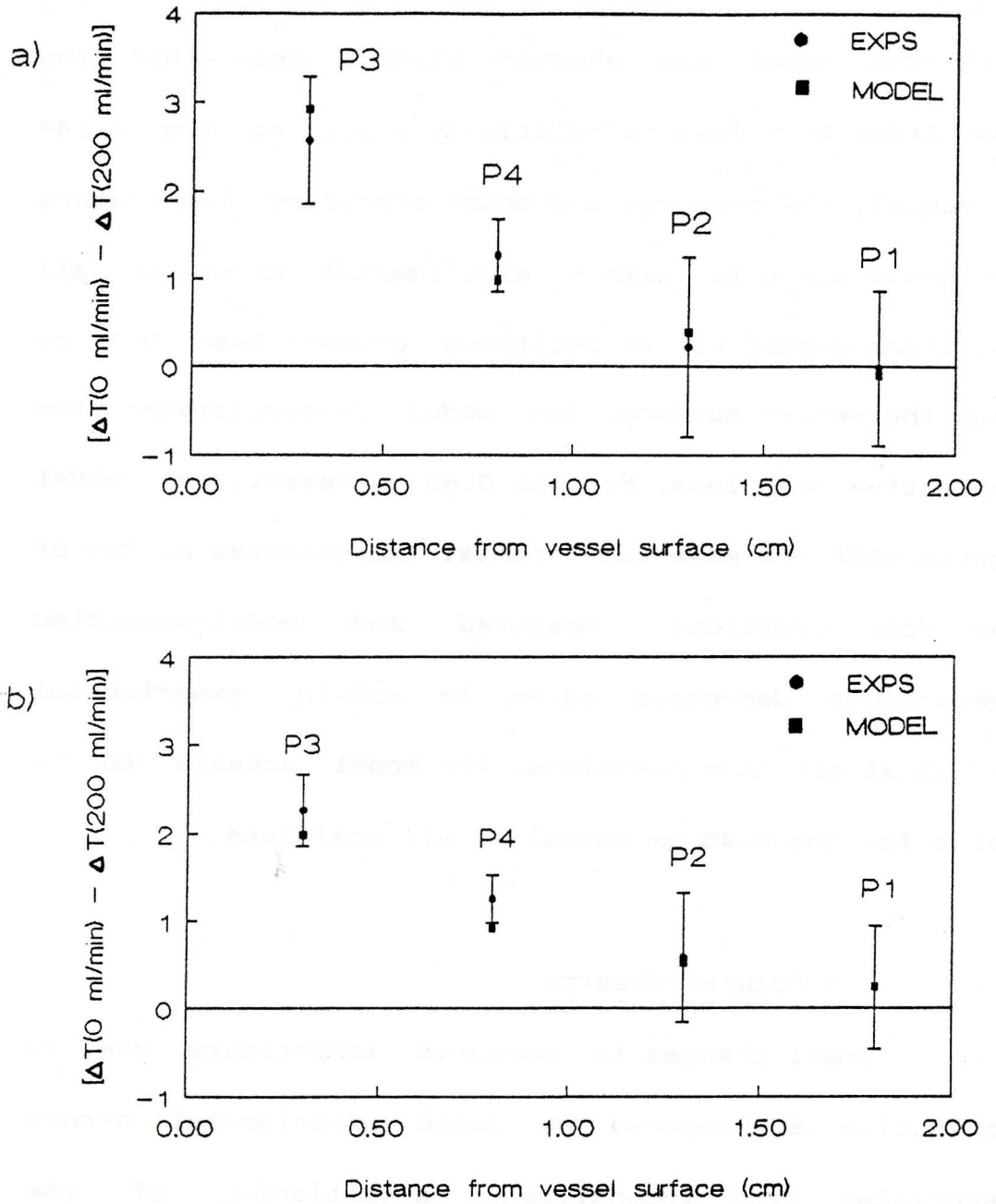

Figure 4.17 Correlation between the predicted and measured temperature decrease due to blood flowing in a 0.40 cm vessel at a rate of 200 ml/min.

a) at 5 minutes following laser pulse.

b) at 10 minutes following laser pulse.

both the model and phantom studies show that the convective heat loss is relatively small. For the 0.144 cm vessel, the measured and model-predicted temperature decreases agree to within experimental error in all positions except P3. At positions closer than 0.9 cm from the vessel surface, the model underestimates the convective heat loss. For the 0.40 cm vessel, the model agrees with the mean experimental temperatures at two of the four positions. Measured and model-predicted temperature decreases agree to within experimental errors at all four positions. The model appears to be valid for the 0.40 cm vessel at all positions.

4.5 Future research

Small changes in measured temperature due to convection is hampered by large experimental errors associated with inconsistent repositioning of the thermocouples. Thermocouple positioning accuracy could be improved using imaging techniques.

The model developed for this project will be used to investigate changes in thermal profiles due to variations in the source-to-fiber spacing, estimated

blood flow rate, the proximity of a "thermally significant" vessel and the treatment time.

The model geometry used in this project is simple when compared to the complex geometry in vivo. A more sophisticated model based on the present one could be developed which would include the effects of radiative heat losses from the surface of the skin and convective heat losses from a distribution of "thermally significant" blood vessels.

CHAPTER 5

SUMMARY

A three-dimensional computer model was developed to predict temperature distributions around large blood vessels during laser-induced hyperthermia. The model is based on the Bioheat Transfer Equation (BHTE) which has been used extensively to model heat transfer in tissue. Separate BHTEs were derived for blood, vessel wall and tissue. The light distribution was determined using transport theory with measured absorption and reduced scattering coefficients. The finite differences method was used to solve the BHTEs for temperatures in blood, vessel and tissue.

The finite differencing scheme was verified by comparing the model results with analytical solutions for the case of an infinite line heat source. A series of dynamic phantom studies were carried out and the results used to establish the validity of the model.

Two vessel diameters each with three flow rates were investigated. Comparisons between the model and

experiments were made at the positions where thermocouples were implanted in the tissue. The absolute temperatures predicted by the model were consistently higher than the average measured values at positions near the light source. The reverse was true at positions far from the source. Large experimental errors associated with inconsistent repositioning of thermocouples during each experiment made a comparison of absolute temperatures difficult.

By isolating the effects of blood flow on the temperature distributions following the laser pulse, the convective heat loss predicted by the model was comparable to the average measured values. For the 0.144 cm vessel, measured and model-predicted temperatures agree to within experimental errors at three of the four measurement sites. The greatest deviation was at the site closest to the surface of the vessel. For the 0.40 cm vessel, the agreement was better. Model-predicted temperatures agreed with the mean experimental temperatures at two of the four sites. At the other two sites the model-predicted temperatures differed slightly from the mean measured values.

Overall, the three dimensional computer model predicts temperature changes due to blood flow. The true validity of the model is unclear because of the large experimental errors. The range of vessel diameters and flow rates for which the model is valid could be determined in the same manner as this project. The statistical value of the experimental results could be improved by the development of a reusable phantom with well known physical, thermal and optical properties. More reliable thermocouple positioning techniques could also reduce experimental errors.

This model can provide useful information about the distances at which large blood vessels can effect temperature perturbations as well as the treatment limitations imposed by the presence of such vessels. Such knowledge is necessary in order to optimize a treatment protocol.

APPENDIX A

FINITE DIFFERENCE EXPRESSIONS FOR THE BIOHEAT TRANFER EQUATIONS

Bioheat transfer equation for tissue

$$T_{i,j,k}^{s+1} =$$

$$\left[\left(\frac{2r\Delta r_2 + \Delta r_2^2}{r\Delta r_1 \Delta r_2(\Delta r_1 + \Delta r_2)}\right) T_{i+1,j,k}^{s+1} + \left(\frac{2r\Delta r_1 - \Delta r_1^2}{r\Delta r_1 \Delta r_2(\Delta r_1 + \Delta r_2)}\right) T_{i-1,j,k}^{s+1} +\right.$$

$$\left(\frac{2\Delta\theta_2}{r^2\Delta\theta_1\Delta\theta_2(\Delta\theta_1 + \Delta\theta_2)}\right) T_{i,j+1,k}^{s+1} + \left(\frac{2\Delta\theta_1}{r^2\Delta\theta_1\Delta\theta_2(\Delta\theta_1 + \Delta\theta_2)}\right) T_{i,j-1,k}^{s+1} +$$

$$\left(\frac{1}{\Delta z^2}\right) T_{i,j,k+1}^{s+1} + \left(\frac{1}{\Delta z^2}\right) T_{i,j,k-1}^{s+1} + \left(\frac{\rho t c t}{kt\Delta t}\right) T_{i,j,k}^{s} + \frac{wbcb}{kt} Ta +$$

$$\left.\left(\frac{Q_M + Q_{L_{i,j,k}}}{kt}\right)\right] \Big/ \left[\frac{\rho t c t}{kt\Delta t} + \frac{2}{\Delta r_1 \Delta r_2} + \frac{(\Delta r_2 - \Delta r_1)}{r\Delta r_1 \Delta r_2} +\right.$$

$$\left.\frac{2}{r^2\Delta\theta_1\Delta\theta_2} + \frac{2}{\Delta z^2} + \frac{wbcb}{kt}\right]$$

Bioheat tranfer equation for vessel

Knowledge of $T_{i-1,j,k}^{s+1}$ is nolonger required because it is replaced by a term containing Tb_k^{s+1}. Therefore the radial component can be differenced evenly, simplifying the expression.

$$T_{i,j,k}^{s+1} =$$

$$\left(\left(\frac{2}{\Delta r^2} \right) T_{i+1,j,k}^{s+1} + \left(\frac{(2r - \Delta r)hs}{r \Delta r kbc} \right) Tb_k^{s+1} + \right.$$

$$\left(\frac{2\Delta\theta_2}{r^2 \Delta\theta_1 \Delta\theta_2 (\Delta\theta_1 + \Delta\theta_2)} \right) T_{i,j+1,k}^{s+1} + \left(\frac{2\Delta\theta_1}{r^2 \Delta\theta_1 \Delta\theta_2 (\Delta\theta_1 + \Delta\theta_2)} \right) T_{i,j-1,k}^{s+1} +$$

$$\left. \left(\frac{1}{\Delta z^2} \right) T_{i,j,k+1}^{s+1} + \left(\frac{1}{\Delta z^2} \right) T_{i,j,k-1}^{s+1} + \left(\frac{\rho vcv}{kbc \Delta t} \right) T_{i,j,k}^{s} + \left(\frac{QM + QL_{i,j,k}}{kbc} \right) \right)$$

$$\Big/ \left(\frac{\rho vcv}{kbc \Delta t} + \frac{2}{\Delta r^2} + \frac{(2r - \Delta r)hs}{r \Delta r kbc} + \frac{2}{r^2 \Delta\theta_1 \Delta\theta_2} + \frac{2}{\Delta z^2} \right)$$

Bioheat transfer equation for blood (no flow)

$$T_{i,j,k}^{s+1} =$$

$$\left(\left(\frac{2r\Delta r_2 + \Delta r_2^2}{r\Delta r_1 \Delta r_2 (\Delta r_1 + \Delta r_2)} \right) T_{i+1,j,k}^{s+1} + \left(\frac{2r\Delta r_1 - \Delta r_1^2}{r\Delta r_1 \Delta r_2 (\Delta r_1 + \Delta r_2)} \right) T_{i-1,j,k}^{s+1} + \right.$$

$$\left(\frac{2\Delta\theta_2}{r^2 \Delta\theta_1 \Delta\theta_2 (\Delta\theta_1 + \Delta\theta_2)} \right) T_{i,j+1,k}^{s+1} + \left(\frac{2\Delta\theta_1}{r^2 \Delta\theta_1 \Delta\theta_2 (\Delta\theta_1 + \Delta\theta_2)} \right) T_{i,j-1,k}^{s+1} +$$

$$\left. \left(\frac{1}{\Delta z^2} \right) T_{i,j,k+1}^{s+1} + \left(\frac{1}{\Delta z^2} \right) T_{i,j,k-1}^{s+1} + \left(\frac{\rho bc\, b}{kb\Delta t} \right) T_{i,j,k}^{s} + \left(\frac{QM + QL_{i,j,k}}{kb} \right) \right)$$

$$\Big/ \left(\frac{\rho bc\, b}{kb\Delta t} + \frac{2}{\Delta r_1 \Delta r_2} + \frac{(\Delta r_2 - \Delta r_1)}{r\Delta r_1 \Delta r_2} + \frac{2}{r^2 \Delta\theta_1 \Delta\theta_2} + \frac{2}{\Delta z^2} \right)$$

Bioheat transfer equation for blood (with flow)

$$T_{i,j,k}^{s+1} =$$

$$\left[\left(\frac{2r\Delta r_2 + \Delta r_2^2}{r\Delta r_1 \Delta r_2 (\Delta r_1 + \Delta r_2)} \right) T_{i+1,j,k}^{s+1} + \left(\frac{2r\Delta r_1 - \Delta r_1^2}{r\Delta r_1 \Delta r_2 (\Delta r_1 + \Delta r_2)} \right) T_{i-1,j,k}^{s+1} + \right.$$

$$\left(\frac{2\Delta\theta_2}{r^2 \Delta\theta_1 \Delta\theta_2 (\Delta\theta_1 + \Delta\theta_2)} \right) T_{i,j+1,k}^{s+1} + \left(\frac{2\Delta\theta_1}{r^2 \Delta\theta_1 \Delta\theta_2 (\Delta\theta_1 + \Delta\theta_2)} \right) T_{i,j-1,k}^{s+1} +$$

$$\left. \left(\frac{\langle v \rangle \rho bcb}{kb\Delta z} \right) Tb_{k-1}^{s+1} + \left(\frac{\rho bcb}{kb\Delta t} \right) T_{i,j,k}^{s} + \left(\frac{QM + QL_{i,j,k}}{kb} \right) \right]$$

$$\Big/ \left[\frac{\rho bcb}{kb\Delta t} + \frac{2}{\Delta r_1 \Delta r_2} + \frac{(\Delta r_2 - \Delta r_1)}{r\Delta r_1 \Delta r_2} + \frac{2}{r^2 \Delta\theta_1 \Delta\theta_2} + \frac{\langle v \rangle \rho bcb}{kb\Delta z} \right]$$

APPENDIX B

CONTROL PROGRAM FOR EXPERIMENTAL TEMPERATURE MEASUREMENTS

```
'     T E M P E R A T U R E   R E S P O N S E   S O F T W A R E
'                                                C.L. Swift  May 90

   ' this routine is designed to pulse one (1) fibre for duration input
   ' thermocouple temperature response determined for a period of time
   ' before and after pulse

   ' input 1) source pulse duration
   '       2) number of thermocouples to be tested
   '       3) labmate channel numbers
   '       4) time between temp measurements
   '       5) total number of temperature measurements before and after pulse
   '       6) filename for temp data storage

 '-----------------------------------------------------------------------

 DECLARE SUB mainmenulevel1 ()
 DECLARE SUB initlevel1 ()
 DECLARE SUB strainsetup ()
 DECLARE SUB timedelay (seconds!)
 DECLARE SUB pulse CDECL (BYVAL tdirect%, BYVAL pultot%, BYVAL deltot%, BYVAL i
 DECLARE SUB interface CDECL ()

 REM $INCLUDE: 'genlev1.cm'
 DEF fnc (x) = INT(x * 100 + .5) / 100

 DIM temp(50, 15), chan%(15), temp2(50, 15), temp3(50, 15)
 DEFINT I

 '-----------------------------------------------------------------------

' I N I T I A L I Z E   S O F T W A R E

   CALL initlevel1
   CALL interface

 '-----------------------------------------------------------------------
```

```
' I N P U T   P A R A M E T E R S

10  CLS
    PRINT
    PRINT "SOURCE SET-UP"
    PRINT "-------------"
    PRINT
    PRINT "DIRECTION of translator motion is TOWARDS motor"
    INPUT "is translator 800 steps off fibre"; C$
        IF C$ = CHR$(89) OR C$ = CHR$(131) THEN GOTO 30 ELSE GOTO 20

20      PRINT
        INPUT "how many STEPS do you want to move"; steps%
        INPUT "what DIRECTION (-1 AWAY; +1 TOWARDS motor)"; direction%
        CALL pulse(direction%, steps%, 500, 2)
        PRINT : INPUT "AGAIN"; G$
        IF G$ = CHR$(89) OR G$ = CHR$(121) THEN GOTO 20
        GOTO 30

30  PRINT
    PRINT "SENSOR SET-UP"

    PRINT "-------------"
    INPUT "NUMBER of thermocouples "; N%
    PRINT "INPUT channel numbers"
        FOR i = 1 TO N%
        INPUT "channel="; chan%(i)
        NEXT i
    PRINT
    INPUT "TIME between temp measurements (secs) "; tdelay
    PRINT
    INPUT "NUMBER of trials before pulse"; tot1%
    INPUT "NUMBER of trials during pulse"; tot2%
    INPUT "NUMBER of trials after pulse"; tot3%
    PRINT
    INPUT "FILENAME for temp data storage "; file$

    PRINT
    INPUT "PRESS any key to START"; C$

'-------------------------------------------------------------------------

'  C O R E

 ' temperature measurements before pulse
    CLS
    LOCATE 2, 1: PRINT "    TEMPERATURE RESPONSE BEFORE pulse"
    LOCATE 4, 1: PRINT "T#\CH";
    PRINT SPC(5);
    FOR i = 1 TO N%
        chan% = chan%(i)
        PRINT chan%;
        PRINT SPC(8);
    NEXT i
    PRINT
    LOCATE 6, 1
    FOR T% = 1 TO tot1%
    PRINT T%;
        FOR i = 1 TO N%
        chan% = chan%(i)
        CALL thermocouple(chan%, 3, "T")
        temp(T%, chan%) = meas
        PRINT SPC(5);
        PRINT USING " ###.##"; temp(T%, chan%);
        NEXT i
    PRINT
    CALL timedelay(tdelay)
    NEXT T%
```

```
' move onto fibre
  CALL pulse(1, 800, 500, 2)

' temperature measurements during pulse
  CLS
  LOCATE 2, 1: PRINT "    TEMPERATURE RESPONSE DURING pulse"
  LOCATE 4, 1: PRINT "T#\CH";
  PRINT SPC(5);
  FOR i = 1 TO N%
      chan% = chan%(i)
      PRINT chan%;
      PRINT SPC(8);
  NEXT i


  PRINT
  LOCATE 6, 1
  FOR T% = 1 TO tot2%
  PRINT T%;
      FOR i = 1 TO N%
      chan% = chan%(i)
      CALL thermocouple(chan%, 3, "T")
      temp2(T%, chan%) = meas
      PRINT SPC(5);
      PRINT USING " ###.##"; temp2(T%, chan%);
      NEXT i
  PRINT
  CALL timedelay(tdelay)
  NEXT T%

' move off fibre
  CALL pulse(-1, 800, 500, 2)

' temperature measurements after pulse
  CLS
  LOCATE 2, 1: PRINT "    TEMPERATURE RESPONSE AFTER pulse"
  LOCATE 4, 1: PRINT "T#\CH";
  PRINT SPC(5);
  FOR i = 1 TO N%
      chan% = chan%(i)
      PRINT chan%;
      PRINT SPC(8);
  NEXT i
  PRINT
  LOCATE 6, 1
  FOR T% = 1 TO tot3%
  PRINT T%;
      FOR i = 1 TO N%
      chan% = chan%(i)
      CALL thermocouple(chan%, 3, "T")
      temp3(T%, chan%) = meas
      PRINT SPC(5);
      PRINT USING " ###.##"; temp3(T%, chan%);
      NEXT i
  PRINT
  CALL timedelay(tdelay)
  NEXT T%
```

```
' store temperature data
  CLS
  PRINT "TEMPERATURE DATA IS STORED IN FILE :"; file$
  PRINT
  PRINT "  form:   1. time between measurements (secs)"
  PRINT "          2. number of thermocouples"
  PRINT "          3. list of channels used"
  PRINT "          4. total number of measurements before"
  PRINT "          5. temperature meas #1 - successive channels"
  PRINT "          6. temperature meas #2 - successive channels"
  PRINT "         etc."
  PRINT "          7. total number of measurements during"
  PRINT "          8. temperature meas #1 - successive channels"
  PRINT "          9. temperature meas #2 - successive channels"
  PRINT "         etc."
  PRINT "         10. total number of measurements after"
  PRINT "         11. temperature meas #1 - successive channels"
  PRINT "         12. temperature meas #2 - successive channels"
  PRINT "         etc."
  OPEN file$ FOR OUTPUT AS #1
      WRITE #1, tdelay
      WRITE #1, N%
      FOR i = 1 TO N%
      WRITE #1, chan%(i)
      NEXT i
      WRITE #1, tot1%
      FOR T% = 1 TO tot1%
          FOR i = 1 TO N%
          chan% = chan%(i)
          WRITE #1, temp(T%, chan%)
          NEXT i
      NEXT T%
      WRITE #1, tot2%
      FOR T% = 1 TO tot2%
          FOR i = 1 TO N%
          chan% = chan%(i)
          WRITE #1, temp2(T%, chan%)
          NEXT i
      NEXT T%
      WRITE #1, tot3%
      FOR T% = 1 TO tot3%
          FOR i = 1 TO N%
          chan% = chan%(i)
          WRITE #1, temp3(T%, chan%)
          NEXT i
      NEXT T%
   CLOSE #1

PRINT
INPUT "ANOTHER SET"; C$
PRINT
IF C$ = CHR$(89) OR C$ = CHR$(121) THEN GOTO 10
END
```

APPENDIX C

COMPUTER CODE FOR DEVELOPED THERMAL MODEL

Symbol	Description
R1	1^{st} radial increment from axis (cm).
EVENR	radial correction to multiple of 0.1 cm.
DELTAR	standard radial increment (cm).
DTHETAD	standard angular increment (degrees).
DELTAZ	standard axial increment (cm).
ZLENGTH	total axial length of model (cm).
DELTAT	time increment (s).
TOTALT	total simulation time (s).
DIV	number of laser pulsing increments.
P	total power from source (W).
Z1, Z2	axial position of line source (cm).
DT	source to vessel axis distance (cm).
MUAt, MUAb	optical absorption coefficient for tissue and blood (cm^{-1}).
MUSPt	reduced optical scattering coefficient for tissue (cm^{-1}).
IFLAG, JFLAG	radial and angular grid point where source is located.

Symbol	Description
LAMBDA	radius of cylindrical boundary (cm).
Rv	inner radius of vessel (cm).
VEL	velocity of blood in vessel (cm/s).
DIFFT	thermal diffusivity of tissue (cm^2/s).
KTISS	thermal conductivity of tissue (W/cm/K).
DIFFB	thermal diffusivity of blood (cm^2/s)
KB	thermal conductivity of blood (W/cm/K).
CB	specific heat of blood (J/g K).
DENB	blood density (g/cm^3).
KV	thermal conductivity of vessel (W/cm/K).
CV	specific heat of vessel (J/g K).
DENV	vessel density (g/cm^3).
QM	metabolic heating rate (W/cm^3).
Ta	temperature of perfuse blood (K).
Wb	average tissue perfusion rate ($g/s/cm^3$).
CRITER	point by point convergence criteria.

```
!Three dimensional model of a functioning blood vessel in a tissue medium.
!Author: Bill Whelan

!------------------------DECLARE VARIABLE TYPES--------------------------------

10    EXTERNAL SUB FORIGIN (DOUBLE,DOUBLE,DOUBLE,DOUBLE,DOUBLE,DOUBLE,DOUBLE, &
                            DOUBLE,DOUBLE,DOUBLE,DOUBLE,DOUBLE)
20    DECLARE REAL RDT,RR,R1,Rv,EVENR,DELTAR,THETAD,DTHETAD,CRITER,RAY,LAMBDA
30    DECLARE DOUBLE R,THETA,ZM,DT,A,B,RESULT,ERREST
40    DECLARE DOUBLE A1,A2,A3,B1,B2,C1,C2,Z1,Z2,TP1,TP2,TP3,RL1,RL2,TM1,TM2,TM3
50    DECLARE DOUBLE DELTAR1,DELTAR2,DTHETA1,DTHETA2,DELTAZ,MLENGTH,ZLENGTH
60    DECLARE DOUBLE OLDTP,OLDTPB,VEL,Ta,HS,WB,AA,BB,CC
70    DECLARE DOUBLE KEFF,DIFFB,DENB,KB,CB,DIFFT,KTISS,DENV,KV,CV,QM,
80    DECLARE DOUBLE P,SL,INTCON,Ko,Kob,Kot,MUA,MUAt,MUAb,MUSP,MUSPt,MUSPb,MUTP
90    DECLARE DOUBLE MUTPb,MUTPt,MUP,MUPb,MUPt,BETA,BETAb,BETAt,D,Db,Dtiss
100   DECLARE INTEGER NR(1 TO 38),INCREM,NZ,TNGP,GPC,TOTAL,DELTAT,TGPC,NEW,OLD
110   DECLARE INTEGER I,J,K,T,NA,TRANS,JINCREM,TNR,DIV,IFLAG,JFLAG
120   DECLARE STRING FILE1$,FILE2$
130   DECLARE REAL TP(0 TO 45,1 TO 38,0 TO 42,1 TO 2),TPB(0 TO 42,1 TO 2)
140   DECLARE REAL RESID(1 TO 45,1 TO 38,1 TO 42),RESIDB(1 TO 42)
150   DECLARE DOUBLE QL(1 TO 45,1 TO 38,1 TO 42),QLB(1 TO 81)
160   DECLARE DOUBLE A(1 TO 45,1 TO 38),B(1 TO 45,1 TO 38),C(1 TO 45,1 TO 38)
170   DECLARE DOUBLE D(1 TO 45,1 TO 38),E(1 TO 45,1 TO 38),F(1 TO 45,1 TO 38)
180   DECLARE DOUBLE G(1 TO 45,1 TO 38),H(1 TO 45,1 TO 38),L(1 TO 45,1 TO 38)
185   DECLARE DOUBLE M(1 TO 45,1 TO 38),N(1 TO 45,1 TO 38)

!-------------------------INPUT PARAMETERS-------------------------------------

190   FILE1$="F1S00GB.DAT"
200   FILE2$="F1S00G.DAT"
210   Rv=0.072
220   R1=Rv
230   DELTAR=0.1
240   EVENR=0.128
250   DTHETAD=10
260   DELTAZ=0.2
270   ZLENGTH=8.0
280   DELTAT=60
290   TOTAL=1200
300   DIV=10
310   DIFFT=0.00127
320   KTISS=0.00493
330   DIFFB=0.0015
340   KB=0.00623
350   CB=4.1783
360   DENB=0.99336
370   CV=1.046
380   DENV=3.414
390   KV=0.0025
400   DT=1.0
410   Z1=3.3 \ Z2=4.8
420   P=2.0
430   MUAt=1.81 \ MUSPt=8.06
440   MUAb=0.2
450   IFLAG=10 \ JFLAG=1
460   LAMBDA=3.2
470   VEL=0
480   WB=0
490   Ta=310
500   QM=0
510   OLD=1 \ NEW=1
520   CRITER=1E-6
530   OPEN FILE1$ FOR OUTPUT AS #1
540   OPEN FILE2$ FOR OUTPUT AS #2
```

```
550   PRINT #2, "TIME";TAB(10);"1";TAB(18);"2";TAB(26);"3";TAB(34);"4"; &
              TAB(42);"5";TAB(50);"6";TAB(58);"7"

!--------------------CALCULATE INCREMENT PARAMETERS--------------------------

560   NA=(360/DTHETAD)
570   DTHETA=DTHETAD*3.14159/180
580   NZ=INT(ZLENGTH/DELTAZ+0.5)
590   INCREM=TOTAL/DELTAT

!-------------------CALCULATE BLOOD FLOW PARAMETERS--------------------------

600   AA=VEL*CB*DENB/DELTAZ \ BB=DENB*CB/DELTAT \ CC=AA+BB
610   HS=(1.08*KB/(2*Rv))*((DENB*CB*VEL*4*Rv^2)/(KB*ZLENGTH))^(1/3)
620   KEFF=4*KTISS*KV*KB/(KB*(KV+KTISS)+KTISS*(KB+KV))

!-------------CALCULATE OPTICAL TRANSPORT EQUATION PARAMETERS-----------------

630   SL=P/(Z2-Z1)
640   INTCON=SL/(4*3.14159)
650   MUTPt=MUSPt+MUAt
660   Kot=SQR(3*MUAt*MUTPt)*(1-(2*MUAt)/(5*MUTPt)) \ MUPt=5*MUTPt/4
670   Dtiss=MUAt/Kot^2 \ BETAt=(2*MUAt/MUSPt)*(MUTPt^2-Kot^2)/(Kot^2-MUAt*MUTPt)
680   MUTPb=MUAb
690   Kob=SQR(3*MUAb*MUTPb)*(1-(2*MUAb)/(5*MUTPb)) \ MUPb=5*MUTPb/4
700   Db=MUAb/Kob^2 \ BETAb=0

!----------------------CALCULATE BHTE COEFFICIENTS-----------------------------

710   TNR=0
720   THETA=0
730   FOR J=1 TO NA
740     R=R1
740     GOSUB 2000
760     TNR=TNR+NR(J)-1
770    FOR I=1 TO 45
780      RR=R
790      IF I=IFLAG AND J=JFLAG THEN  !Omit BHTE coefficients at light source.
            I=I+1
         END IF
800      GOSUB 3000
810      IF J=JFLAG AND I=(IFLAG-1) OR J=JFLAG AND I=(IFLAG+1) THEN
            GOSUB 4000
         END IF
820      IF J=NA AND I=IFLAG OR J=(JFLAG+1) AND I=IFLAG THEN
            GOSUB 5000
         END IF
830      R=R+DELTAR1
840    NEXT I
850    THETA=THETA+DTHETA1
860   NEXT J

!----------------------SET TOTAL NUMBER OF GRID POINTS-------------------------

870   IF VEL > 0 THEN
         TNGP=(TNR+1)*(NZ-1) !Fof flowing blood.
      ELSE
         TNGP=(TNR)*(NZ-1)   !For stationary blood.
      END IF

!--------------------CALCULATE ABSORBED LIGHT DISTRIBUTION---------------------

880   ZM=DELTAZ
890   FOR K=1 TO (NZ-1)
900     THETA=0
```

```
910      IF VEL > 0 THEN
            A=Z1 \ B=Z2 \ RESULT=0 \ ERREST=0
            MUA=MUAb \ MUP=MUPb \ Ko=Kob \ BETA=BETAb \ D=Db \ R=0
            CALL FORIGIN (R,THETA,ZM,Ko,BETA,D,MUP,DT,A,B,RESULT,ERREST)
            QLB(K)=MUA*INTCON*RESULT  !Absorbed light in flowing blood along
                                      !vessel axis.
         END IF
920     FOR J=1 TO NA
930       R=R1
940      FOR I=1 TO (NR(J)-1)
950        RR=R
960        IF I=IFLAG AND J=JFLAG THEN  !Omit light absorption at source.
              GOTO 1020
           END IF
970        A=Z1 \ B=Z2 \ RESULT=0 \ ERREST=0
980        IF RR < Rv THEN
              MUA=MUAb \ MUP=MUPb \ Ko=Kob \ BETA=BETAb \ D=Db
           ELSE
              MUA=MUAt \ MUP=MUPt \ Ko=Kot \ BETA=BETAt \ D=Dtiss
           END IF
900        CALL FORIGIN (R,THETA,ZM,Ko,BETA,D,MUP,DT,A,B,RESULT,ERREST)
1000       QL(I,J,K)=MUA*INTCON*RESULT !Absorbed light in tissue and
                                       !stationary blood.
1010       IF RR = Rv THEN             !Set absorbed light at vessel to zero.
              QL(I,J,K)=0
           END IF
1020       SELECT RR                   !Distributed radial increments due to
             CASE < Rv                 !nonuniform differencing at vessel.
              DELTAR1=DELTAR
             CASE = Rv
              DELTAR1=EVENR
             CASE ELSE
              DELTAR1=DELTAR
           END SELECT
1030       R=R+DELTAR1
1040     NEXT I
1050      THETA=THETA+DTHETA
1060    NEXT J
1070     ZM=ZM+DELTAZ
1080   NEXT K

!--------------------INITIALIZE ALL GRID POINTS TO 310 K----------------------

1090   FOR K=0 TO NZ
1100     TPB(K,OLD)=310
1110    FOR J=1 TO NA
1120     FOR I=1 TO 45
1130       TP(I,J,K,OLD)=310
1140     NEXT I
1150    NEXT J
1160   NEXT K
1170   T=1

!----------CALCULATE TEMPERATURE DISTRIBUTIONS FOR THE TIME INTERVAL------------

1180   IF NEW=1 THEN
          NEW=2
       ELSE
          NEW=1
       END If

!Due to implicit differencing, reset all temps. at start of new time interval
!to 310 K.

1190   FOR K=0 TO NZ
```

```
1200     TPB(K,NEW)=310
1210    FOR J=1 TO NA
1220     FOR I=1 TO 45
1230       TP(I,J,K,NEW)=310
1240     NEXT I
1250    NEXT J
1260   NEXT K
1270   CTR=0                !Initialize the iterative counter.
1280   GPC=0                !Initialize number of converged grid points
1290   FOR K=1 TO (NZ-1)
1300     IF VEL > 0 THEN
            IF CTR > 20 AND RESIDB(K) < CRITER THEN
               GPC=GPC+1          !Count number of converged grid points in
               GOTO 1320          !flowing blood.
            END IF

!Calculate blood temperature and residual if blood velocity > 0.

            OLDTPB=TPB(K,NEW)
            TPB(K,NEW)=(QLB(K)+(AA*TPB(K-1,NEW))+(BB*TPB(K,OLD)))/CC
            RESIDB(K)=ABS(OLDTPB-TPB(K,NEW))*2/(OLDTPB+TPB(K,NEW))

         END IF
1320    FOR J=1 TO NA
1330     FOR I=1 TO (NR(J)-1)
1340       IF CTR > 20 AND RESID(I,J,K) < CRITER THEN
              GPC=GPC+1          !Count number of converged grid points in
              GOTO 1530          !tissue, vessel and stationary blood.
           END IF
1350       TEMP1=0 \ TEMP2=0 \ TEMP3=0 \ TEMP4=0 \ TP1=0 \ TP2=0 \ TP3=0
1360       IF I=IFLAG AND J=JFLAG THEN !Omit temp. calculation at source.
              I=I+1
           END IF
1370       IF J < (NA/2)+1 THEN
              JINCREM=J+(180/DTHETAD)
           ELSE
              JINCREM=J-(180/DTHETAD)
           END IF
1380       TEMP1=TP(I+1,J,K,NEW)
1390       IF VEL > 0 THEN
              TEMP2=TP(I-1,J,K,NEW)
           ELSE
              IF I=1 THEN
                 TEMP2=TP(1,JINCREM,K,NEW)
              ELSE
                 TEMP2=TP(I-1,J,K,NEW)
              END IF
           END IF
1400       IF J=NA THEN
              TEMP3=TP(I,1,K,NEW)
           ELSE
              TEMP3=TP(I,J+1,K,NEW)
           END IF
1410       IF J=1 THEN
              TEMP4=TP(I,NA,K,NEW)
           ELSE
              TEMP4=TP(I,J-1,K,NEW)
           END IF
1420       IF J=JFLAG AND I=(IFLAG-1) THEN
              TEMP1=TP(I+2,J,K,NEW)
           END IF
1430       IF J=JFLAG AND I=(IFLAG+1) THEN
              TEMP2=TP(I-2,J,K,NEW)
           END IF
1440       IF J=NA AND I=IFLAG THEN
```

```
            TEMP3=TP(I,JFLAG+1,K,NEW)
         END IF
1450     IF J=(JFLAG+1) AND I=IFLAG THEN
            TEMP4=TP(I,NA,K,NEW)
         END IF
1460     IF T > DIV THEN              !End light absorption after a
            QL(I,J,K)=0               !specified time.
         END IF
1470     OLDTP=TP(I,J,K,NEW)          !Rename temperture of previous interation
                                      !to calculate residual.
1480     TP1=B(I,J)*TEMP1 + C(I,J)*TEMP2 + D(I,J)*TEMP3 + E(I,J)*TEMP4
1490     TP2=F(I,J)*TP(I,J,K+1,NEW) + G(I,J)*TP(I,J,K-1,NEW)
1500     TP3=H(I,J)*TP(I,J,K,OLD) + L(I,J) + M(I,J)*TPB(K,NEW)+(QM + QL(I,J,K))/N(I
1510     TP(I,J,K,NEW)=(TP1 + TP2 + TP3) / A(I,J)    !Update temperature.
1520     RESID(I,J,K)=ABS(OLDTP-TP(I,J,K,NEW))*2/   &
                    (OLDTP+TP(I,J,K,NEW))          !Calculate residual.
1530    NEXT I
1540   NEXT J
1550  NEXT K
1560  CTR=CTR+1
1570  IF GPC < TNGP THEN              !Are all grid points at the time
         GOTO 1280                    !interval converged.
      END IF

!---------------------------PRINT RESULTS-------------------------------------

1580  PRINT #2, T;TAB(8);TP(10,10,19,NEW);TAB(16);TP(5,1,19,NEW); &
                TAB(24);TP(15,1,19,NEW);TAB(32);TP(20,1,19,NEW);  &
                TAB(40);TP(10,28,19,NEW);TAB(48);TP(5,19,19,NEW); &
                TAB(56);TP(10,19,19,NEW)

!Print blood temperatures.

1590  FOR K=1 TO (NZ-1)
1600    PRINT #1, "TPB(";K;",";T;")=";TPB(K,NEW)
1610  NEXT K

!Print radial temps from vessel to source at plane of interest.

1620  FOR J=1 TO 19 STEP 18
1630   FOR I=1 TO 10
1640     K=19
1650     IF I=1 AND J=1 THEN
            PRINT "TPB(";K;",";T;")=";TPB(K,NEW)
         END IF
1660     PRINT "TP(";I;",";J;",";K;",";T;")=";TP(I,J,K,NEW)
1670   NEXT I
1680  NEXT J

1690  IF OLD=1 THEN
         OLD=2
      ELSE
         OLD=1
      END IF

1700  IF T < INCREM THEN        !Is the modelling time complete?
         T=T+1
         GOTO 1180
      END IF

1710  CLOSE #1
1720  CLOSE #2
1730  GOSUB 10000
```

```
!-------------------------------------------------------------------------------
!   SUBROUTINE #1: DETERMINE THE NUMBER OF RADIAL INCREMENTS AT EACH ANGLE
!-------------------------------------------------------------------------------
2000  RL1=DT*COS(THETA)+SQR(DT^2*((COS(THETA))^2-1)+LAMBDA^2)
2020  RL2=DT*COS(THETA)-SQR(DT^2*((COS(THETA))^2-1)+LAMBDA^2)
2030  IF RL1 > 0 THEN          !Calculate distance from vessel axis to boundary
        RAY=RL1                !of cylinder defined by lambda.
      ELSE
        RAY=RL2
      END IF
2070  MLENGTH=RAY-.2           !Subtract region at vessel with nonuniform radial
                               !differencing.
2080  NR(J)=INT((MLENGTH/DELTAR)+0.5) + 2 !Add number of increments in this
                                          !region.
2090  RETURN

!-------------------------------------------------------------------------------
!             SUBROUTINE #2: CALCULATE BHTE COEFFICIENTS
!-------------------------------------------------------------------------------
3000  DTHETA1=DTHETA \ DTHETA2=DTHETA
      SELECT RR
        CASE < Rv
          DELTAR2=2*DELTAR \ DELTAR1=DELTAR
          A1=1/(DIFFB*DELTAT) + 2/(DELTAR1*DELTAR2)
          A2=(DELTAR2-DELTAR1)/(R*DELTAR1*DELTAR2) + 2/(R^2*DTHETA1*DTHETA2)
          A3=2/DELTAZ^2
          A(I,J)= A1 + A2 + A3
          B(I,J)=(2*R*DELTAR2+DELTAR2^2)/(R*DELTAR1*DELTAR2*(DELTAR1+DELTAR2))
          C(I,J)=(2*R*DELTAR1-DELTAR1^2)/(R*DELTAR1*DELTAR2*(DELTAR1+DELTAR2))
          D(I,J)=2/(R^2*DTHETA1*(DTHETA1+DTHETA2))
          E(I,J)=2/(R^2*DTHETA2*(DTHETA1+DTHETA2))
          F(I,J)=1/DELTAZ^2
          G(I,J)=1/DELTAZ^2
          H(I,J)=1/(DIFFB*DELTAT)
          L(I,J)=0
          M(I,J)=0
          N(I,J)=KB
        CASE = Rv
          IF VEL > 0 THEN
            DELTAR1=EVENR
            A1=DENV*CV/(KEFF*DELTAT) + 2/DELTAR1^2
            A2=2/(R^2*DTHETA1*DTHETA2)
            A3=2/DELTAZ^2 + (2*R-DELTAR1)*HS/(R*DELTAR1*KEFF)
            A(I,J)=A1+A2+A3
            B(I,J)=2/DELTAR1^2
            C(I,J)=0
            D(I,J)=2/(R^2*DTHETA1*(DTHETA1+DTHETA2))
            E(I,J)=2/(R^2*DTHETA2*(DTHETA1+DTHETA2))
            F(I,J)=1/DELTAZ^2
            G(I,J)=1/DELTAZ^2
            H(I,J)=DENV*CV/(KEFF*DELTAT)
            L(I,J)=0
            M(I,J)=(2*R-DELTAR1)*HS/(R*DELTAR1*KEFF)
            N(I,J)=KEFF
          ELSE
            DELTAR2=Rv \ DELTAR1=EVENR
            A1=DENV*CV/(KEFF*DELTAT) + 2/(DELTAR1*DELTAR2)
            A2=(DELTAR2-DELTAR1)/(R*DELTAR1*DELTAR2)
            A3=2/(R^2*DTHETA1*DTHETA2) + 2/DELTAZ^2
            A(I,J)= A1 + A2 + A3
            B(I,J)=(2*R*DELTAR2+DELTAR2^2)/(R*DELTAR1*DELTAR2*(DELTAR1+DELTAR2))
            C(I,J)=(2*R*DELTAR1-DELTAR1^2)/(R*DELTAR1*DELTAR2*(DELTAR1+DELTAR2))
            D(I,J)=2/(R^2*DTHETA1*(DTHETA1+DTHETA2))
            E(I,J)=2/(R^2*DTHETA2*(DTHETA1+DTHETA2))
            F(I,J)=1/DELTAZ^2
```

```
            G(I,J)=1/DELTAZ^2
            H(I,J)=DENV*CV/(KEFF*DELTAT)
            L(I,J)=0
            M(I,J)=0
            N(I,J)=KEFF
          END IF
        CASE = (Rv+EVENR)
          DELTAR2=EVENR \ DELTAR1=DELTAR
          A1=1/(DIFFT*DELTAT) + 2/(DELTAR1*DELTAR2)
          A2=(DELTAR2-DELTAR1)/(R*DELTAR1*DELTAR2) + 2/(R^2*DTHETA1*DTHETA2)
          A3=2/DELTAZ^2 + WB*CB/KTISS
          A(I,J)= A1 + A2 + A3
          B(I,J)=(2*R*DELTAR2+DELTAR2^2)/(R*DELTAR1*DELTAR2*(DELTAR1+DELTAR2))
          C(I,J)=(2*R*DELTAR1-DELTAR1^2)/(R*DELTAR1*DELTAR2*(DELTAR1+DELTAR2))
          D(I,J)=2/(R^2*DTHETA1*(DTHETA1+DTHETA2))
          E(I,J)=2/(R^2*DTHETA2*(DTHETA1+DTHETA2))
          F(I,J)=1/DELTAZ^2
          G(I,J)=1/DELTAZ^2
          H(I,J)=1/(DIFFT*DELTAT)
          L(I,J)=WB*CB*Ta/KTISS
          M(I,J)=0
          N(I,J)=KTISS
        CASE ELSE
          DELTAR2=DELTAR \ DELTAR1=DELTAR
          A1=1/(DIFFT*DELTAT) + 2/(DELTAR1*DELTAR2)
          A2=(DELTAR2-DELTAR1)/(R*DELTAR1*DELTAR2) + 2/(R^2*DTHETA1*DTHETA2)
          A3=2/DELTAZ^2 + WB*CB/KTISS
          A(I,J)= A1 + A2 + A3
          B(I,J)=(2*R*DELTAR2+DELTAR2^2)/(R*DELTAR1*DELTAR2*(DELTAR1+DELTAR2))
          C(I,J)=(2*R*DELTAR1-DELTAR1^2)/(R*DELTAR1*DELTAR2*(DELTAR1+DELTAR2))
          D(I,J)=2/(R^2*DTHETA1*(DTHETA1+DTHETA2))
          E(I,J)=2/(R^2*DTHETA2*(DTHETA1+DTHETA2))
          F(I,J)=1/DELTAZ^2
          G(I,J)=1/DELTAZ^2
          H(I,J)=1/(DIFFT*DELTAT)
          L(I,J)=WB*CB*Ta/KTISS
          M(I,J)=0
          N(I,J)=KTISS
      END SELECT
3800  RETURN

!-------------------------------------------------------------------------
!SUBROUTINE #3: RECALCULATE COEFFICIENTS ONE INCREMENT ABOVE AND BELOW
!               THE LIGHT SOURCE.
!-------------------------------------------------------------------------
4000  DTHETA2=DTHETA \ DTHETA1=DTHETA
4002  SELECT I
        CASE = (IFLAG-1)
          DELTAR2=DELTAR \ DELTAR1=2*DELTAR
        CASE = (IFLAG+1)
          DELTAR2=2*DELTAR \ DELTAR1=DELTAR
      END SELECT
4100  A1=1/(DIFFT*DELTAT) + 2/(DELTAR1*DELTAR2)
      A2=(DELTAR2-DELTAR1)/(R*DELTAR1*DELTAR2) + 2/(R^2*DTHETA1*DTHETA2)
      A3=2/DELTAZ^2 + WB*CB/KTISS
      A(I,J)= A1 + A2 + A3
      B(I,J)=(2*R*DELTAR2+DELTAR2^2)/(R*DELTAR1*DELTAR2*(DELTAR1+DELTAR2))
      C(I,J)=(2*R*DELTAR1-DELTAR1^2)/(R*DELTAR1*DELTAR2*(DELTAR1+DELTAR2))
      D(I,J)=2/(R^2*DTHETA1*(DTHETA1+DTHETA2))
      E(I,J)=2/(R^2*DTHETA2*(DTHETA1+DTHETA2))
      F(I,J)=1/DELTAZ^2
      G(I,J)=1/DELTAZ^2
      H(I,J)=1/(DIFFT*DELTAT)
      L(I,J)=WB*CB*Ta/KTISS
      M(I,J)=0
```

```
      N(I,J)=KTISS
4800  RETURN

!-------------------------------------------------------------------------
!SUBROUTINE #4: RECALCULATE COEFFICIENTS ONE ANGULAR INCREMENT ON EITHER
!               SIDE OF THE LIGHT SOURCE.
!-------------------------------------------------------------------------
5000  DELTAR2=DELTAR \ DELTAR1=DELTAR
5002  SELECT J
         CASE = NA
           DTHETA2=DTHETA \ DTHETA1=2*DTHETA
         CASE = (JFLAG+1)
           DTHETA2=2*DTHETA \ DTHETA1=DTHETA
      END SELECT
5100  A1=1/(DIFFT*DELTAT) + 2/(DELTAR1*DELTAR2)
      A2=(DELTAR2-DELTAR1)/(R*DELTAR1*DELTAR2) + 2/(R^2*DTHETA1*DTHETA2)
      A3=2/DELTAZ^2 + WB*CB/KTISS
      A(I,J)= A1 + A2 + A3
      B(I,J)=(2*R*DELTAR2+DELTAR2^2)/(R*DELTAR1*DELTAR2*(DELTAR1+DELTAR2))
      C(I,J)=(2*R*DELTAR1-DELTAR1^2)/(R*DELTAR1*DELTAR2*(DELTAR1+DELTAR2))
      D(I,J)=2/(R^2*DTHETA1*(DTHETA1+DTHETA2))
      E(I,J)=2/(R^2*DTHETA2*(DTHETA1+DTHETA2))
      F(I,J)=1/DELTAZ^2
      G(I,J)=1/DELTAZ^2
      H(I,J)=1/(DIFFT*DELTAT)
      L(I,J)=WB*CB*Ta/KTISS
      M(I,J)=0
      N(I,J)=KTISS
5800  RETURN

10000 END
```

BIBLIOGRAPHY

Anderson, A.E., 1989 "Flow mediated and reflex changes in large peripheral artery tone in humans" Circulation 79 pp. 93-100.

Arnfield, M.R., Tulip, J. and McPhee, M.S., 1988, "Optical propagation in tissue with anisotropic scattering" IEEE Trans. Biomed. Eng. 35 pp. 372-381.

Astrahan, M.A., 1979 "Concerning hyperthermia phantom" Med. Phys. 6 p. 235.

Blechinger, J.C., Madsen, E.L. and Frank, G.R., 1988 "Tissue-mimicking gelatin-agar geals for use in magnetic resonance imaging phantoms" Med Phys. 15 pp. 629-636.

Borrelli, A., 1986 "A direct correlation between hyperthermia induced membrane blebbing and survival in synchronous G1 CHO cells", J. Cell. Physiol. 126 p.181-190.

Boulnois, J., 1986 "Photophysical processes in recent medical laser developements: a review" Lasers in Med. Sci. 1 pp. 47-66.

Bowman, H.F., Cravalho, E.G. and Woods, M., 1975 "Theory, measurements and applications of thermal properties of biomaterials" Annu. Rev. Biophys. Bioeng. 4 pp. 43-80.

Bibliography (continued)

Bowman, H.F., 1882 "Thermodynamics of tissue heating: Modelling and measurements for temperature distributions" in Physical Aspects of Hypthermia, G.H Nussbaum Ed., New York: Amer. Inst. Physics, pp. 511-548.

Bown, S.G., Salmon, P.R., Storey, D.W. et al, 1980, "Nd:YAG laser photocoagulation in the dog stomach" Gut 21 pp. 818-825.

Brandts, J.F. et al., 1978, "Calorimetric studies of the structural transitions of the human erythrocyte membrane -- Studies of the B and C transitions", Biochem. Biophys. Acta. 512 pp. 566-578.

Bruns, P., 1877 "Die Heilwirkung des Erysipels auf Geschwulste", Beitr. Klin. Chir. 3 p.433.

Busch, H. and Smetana, K., 1970 The Nucleolus, Academic Press, New York.

Bush, W., 1866 "Uber den Einfluss weichen Heftigere Erysipelen Zuweilen auf Organisierte Neubildungen Ausuken Verhandl", Rheinisch-Westfael. Akad. Wiss. Nat. Ing. Wirtschaftswiss, Votr. 23 p.28.

Carslaw, H.S. and Jaegar, J.C., 1959 Conduction of heat in solids, Oxford: Clarendon Press, 2nd ed.

Cavaliere, R. et al, 1967 "Selective heating of cancer cells: biochemical and clinical studies" Cancer 20 pp. 1351-1381.

Chen, M.M. and Holmes, K.R., 1980 "Microvascular contributions in tissue heat transfer" Ann. N.Y. Acad. Sci. 335 pp 137 - 150.

Bibliography (continued)

Christensen, D.A., 1979 "Thermal dosimetry and temperature measurements", Cancer Res. 39 pp 2325 - 2327.

Coley, W.B., 1893 "The treatment of malignant tumors by repeated inoculations of erysipelas with a report of ten original cases" Am. J. Med. Sci. 105 p.487.

Cravalho, E.G., Fox, L.R. and Kan, J.C., 1980 "The application of the bioheat transer equation to the design of thermal protocols for local hyperthermia" Annals NYAS 335 pp. 86-96.

CRC Handbook of Chemistry and Physics, 1983-1984 64th edition, CRC Press Inc., Boca Raton, Florida.

Crile, G. Jr., 1961 "Heat as an adjunct to the treatment of cancer; experimental studies" Cleve. Clin. Q. 28 p.75-89.5-89.

Daikuzono, N., Suzuki, S., Tajiri, H., Tsunekawa, H., Ohyama, M. and Joffe, S., 1988, "Laserthermia: A new computer-controlled contact Nd:YAG system for interstitial local hyperthermia" Lasers Med. Surg. 8 pp. 254-258.

Davies, M., Dowden, J., Steger, A., Kapadia, P. and Whiting, P., 1989, "A mathematical model for interstitial laser treatment of tumors using four fibers" Lasers Med. Sci. 4 pp. 41-53.

Dewey, W.C., 1989 "Mechanisms of thermal radiosensitization", in Hyperthermia and Oncology, M. Urano and E. Douple, Eds.), Vol. 2, pp. 1-15. VSP, The Netherlands.

Bibliography (continued)

Dewey, W.C., 1988 "Cell cycle effects: Killing, division delay, and chromosomal aberations, Symposium Lecture", Proceedings of 5th International Symposium on Hyperthermic Oncology, Kyoto, Japan, in press.

Dewey, W.C.; Hopwood, L.E.; Sapareto, L.A. and Gerweck, L.E., 1977 "Cellular responses to combinations of hyperthermia and radiation" Radiology 123 p.463-474.

Dewey, W.C., Saparetto, S.A.and Bretton, D.A., 1980 "Hyperthermic radiosensitization of synchronous Chinese hamster cells: relation between lathality and chromosomal abberations" Radiat. Res. 76 p.48-59.

Divrik, M.A., Roemer, R.B. and Cetas, T.C., 1984, "Inference of complete tissue temperature fields from a few measured termperatures: An unconstrained optimization model" IEEE Biomed. Eng. BME-31, pp. 150-160.

Doss, J.D., 1985, "Simulations of automatic temperature control in tissue hyperthermia calculations" Med. Phys. 12 pp. 693-697.

Dowden, J., Davies, M., Kapadia, P. and Matthewson, K., 1987, "Heat flow in laser treatment by local hyperthermia" Lasers Med. Sci. 2 pp. 211-221.

Bibliography (continued)

Dowden, J., Jordan, T. and Kapadia, P., 1988, "Temperature distribution produced by a cylindrical etched fiber tip in laser treatment of tumors by local hyperthermia" Lasers Med. Sci. 3 pp. 47-54.

Drew, T.B., Hottel, H.C. and McAdams, W.H., 1936 "Heat transmission" Trans. Am. Inst. Chem. Eng. 32 pp. 271-305.

Duderstadt, J.J. and Hamilton, L.J., 1976, Nuclear Reactor Analysis, Wiley and Sons Inc.

Dunlop, P.R.C. and Howard, G.C.W., 1989 "Has hyperthermia a place in cancer treatment" Clinical Radiology 40 p.76-82.

Eberhart, R.C., Shitzer, A., and Hernandez, E.J., 1980, "Thermal dilution methods: Estimation of tissue blood flow and metabolism" Ann. N.Y. Acad. Sci. 3 pp. 107-131.

Engler, M.J., Dewhirst, M.W. and Oleson, J.R., 1989, "Stability of temperatures during hyperthermia treatments" Int. J. Hyperthermia 5 pp. 59-67.

Freeman, M.L., Dewey, W.C. and Hopwood, L.E., 1977, "Effect of pH on hyperthermic cell survival" J. Natl. Cancer Inst. 58 pp. 1837-1839.839.

Gerner, E.W. and Russel, D.H., 1977 "The relationship between polyamine accumulation and DNA replication kinetics in synchronized CHO cells after heat shock" Cancer Res. 37 p.482-489.

Gerner, E.W. and Schneider, M.J., 1975 "Induced thermal resistance in HeLa cells" Nature 256 p.500-502.

Bibliography (continued)

Gessler, A.E.; McCarthy, K.S. and Parkinson, M.D., 1950 "Eradication of spontaneous mouse tumors by high frequency radiation", Exp. Med. Surg. 8 p.143-148.

Glazebrook, G.A., Jackson, F.I. and Usiskin, S.R., 1985, "The cooling effect of tubular liquid flow during radiofrequency heating: the "Rind" survival hypothesis" J. Can. Ass. of Radiologists 36 pp. 127-132.

Gordon, S., 1965 Numerical Solutions of PDE with Excercises and Worked Solutions, Oxford University Press, London.

Guyton, 1981, Textbook of Medical Physiology, Saunders Publications, 6th edition.

Hahn, G.M., Li, G.C. and Shui, E., 1977 "Interaction of Amphotericin B and 43°C hyperthermia", Cancer Res. 37 p.761-764.

Hall, E.J., 1988 Radiobiology for the Radiologist J.B. Lippincott Co., Philadelphia, 3rd ed.

Handbook of Optics, 1978, W.G. Driscoll ed., McGraw Hill Book Co., New York.

Hayes, L.J., Diller, K.R., Pearce, J.A., Schick, M.R. and Colvin, D.P., 1985, "Prediction of transient temperature fields and cumulative tissue destruction for radiofrequency heating of a tumor" Med. Phys. 12 pp. 684-692.

Henle, K.J., 1980, J. Natl. Cancer Inst. 64 p. 1479.

Bibliography (continued)

Hofer, K.G. and Mivechi, N.F., 1980, "Tunor cell sensitivity to hyperthermia as a function of extracellular and intracellular pH" J. Natl. Cancer Inst. 65 pp. 621-625.

Hynynen, K. and Edwards, D.K., 1989, "Temperature measurements during ultrasound hyperthermia" Med. Phys. 16 pp. 618-626.

Hornbeck G., 1984 Hyperthermia and Cancer: Human Clinical Trial Experience Vol I and II, CRC Press Boca Raton, Florida.

Jacques, S. and Prahl, S., 1987, "Modeling optical and thermal distributions in tissue during laser irradiation" Lasers Surg. Med. 6 pp. 494-503.

Jain, R.K., 1982, "Bioheat transfer: Mathematical models of thermal systems, in Hyperthermia in Cancer Therapy, K.F. Storm ed., Hall Medical Publishers, Boston.

Jain, R.K., Grantham, F.H. and Gullino, P.M>, 1979 "Blood flow and heat transfer in Walker 256 mammary carcinoma" J. of the Natl. Cancer Inst. 62 pp. 927-933.

Johnson, F.H. et al., 1954, The Kinetics Basic of Molecular Biology, Wiley, New York.

Lagendijk, J.J.W., 1982, "The influence of bloodflow in large blood vessels on the temperature distributions in hyperthermia" Phys. Med. Biol. 27 pp. 17-23.

Bibliography (continued)

Lagendijk, J.J.W., Schellekens, M., Schipper, J. and van der Linden, P.M., 1984, "A three-dimensional description of heating patterns in vascularized tissues during hyperthermic treatment" Phys. Med. Biol. 29 pp. 495-507.

Lagendijk, J.J.W. and Crezee, J., 1990 "Experimental verification of bioheat theories: measurement of temperature profiles around large artificial vessels in perfused tissues" Phys. Med. Biol. 35 pp. 905-923.

Lele, P.P. and Parker, K.J., 1982 "Temperature distributions in tissues during local hyperthermia by stationary or steered beams of unfocused or focused ultrasound" Br. J. Cancer 45 (suppl. V) pp. 108-121.

McCormick, W. and Penman, S., 1969 "Regulation of protein synthesis in HeLa cells; translation at elevated temperatures", J. Mol. Biol. 39 p. 315.

Mondovi, B., 1976, "Biochemical and ultrasonic lesions" In Proceedings of the First International Symposium on Cancer Therapy by Hyperthermia and Radiation, eds M.J. Wizenberg and J.E. Robinson, Chicago: American College of Radiology pp. 3-15.

Moricca, G et al, 1977 "Hyperthermia treatment of tumors: experimental and clinical applications" Recent Results Cancer Res. 59 pp. 112-151.

Bibliography (continued)

Oleson, J.R. and Samulski, T.V., 1989, "Improved coupling of ultrasound hyperthermia applicators to patients" Int. J. Radiation Oncology Biol. Phys. 16 pp. 609-612.

Overgaard, J., '1977 "Effect of hyperthermia on malignant cells in vivo. A review and a hypothesis" Cancer 39 p.2637-2646.

Overgaard, J., 1982 "The design of clinical trials" in Hyperthermia Oncology: Physics and Technology of Hyperthermia, Martinus Nijhuff Publishers, Amsterdam.

Paglione, R.W., 1982 "Power deposition with microwaves", in Physical Aspects of Hyperthermia, pp. 192-208.

Pennes, H.H., 1948 "Analysis of tissue and arterial blood temperatures in the resting forearm" J. Appl. Physiol. 1 p. 93.

Peters, V.G., Wyman, D.R., Patterson, M.S. and Frank, G.L., 1990 "Optical properties of normal and diseased human breast tissues in the visible and near infrared" Phys. Med. Biol. 35 pp. 1317-1334.

Reece, G., 1986 Microcomputer Modelling by Finite Differences, John Wiley and Sons, New York.

Samulski, T.V., Cox, R.S., Lyons, B.E. and Fessenden, P., 1989, "Heat loss and blood flow during hyperthermia in normal canine brain II:Mathematical model" Int. J. Hyperthermia 5 pp. 249-263.

Bibliography (continued)

Song, C.W., 1980 "Effect of hyperthermia on vascular function, pH and cell survival" Radiology 137 pp. 795-803.

Stauffer, P.R., Sneed, P.K., Suen, S.A., Satoh, T., Matsumoto, K., Fike, J.R., and Phillips, T.L., 1989, "Comparative thermal dosimetry of interstitial microwave and radiofrequency-LCF hyperthermia" Int. J. Hyperthermia 5 pp. 307-318.

Strohbehn, J.W., Curtis, E.H., Paulsen, K.D., Yuan, X. and Lynch, D.R., 1989, "Optimization of the absorbed power distributions for an annular phased array hyperthermia system" Int. J. Radiation Oncology Biol. Phys. 16 pp. 589-599.

Strohbehn, J.W. and Roemer, R.B., 1984, "A survey of computer simulations of hyperthermia treatments" IEEE Trans. Biomed. Eng. BME-31, pp. 136-149

Svaasand, L.O., Boerslid, T. and Oeveraasen, M., 1985, "Thermal and optical properties of living tissue: Application to laser-induced hyperthermia" Lasers Med. Surg. 5 pp. 589-602.

Svaasand, L.O., 1989 "Dosimetry for laser induced hyperthermia" Lasers in Med. Sci. pp. 309-315.

Turner, P.F., 1984 "Regional hyperthermia with an annular phased array" IEEE Trans. Biomed. Eng. 31 pp. 106-114.

Bibliography (continued)

Waterman, F.M., Tupchong, L., Matthews, J., and Nerlinger, R., 1989, "Mechanisms of heat removal during local hyperthermia" Int. J. Radiation Oncology Biol. Phys. 17 pp. 1049-1055.

Weinberg, A. and Wigner, E., 1958 The Physical Theory of Neutron Chain Reactors, U of Chicago Press, Chicago.

Welch, A.J., 1984 "The thermal response of laser irradiated tissue" IEEE J. Quantum Electronic QE-20, pp. 1471-1480.

Westra, A. and Dewey, W.C., 1971 "Variation in sensitivity to heat shock during the cell cycle of Chinese hamster cells in vitro", Int. J. Radiat. Biol. 19 pp. 467-477.

Wong, R.S.L. et al., 1989, "Mechanism of killing Chinese hamster ovary cells heated in G1: Effects of DNA synthesis and blocking in G2" Radiat. Res. 118 pp. 295-310.

Wulff, W., 1974 "The energy conservation equation for the living tissue" IEEE Trans. BME 21 p. 494.

Wyman, D., Wilson, B., Swift, C. and Siwek, R.A., 1990 "Spatial distribution of light emitted from optical fibre diffusing tips" Phys. Med. Biol. 35 pp. 561-564.

Wyman, D., Swift, C., Siwek, R. and Wilson, B., 1991, "A control method for a nonlinear multivariable system: Application to interstitial laser hyperthermia" IEEE Trans. Biomed. Eng 38 (in press).